# 上节课回顾

The vorticity in the $x$–$z$ plane $\xi$ is governed by (2.61), which we write here as

$$\frac{D\xi}{Dt} + g\frac{\partial}{\partial x}\left(\frac{\theta^*}{\hat{\theta}}\right) = 0 \quad (9.3)$$

$$\xi = \frac{\partial u}{\partial z} - \frac{\partial w}{\partial x}$$

We may define a

$$(u, w) = (\psi_z, -\psi_x) \quad (9.4)$$

$$\frac{B}{g} \approx \frac{\theta'}{\theta} + 0.61q_v' - \frac{c_v}{c_p}\frac{p'}{p} - q_h$$

Then the vorticity, $\xi \equiv u_z - w_x$ [see (2.56)], becomes

$$\xi = \psi_{zz} + \psi_{xx} \quad (9.5)$$

Substituting (9.4) and (9.5) into (9.3) and applying the steady state assumption, we obtain

$$\psi_z\frac{\partial}{\partial x}(\psi_{zz}+\psi_{xx}) - \psi_x\frac{\partial}{\partial z}(\psi_{zz}+\psi_{xx}) + g\frac{\partial}{\partial x}\left(\frac{\theta^*}{\hat{\theta}}\right) = 0 \quad (9.6)$$

请参考《Cloud Dynamics》第250页

# 上节课回顾

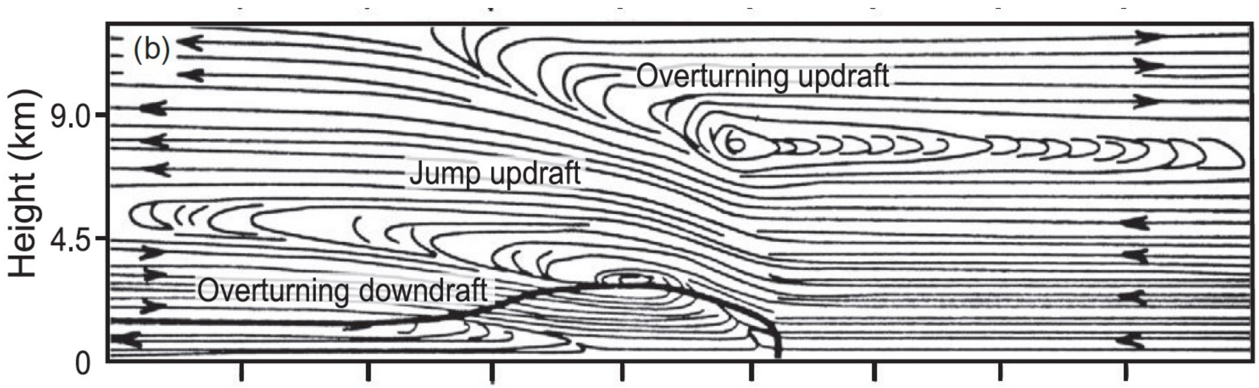


**FIGURE 9.18** Time averaged numerical model simulation of a squall line with trailing stratiform precipitation. (a) Simulated radar reflectivity (in intervals of 5 dBZ). (b) Streamlines of system relative airflow. (c) Equivalent potential temperature (intervals of 3 K). Bold solid contour outlines cold pool (region of negative potential temperature perturbation). *From Fovell and Ogura (1988). Republished with permission of the American Meteorological Society.*

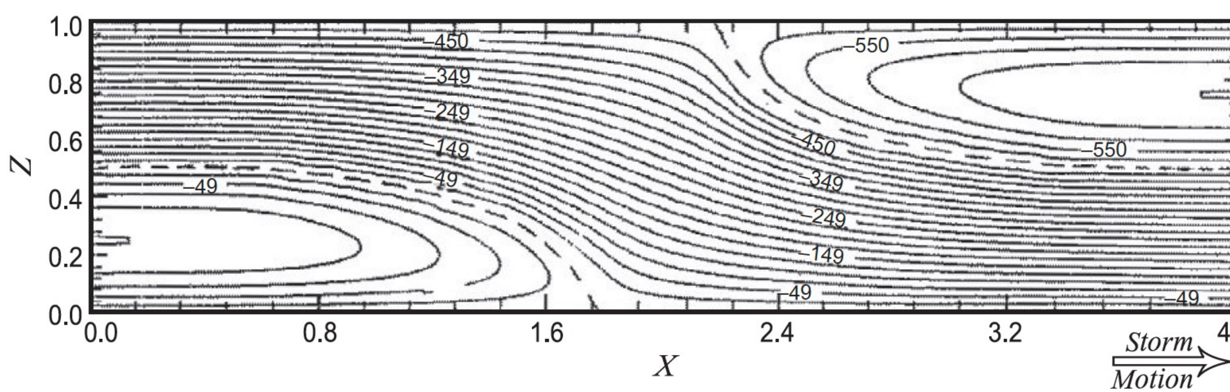


**FIGURE 9.19** Two-dimensional relative stream function $\psi$ calculated for the conditions of a squall-line MCS. Height $z$ and horizontal distance $x$ are in arbitrary units. *From Moncrieff (1992). Republished with permission of the Royal Meteorological Society.*

# 上节课回顾

Consider a steady solution with all varable u only depending on $\psi$ and z

$$u = u\left(\psi\left(x, z\right), z\right)$$

3D momentum equations reads as follows

$$\frac{\mathrm{D}\mathbf{v}}{\mathrm{D}t} = -\frac{1}{\rho_o}\nabla p^* - f\mathbf{k}\times\mathbf{v} + B\mathbf{k} + \mathbf{F} \qquad (2.47)$$

Making Boussinesq assumption $\rho_0$=const.

$$wB = \frac{D}{Dt}\int_{z_{in}}^{z} B\left(\psi, z'\right)dz'$$

Taking $\mathbf{v}\cdot$(2.47), making the Boussinesq assumption, ignoring friction, and using the identity (9.9), we obtain the Bernoulli equation

$$\frac{1}{2}\left(u^2 + w^2\right) + \frac{p^*}{\rho_o} - \int_{z_{in}}^{z(t)} g\left(\frac{\theta^*}{\hat{\theta}}\right)\mathrm{d}z = \text{constant on streamline}$$

# 上节课回顾

Ertel PV theorem

$$\frac{d}{dt}\left\{\frac{\boldsymbol{\omega}_a}{\rho}\cdot\nabla\lambda\right\} = \frac{\boldsymbol{\omega}_a}{\rho}\cdot\nabla\Psi + \nabla\lambda\cdot\left[\frac{\nabla\rho\times\nabla p}{\rho^3}\right] + \frac{\nabla\lambda}{\rho}\cdot\left\{\nabla\times\frac{\mathscr{F}}{\rho}\right\}.$$

Geophysical Fluid Dynamics by Pedlosky (1986)

The derivation begins with the hydrostatic primitive equations with minor approximation in the thermodynamic terms

$$d\mathbf{v}/dt + \theta_0\nabla\pi' + f\mathbf{k}\times\mathbf{v} = \mathbf{F}, \quad (1)$$

$$\theta_0(\partial\pi'/\partial z) - b' = 0, \quad (2)$$

$$\nabla\cdot\mathbf{v} + \rho_0{}^{-1}(\partial\rho_0 w/\partial z) = 0, \quad (3)$$

$$db'/dt + N^2 w = gH/\theta_0, \quad (4)$$

$$u = -\frac{\partial\psi}{\partial y} \qquad v = \frac{\partial\psi}{\partial x}$$

见板书!

To the extent that vertical velocities are small, $\phi$ can be ignored, and the $x$ and $y$ components of vorticity can be approximated as

$$\zeta_x \approx -\partial^2\psi/\partial x\partial z, \quad \zeta_y \approx -\partial^2\psi/\partial y\partial z. \quad (10)$$

The potential vorticity $q = \rho^{-1}(\boldsymbol{\zeta} + f\mathbf{k})\cdot\nabla\theta$ thus becomes, to this degree of approximation,

$$q = \frac{1}{\rho_0}\left[-\frac{\partial^2\psi}{\partial x\partial z}\frac{\partial\theta}{\partial x} - \frac{\partial^2\psi}{\partial y\partial z}\frac{\partial\theta}{\partial y} + (f + \nabla^2\psi)\frac{\partial\theta}{\partial z}\right], \quad (11)$$

Raymond and Jiang (1990)

Any difference from QG theory?

$$\frac{g\rho_0 q'}{\theta_0} = \frac{f}{\theta_0}\frac{\partial}{\partial z}\left(\theta_0{}^2\frac{\partial\pi'}{\partial z}\right) + N^2\nabla^2\psi - \theta_0\left(\frac{\partial^2\psi}{\partial x\partial z}\frac{\partial^2\pi'}{\partial x\partial z} + \frac{\partial^2\psi}{\partial y\partial z}\frac{\partial^2\pi'}{\partial y\partial z}\right). \quad (12)$$

$$\nabla^2(\theta_0\pi' - f\psi) = 2\frac{\partial^2\psi}{\partial x^2}\frac{\partial^2\psi}{\partial y^2} - 2\left(\frac{\partial^2\psi}{\partial x\partial y}\right)^2. \quad (13)$$

请参考Raymond and Jiang (1990)

# 上节课回顾

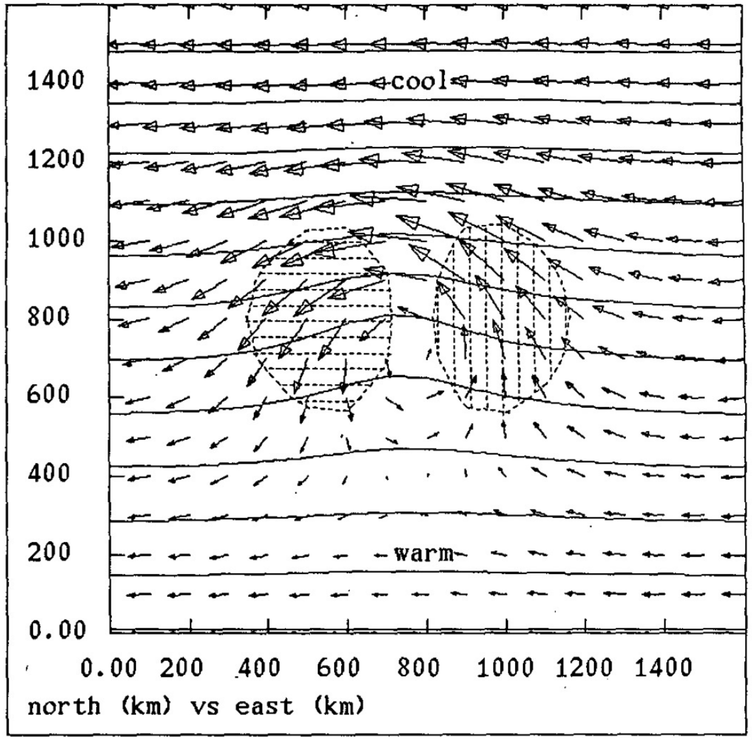


FIG. 6. Flow and potential temperature at $z = 3$ km and $t = 10$ ks. Contours indicate constant values of potential temperature at 1°K intervals, with cooler regions to the north. Vectors show the horizontal flow with a scale of 3 m $s^{-1}$ per 100 km. Vertical hatching shows updrafts in excess of 0.5 cm $s^{-1}$, while downdrafts less than $-0.5$ cm $s^{-1}$ are indicated by horizontal hatching.

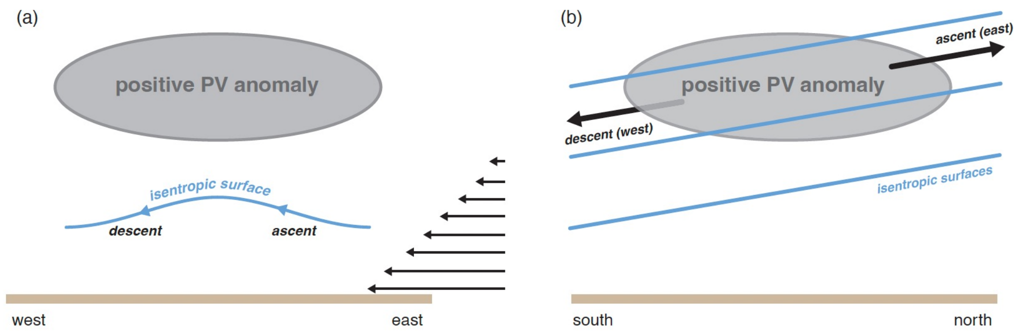


**Figure 9.34** Illustrations of the mechanisms by which ascent can occur in the presence of a potential vorticity anomaly in shear. The environmental shear is westerly in the illustration and only shown below the positive potential vorticity anomaly for clarity. (a) In a frame of reference moving with the potential vorticity anomaly, the relative environmental wind causes flow on the perturbation isentropic surface caused by the potential vorticity anomaly, with ascent (descent) upwind (downwind) of the anomaly. (b) The potential vorticity anomaly, as viewed from the east. The tilted isentropic surfaces are associated with the environmental westerly wind shear indicated in (a). The cyclonic circulation around the potential vorticity anomaly causes ascent (descent) in the southerlies (northerlies) east (west) of the anomaly. (Adapted from Raymond and Jiang [1990].)

# 上节课回顾

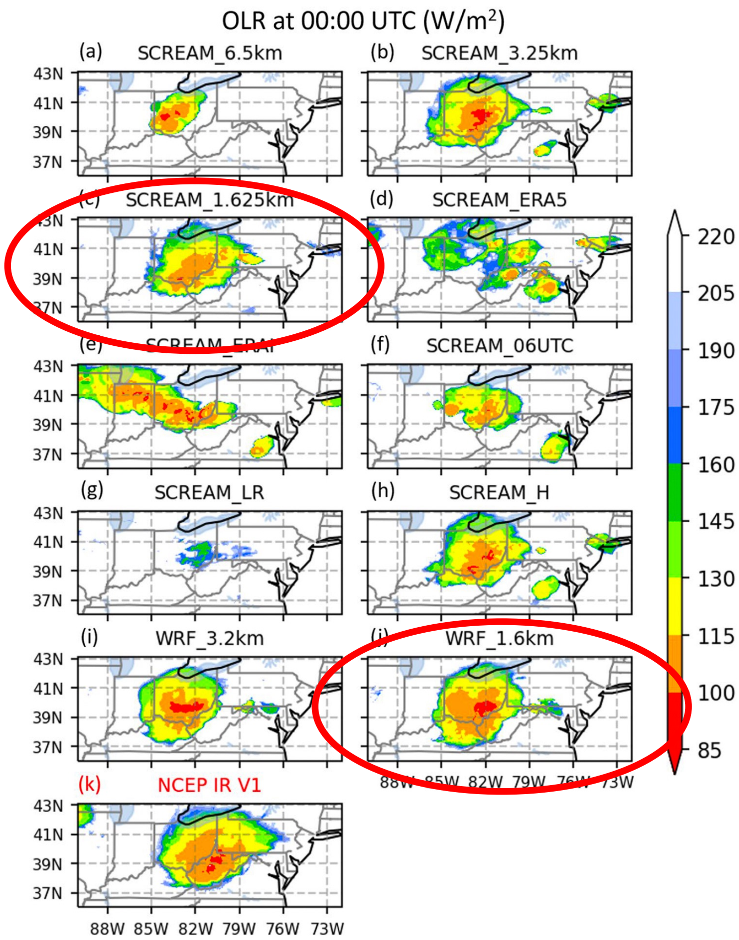


**Figure 2.** Outgoing longwave radiation ($W/m^2$) at 00:00 UTC 30 June 2012 in (a) SCREAM_6.5 km, (b) SCREAM_3.25 km, (c) SCREAM_1.625 km, (d) SCREAM_ERA5, (e) SCREAM_ERAI, (f) SCREAM_06UTC, (g) SCREAM_LR, (h) SCREAM_H, (i) WRF_3.2 km, (j) WRF_1.6 km, and (k) NCEP IR V1. All datasets are remapped to 0.05° resolution. The panel with red title denotes the reference data set.

# 上节课回顾

Pseudo-global warming (PGW) approach

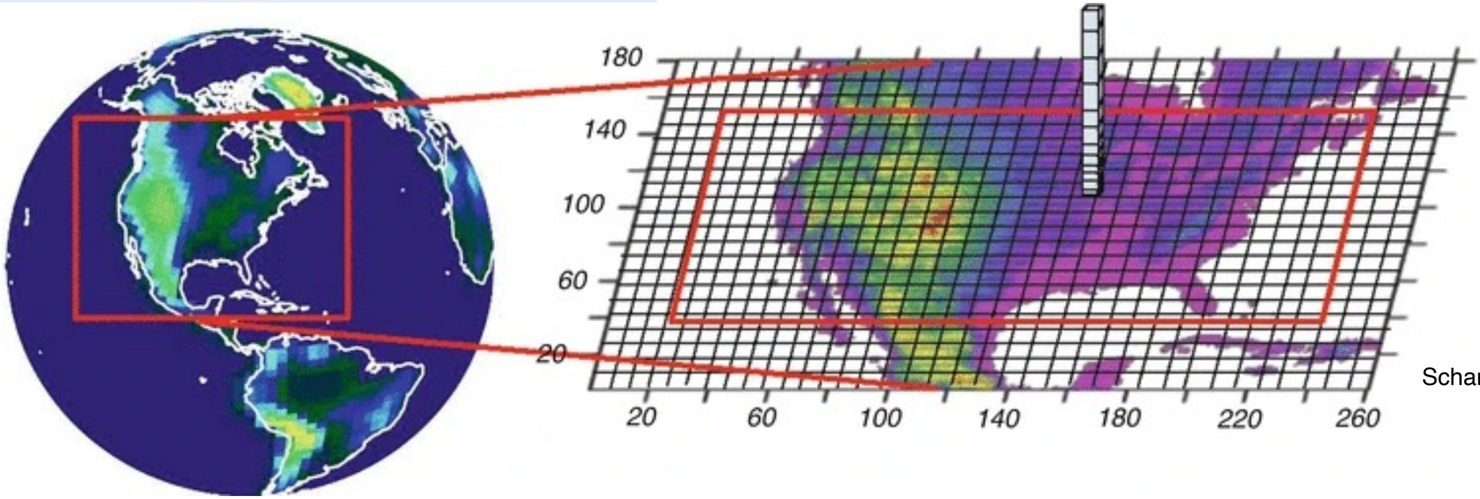


Schar et al. (1996); Sato et al. (2007) ...

change signal for the RCP8.5 scenario. As described in Liu et al. (2016), the WRF input for the PGW simulation is as follows:

$$WRF_{INPUT} = ERA - Interim + \Delta CMIP5_{RCP8.5} \quad (1)$$

where $\Delta CMIP5_{RCP8.5}$ is the 95-year CMIP5 multi-model ensemble-mean monthly change under the RCP8.5 scenario:

$$\Delta CMIP5_{RCP8.5} = CMIP5_{2071-2100} - CMIP5_{1976-2005} \quad (2)$$

The perturbed fields that were used to generate the WRF input for the PGW simulation include horizontal wind, geopotential, temperature, specific humidity, sea surface temperature, soil temperature, sea level pressure, and sea ice. Across the CONUS domain, temperature changes in

# 上节课回顾

LETTERS
https://doi.org/10.1038/s41558-017-0007-7
nature climate change

## Increased rainfall volume from future convective storms in the US

Andreas F. Prein*, Changhai Liu, Kyoko Ikeda, Stanley B. Trier, Roy M. Rasmussen, Greg J. Holland and Martyn P. Clark

**Fig. 1 | Schematic of Lagrangian tracking of MCS precipitation and future changes in MCSs. a**, MCS hourly precipitation accumulations above 5 mm $h^{-1}$ are identified and tracked over space and time (time corresponds to the vertical axis). **b**, Characteristics such as storm motion, rain rates or cloud top heights are identified for MCSs in the current and future climate. Highest increases are found for MCS precipitation volumes, which is positively related to increasing rain rates and rain areas and negatively to changes in storm motion (**b**).

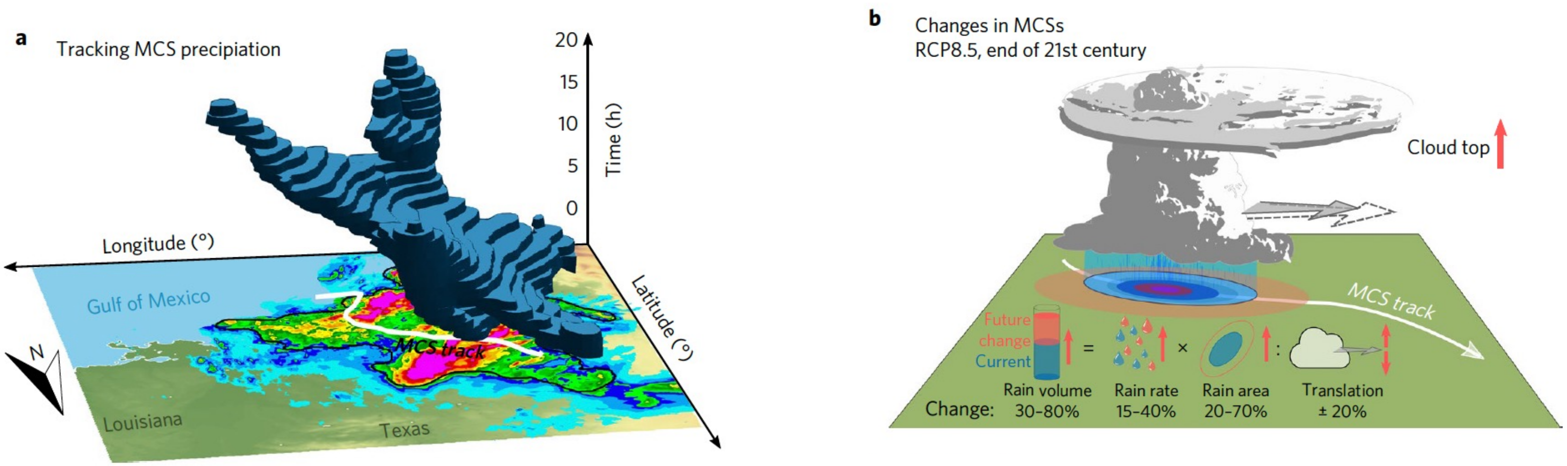

## Chapter 5

# Hazards associated with DMC

- Tornado
- Straight Wind
- Hail
- Flash flood

# What is tornado?

*A rotating column of air, in contact with the surface, pendant from a cumuliform cloud, and often visible as a funnel cloud and/or circulating debris/dust at the ground* (AMS 2015).

# 龙卷视频:派比安台风龙卷

2006年8月4日，受“派比安”台风外围环流的影响,两股威力超强的龙卷风袭击广东4个市（区）。其中一股龙卷风上午从南海西樵镇崇南村向丹灶镇方向扫过，波及途经的8个村委会并吹向三水白坭镇；另一股龙卷风则在下午3时30分前后袭击南海大沥镇。

# 龙卷视频：彩虹台风龙卷


**龙卷位置：**
**龙眼博澳城**
（网络视频）
约**15:30 BJT**

# 龙卷视频：彩虹台风龙卷

# 龙卷视频：彩虹台风龙卷

开心美食
餐厅监控


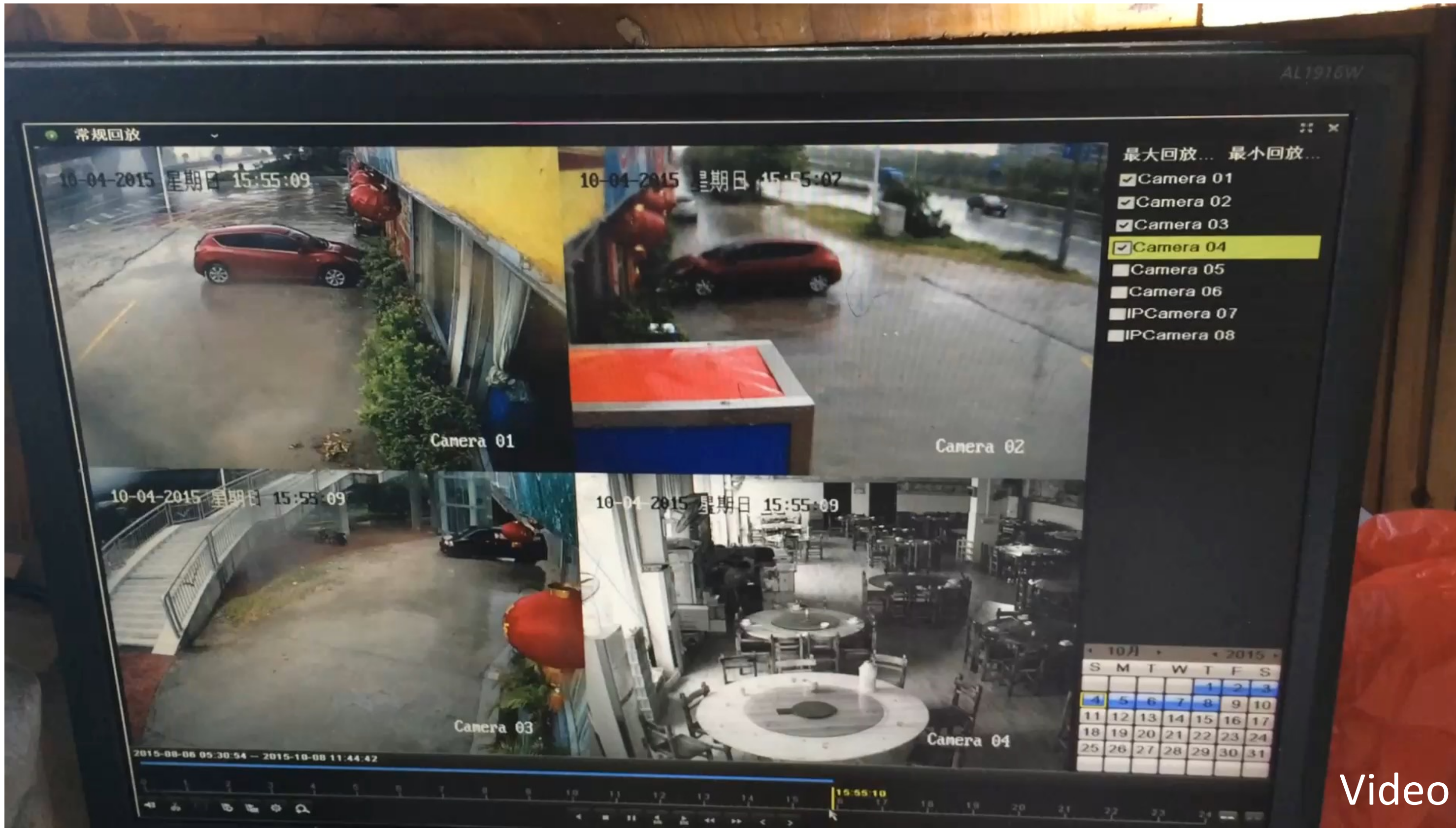


# 龙卷视频：彩虹台风龙卷

## 道路摄像头

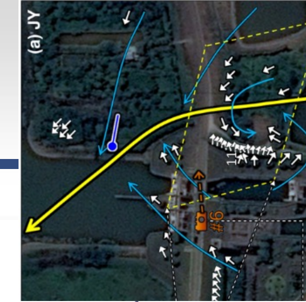

# 龙卷视频：赤峰冷涡龙卷

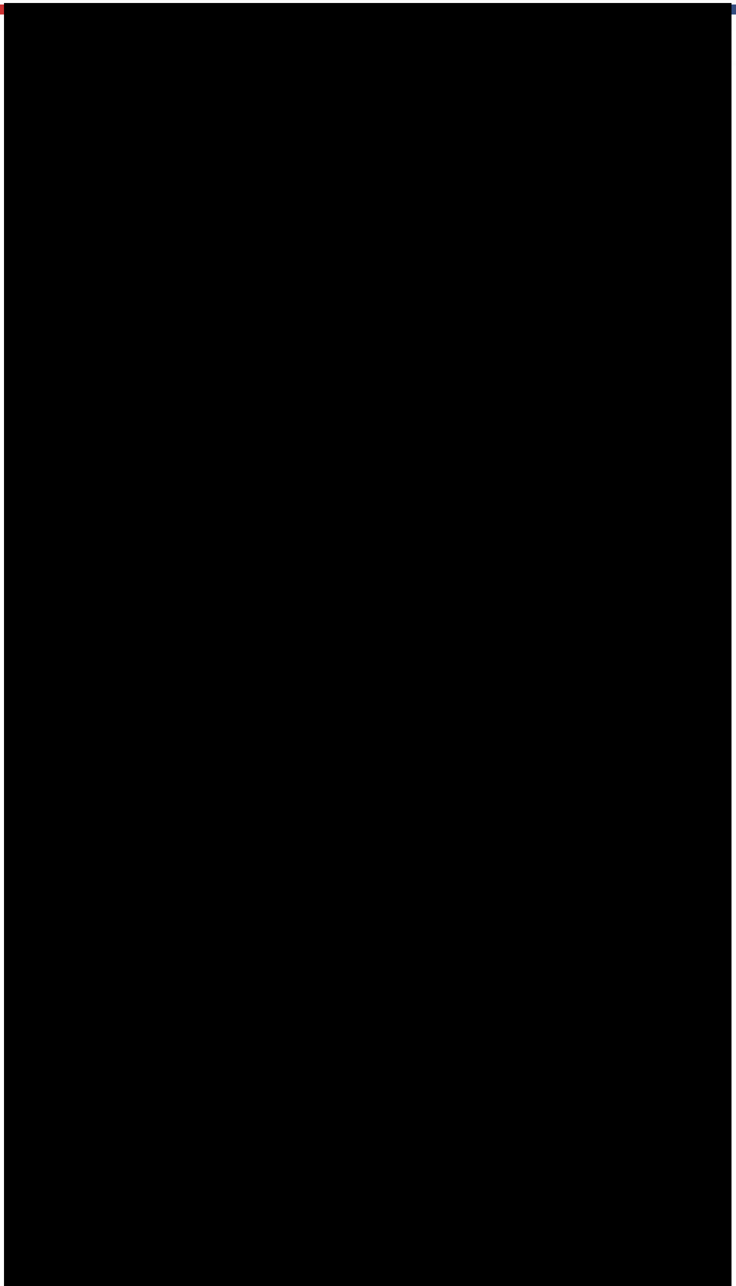

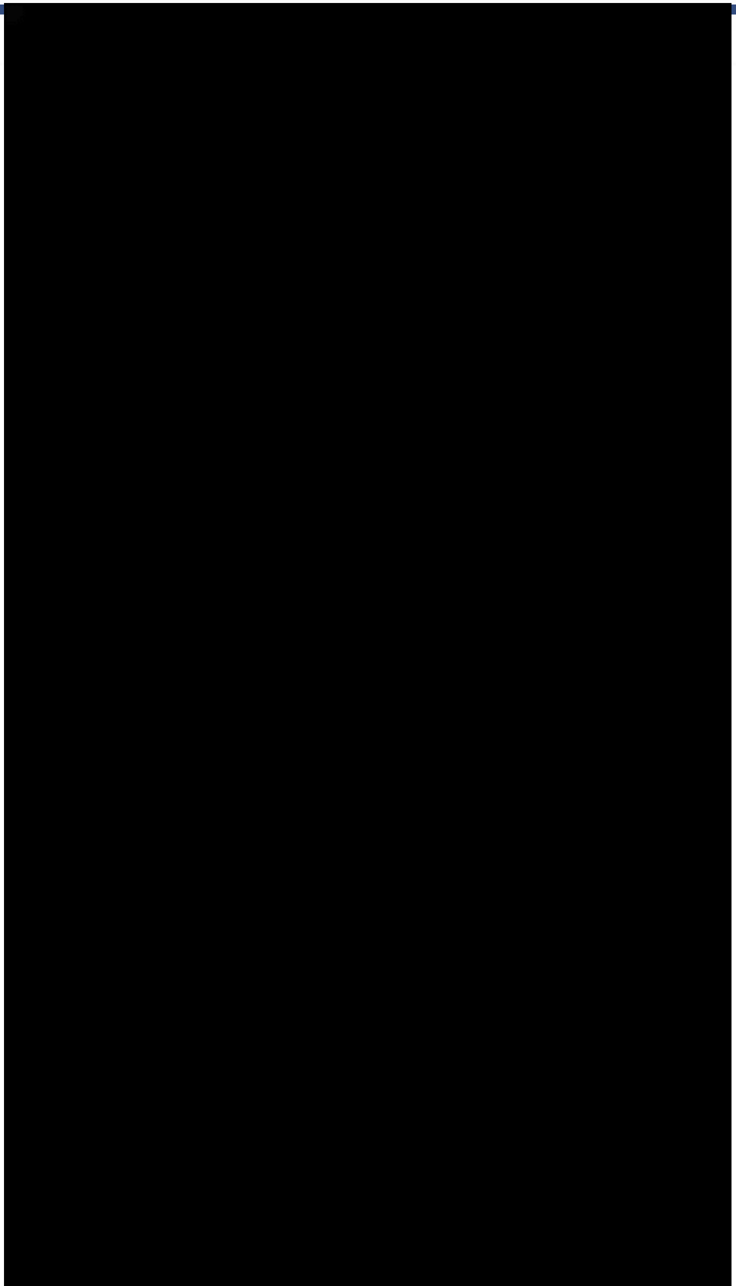

# 龙卷视频：阜宁龙卷风

# 龙卷视频：开原龙卷

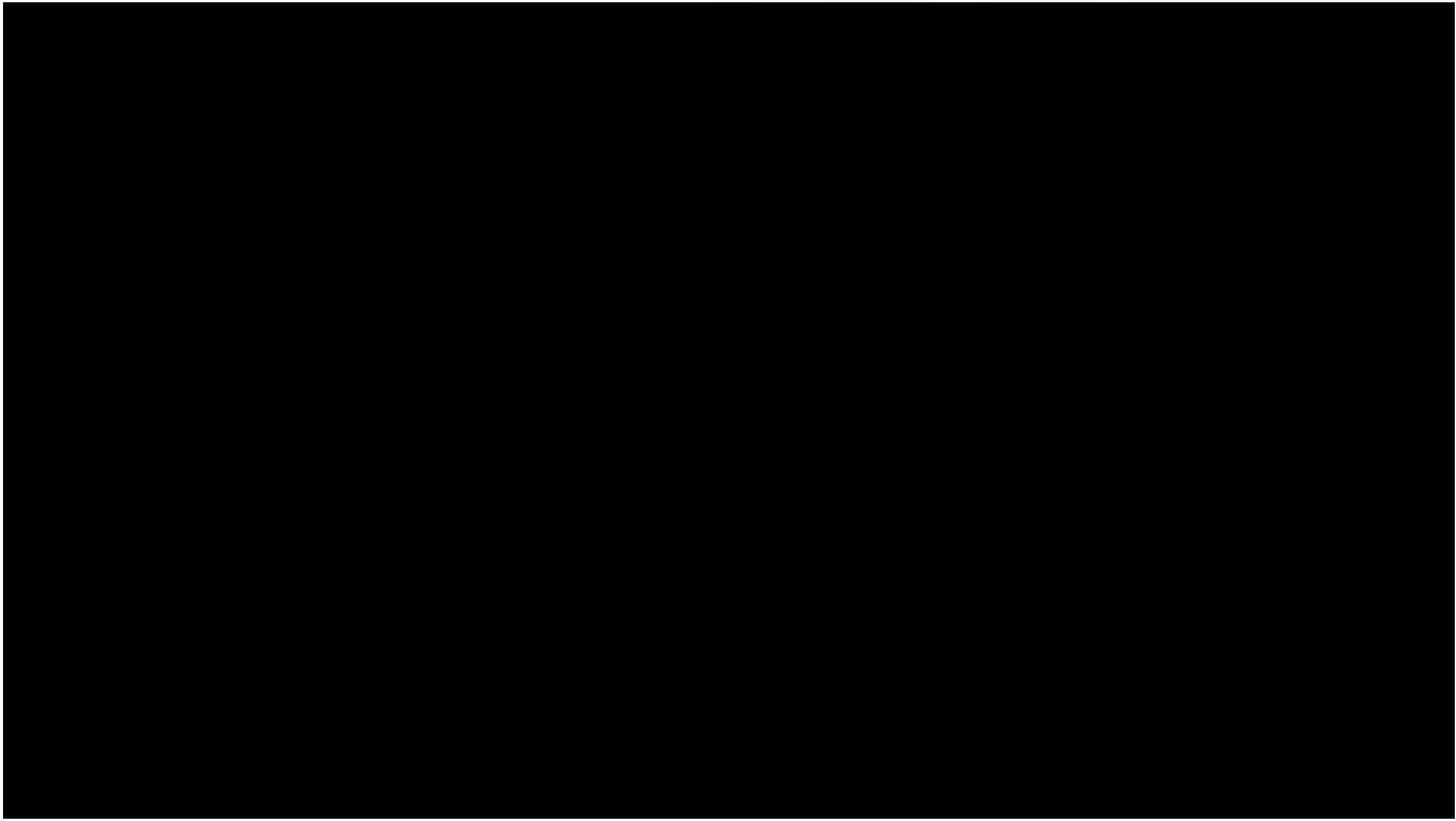

**2019年7.3辽宁开原EF4龙卷**

# 龙卷灾害等级：F等级

表1 Fujita 龙卷等级[25]（1971）

| F等级 | 估计最大风速（m/s） | 损害描述 |
|---|---|---|
| F0 | 18~33 | 轻微损害。烟囱会有一些损害，一些树枝被刮掉，树根浅的树可能被刮倒，指路牌被损坏。 |
| F1 | 33~50 | 中等程度损害。可以刮掉房屋屋顶的表面，将移动房屋刮离地基或侧翻，正在开动的汽车被推离公路。 |
| F2 | 50~70 | 相当大的损害。框架结构的屋顶被刮掉，移动房屋被推毁，集装箱卡车侧翻，大树被折断或被连根拔起，轻的物体快速飞到空中。 |
| F3 | 70~92 | 严重损害。屋顶严重损坏，一些结构比较结实的房屋的墙被刮倒，火车被刮翻，森林里大多数树木被连根拔起，汽车被掀离地面并被抛到一定距离以外。 |
| F4 | 92~117 | 巨大损害。较结实的房屋被夷平，一些房屋部件被抛到一定距离以外，汽车被抛到空中，一些大的物体高速飞入空中。 |
| F5 | 117~143 | 难以想象的损害。非常结实的房屋被推离地基并被带到相当距离之外碎成几块。汽车大小的物体以超过100m/s的速度被抛入空中，会发生难以置信的现象。 |

- Wind speed: usually < 50 m/s， EF4 or EF5 may > 75 m/s

  1% of total tornadoes account for 70% fatalities

# 龙卷灾害等级：EF等级

**Enhanced Fujita（EF) scale； 2007年2月1日 （WSEC 2006）**

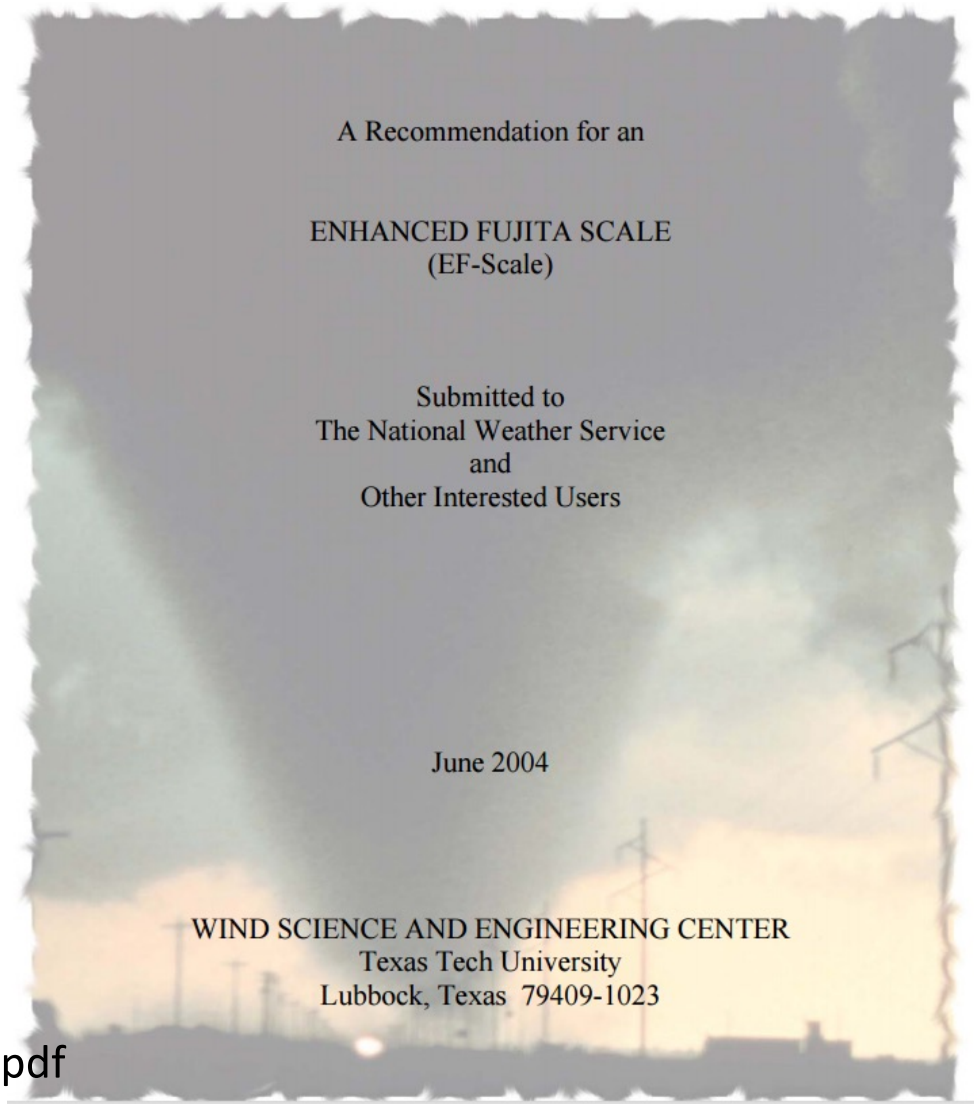


http://www.spc.noaa.gov/faq/tornado/ef-ttu.pdf

# Damage Indicators for EF Scale

| DI No. | Damage indicator (DI) |
|---|---|
| 1 | Small Barns or Farm Outbuildings (SBO) |
| 2 | One- or Two-Family Residences (FR12) |
| 3 | Manufactured Home – Single Wide (MHSW) |
| 4 | Manufactured Home – Double Wide (MHDW) |
| 5 | Apartments, Condos, Townhouses [3 stories or less] (ACT) |
| 6 | Motel (M) |
| 7 | Masonry Apartment or Motel Building (MAM) |
| 8 | Small Retail Building [Fast Food Restaurants] (SRB) |
| 9 | Small Professional Building [Doctor's Office, Branch Banks] (SPB) |
| 10 | Strip Mall (SM) |
| 11 | Large Shopping Mall (LSM) |
| 12 | Large, Isolated Retail Building [K-Mart, Wal-Mart] (LIRB) |
| 13 | Automobile Showroom (ASR) |
| 14 | Automobile Service Building (ASB) |
| 15 | Elementary School [Single Story; Interior or Exterior Hallways] (ES) |
| 16 | Junior or Senior High School (JHSH) |
| 17 | Low-Rise Building [1-4 Stories] (LRB) |
| 18 | Mid-Rise Building [5-20 Stories] (MRB) |
| 19 | High-Rise Building [More than 20 Stories] (HRB) |
| 20 | Institutional Building [Hospital, Government or University Building] (IB) |
| 21 | Metal Building System (MBS) |
| 22 | Service Station Canopy (SSC) |
| 23 | Warehouse Building [Tilt-up Walls or Heavy-Timber Construction](WHB) |
| 24 | Transmission Line Towers (TLT) |
| 25 | Free-Standing Towers (FST) |
| 26 | Free-Standing Light Poles, Luminary Poles, Flag Poles (FSP) |
| 27 | Trees: Hardwood (TH) |
| 28 | Trees: Softwood (TS) |

# 龙卷定级

## 27. TREES:  HARDWOOD

Typical Construction

- Hardwood:  Oak, Maple, Birch, Ash

| DOD* | Damage description | EXP | LB | UB |
|---|---|---|---|---|
| 1 | Small limbs broken  (up to 1" diameter) | 60 | 48 | 72 |
| 2 | Large branches broken  (1"-3" diameter) | 74 | 61 | 88 |
| 3 | Trees uprooted | 91 | 76 | 118 |
| 4 | Trunks snapped | 110 | 93 | 134 |
| 5 | Trees debarked with only stubs of largest branches remaining | 143 | 123 | 167 |

* Degree of Damage

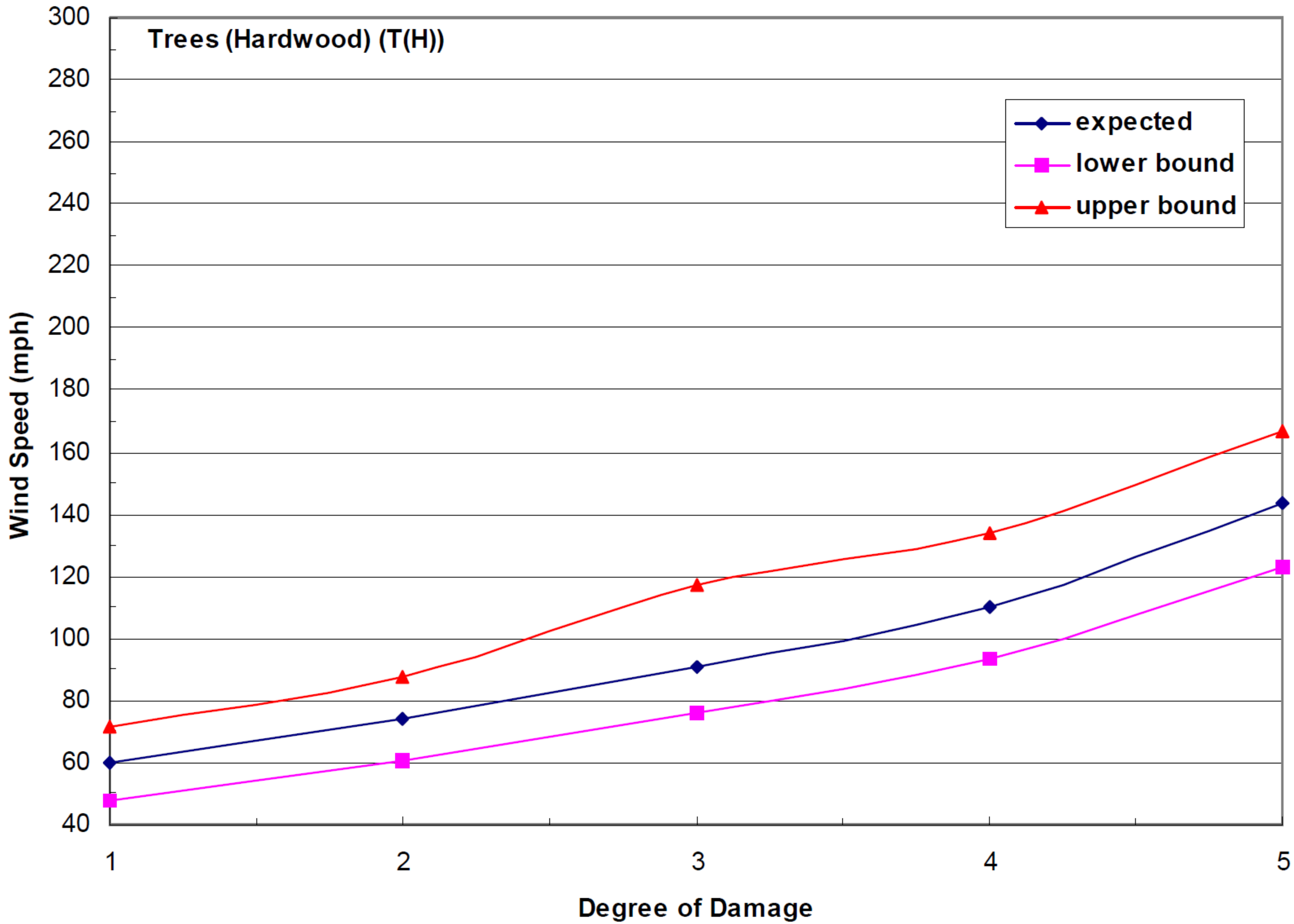

Trees (Hardwood) (T(H))
expected
lower bound
upper bound
Wind Speed (mph)
300
280
260
240
220
200
180
160
140
120
100
80
60
40
1
2
3
4
5
Degree of Damage

| | Recommended EF Scale |
|---|---|
| EF Classes | 3-Second Gust Speed, mph |
| EF0 | 65 - 85 |
| EF1 | 86 - 110 |
| EF2 | 111 - 135 |
| EF3 | 136 - 165 |
| EF4 | 166 - 200 |
| EF5 | >200 |

# EF等级和F等级的对应关系

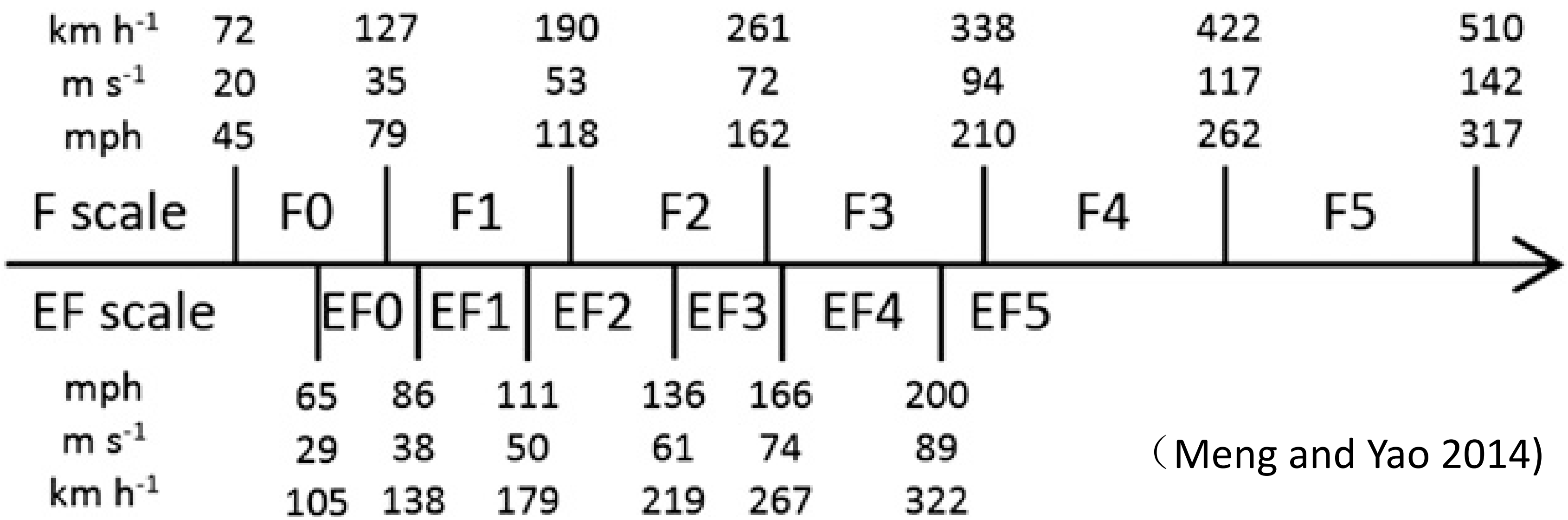


（Meng and Yao 2014)

# General characteristics

- Vertical vorticity: 1 /s, mostly cyclonic
- Diameters : ~ 100 m
- Lift span: 10 min–1 h
- Environmental  system
  - most significant tornadoes (F2 or above) and all violent tornadoes are associated with supercell storms.

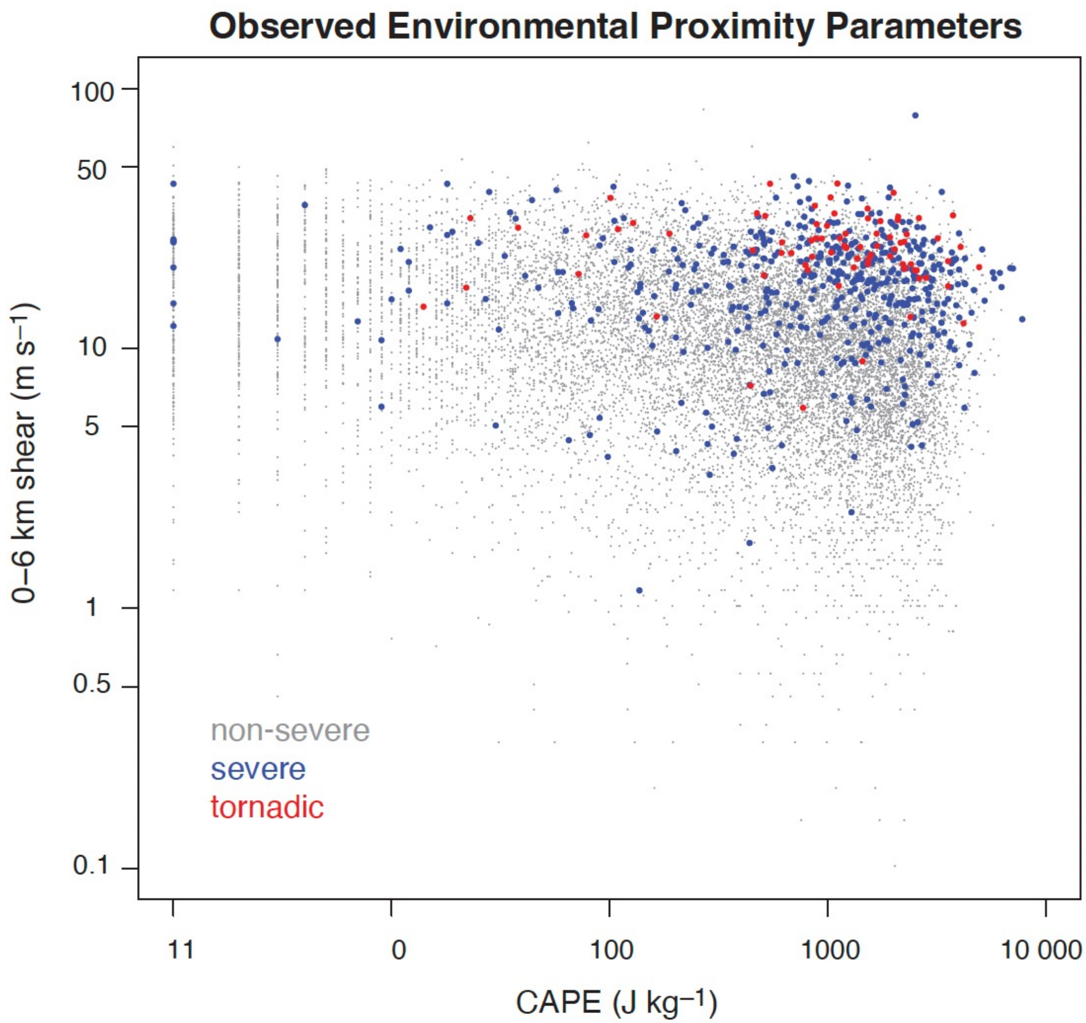


**Figure 10.1** Relationship between severity of observed thunderstorms and the CAPE and vertical wind shear of the environments, as determined by proximity soundings. Red dots indicate tornado reports. Green dots indicate nontornadic damaging wind and/or large hail reports. Black dots indicate nonsevere thunderstorm reports. Courtesy of Harold Brooks, adapted from a figure originally appearing in Brooks *et al.* (2003).

# Spatial distribution

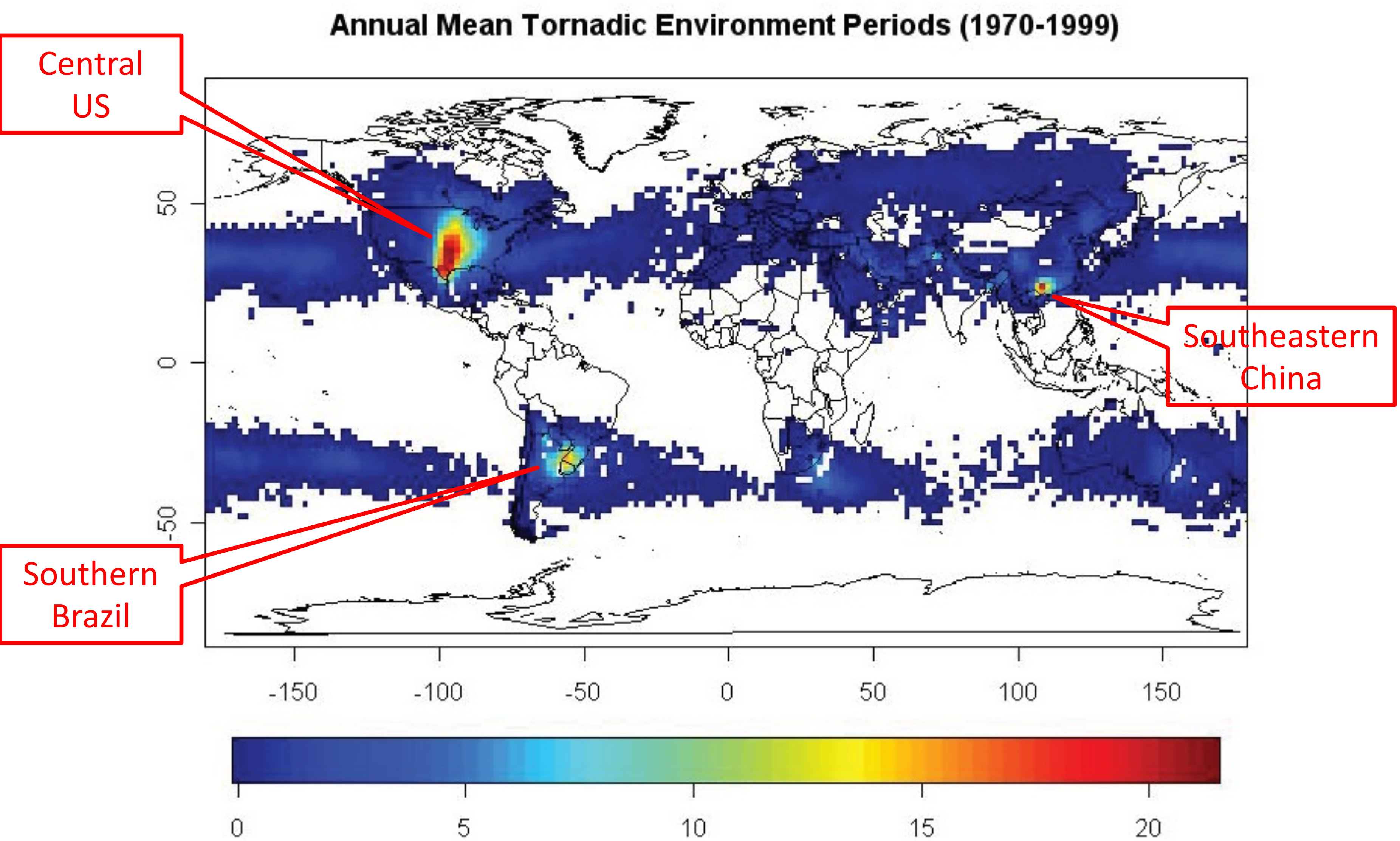

# 我国龙卷分布 (1948-2012)

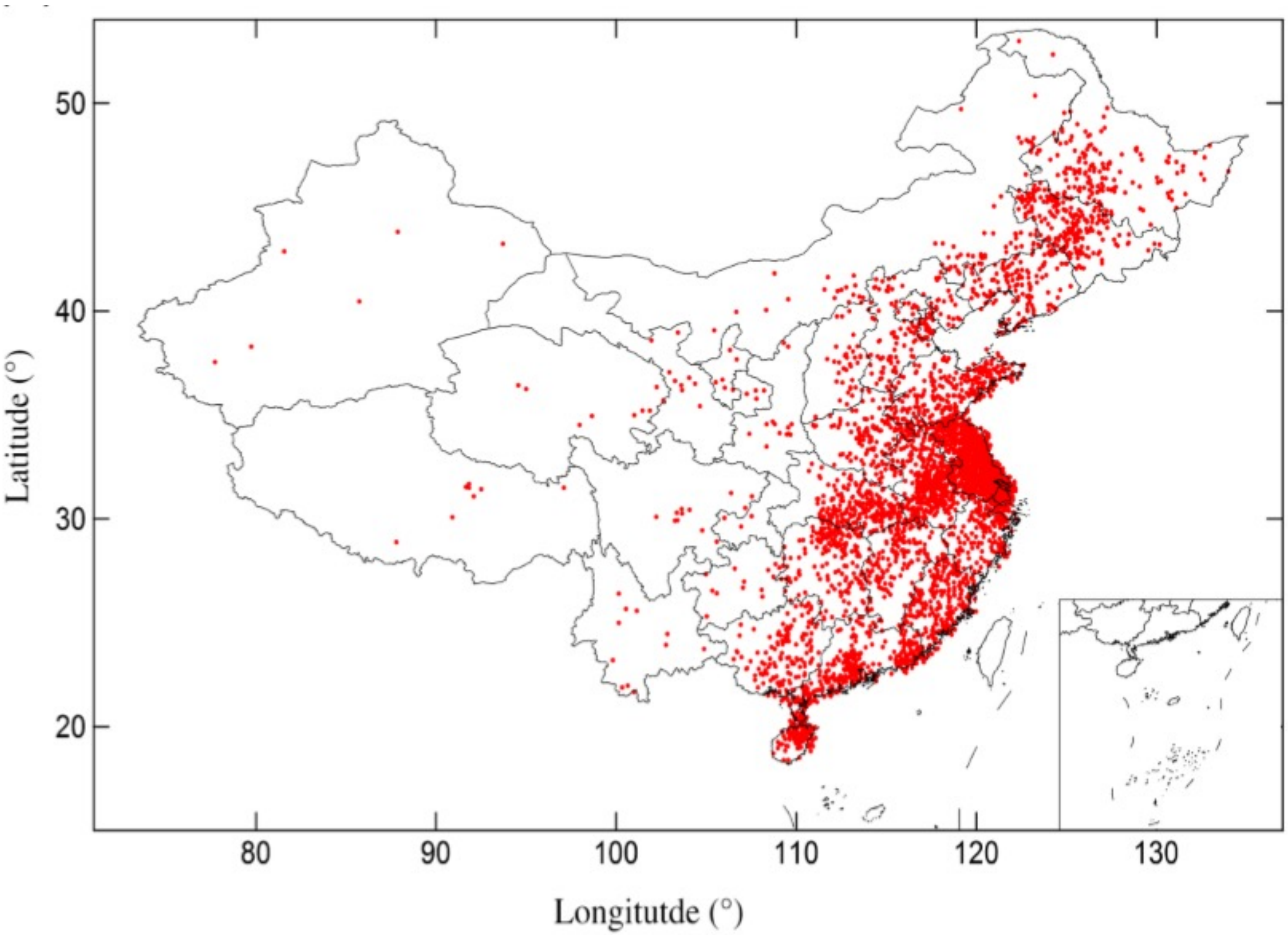


(Chen et al. 2017, International Journal of Climatology)

# 我国龙卷分布 (1948-2012)

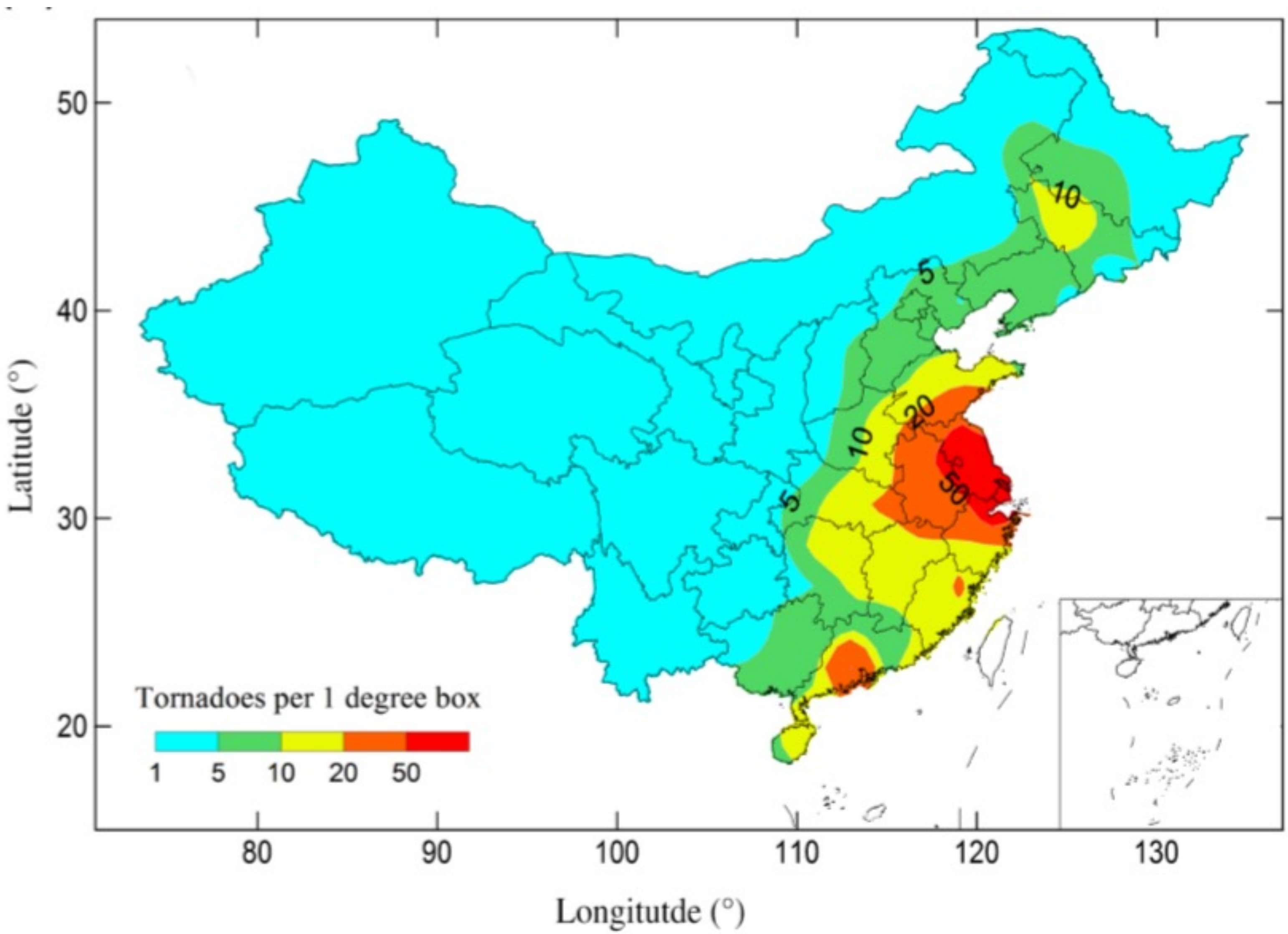

# 我国龙卷分布 (1948-2012)

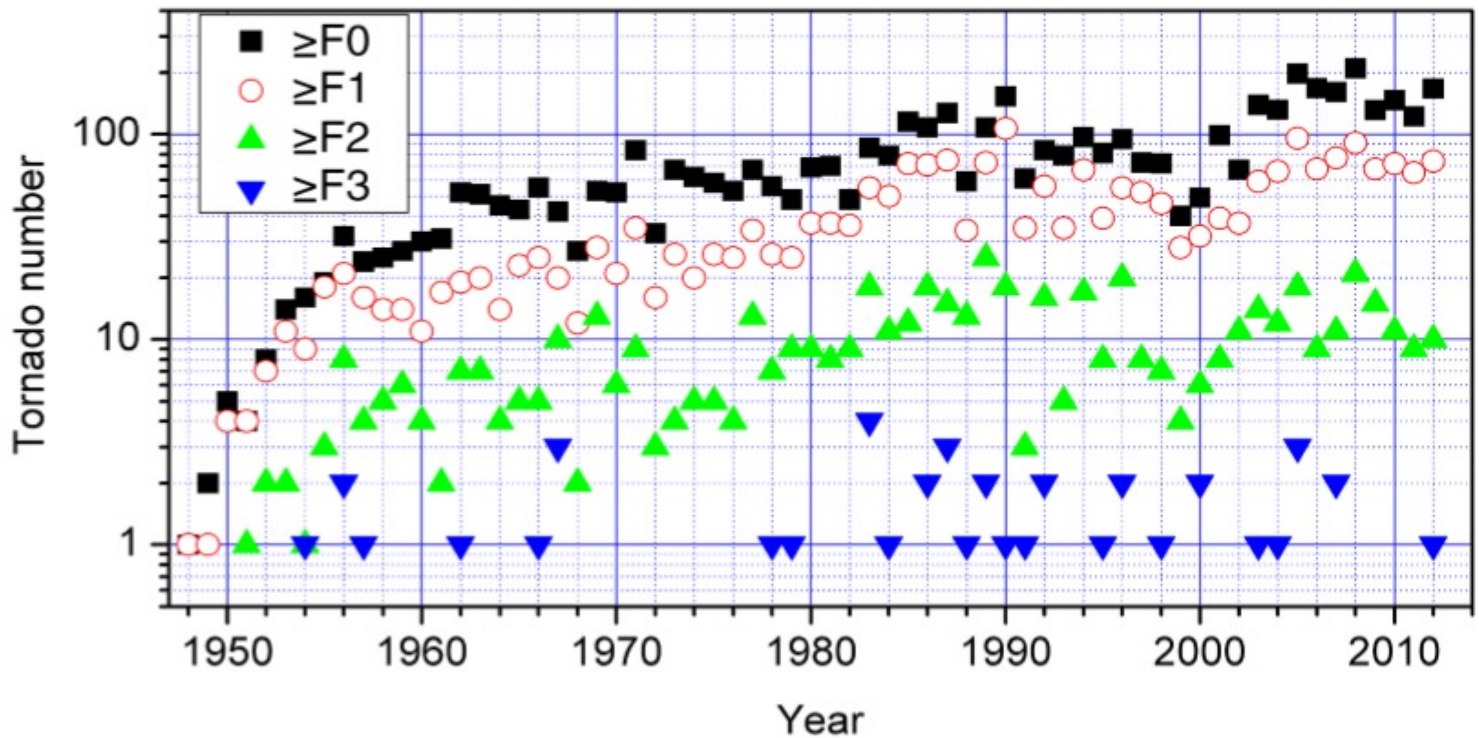


Figure 4. Annual tornado numbers in China from 1948 to 2012 in the data set. Symbols denote different Fujita scale classes, with the number of tornadoes (*N*) that were ≥F0, F1, F2, and F3 being 4676, 2467, 555, and 42, respectively. [Colour figure can be viewed at wileyonlinelibrary .com].

# 我国龙卷分布 (1948-2012)

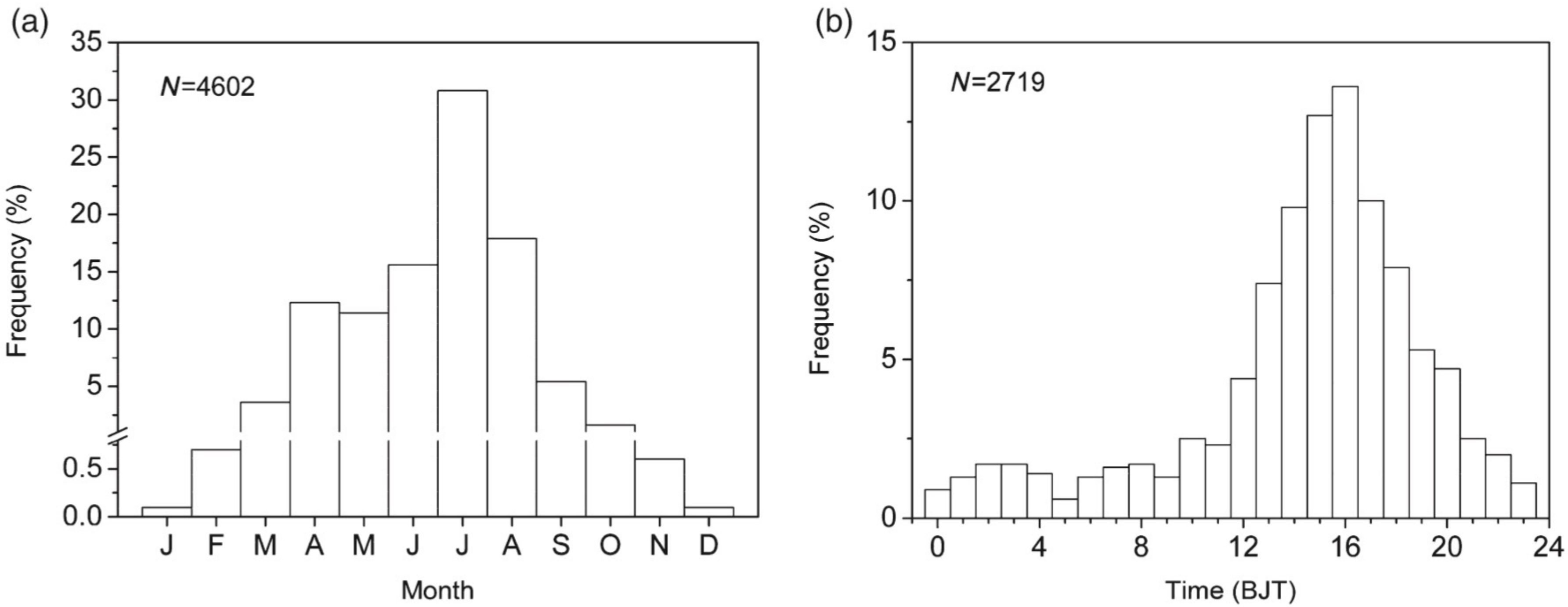


Figure 6. Seasonal (a) and diurnal (b) variation in tornado frequency. BJT is Beijing standard time (UTC + 8). The number of tornadoes is indicated (*N*).

# Tentative location of tornadoes

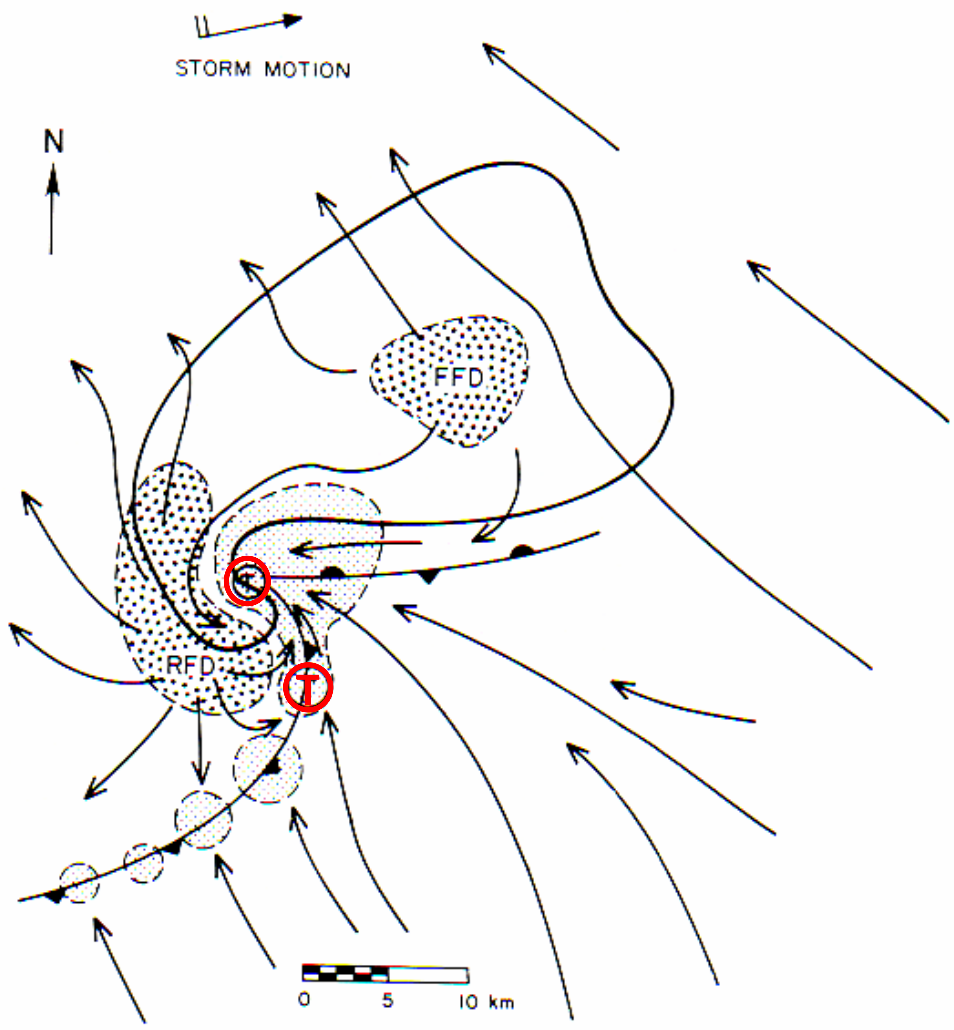

# Tornado Genesis (1)

- It needs large vertical vorticity arises at the ground

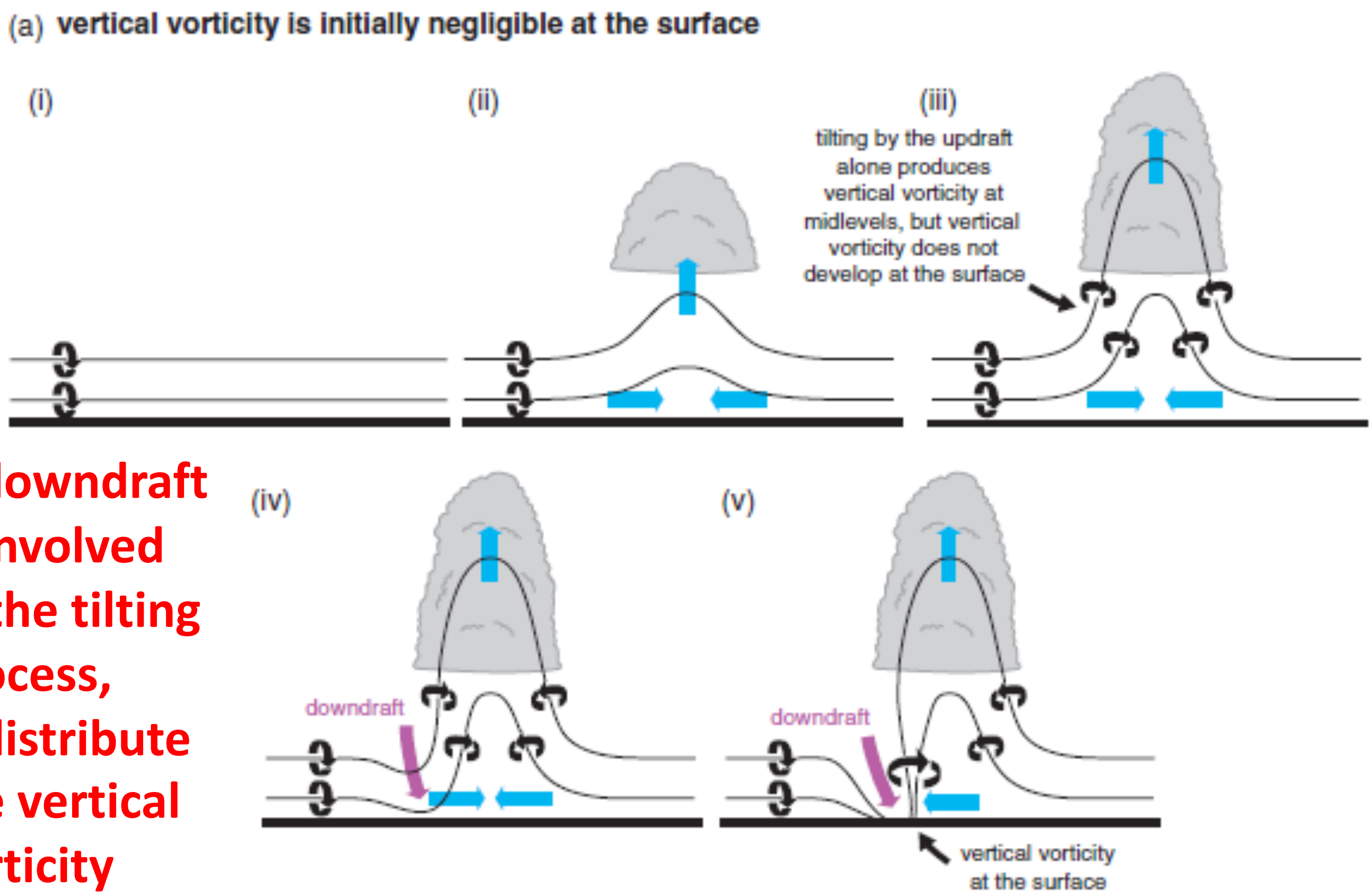


**A downdraft is involved in the tilting process, redistribute the vertical vorticity**

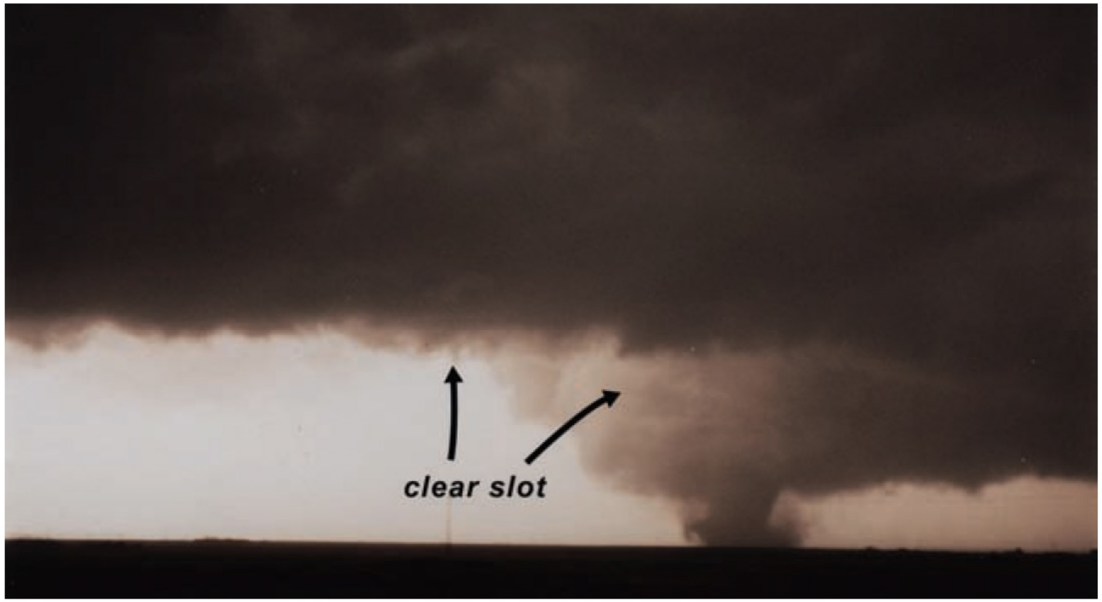


**Figure 10.4** A clear slot like that shown above near the Dimmitt, TX, tornado on 2 June 1995 is a visual manifestation of sinking air, probably in what ought to be regarded as an *occlusion downdraft* (defined in Section 8.4 as a local, dynamically driven intensification of sinking motion within the larger-scale RFD). Photograph by Paul Markowski.

# Observational facts

Trajectories in the RFD region (dual-Doppler observations of supercell thunderstorms,);

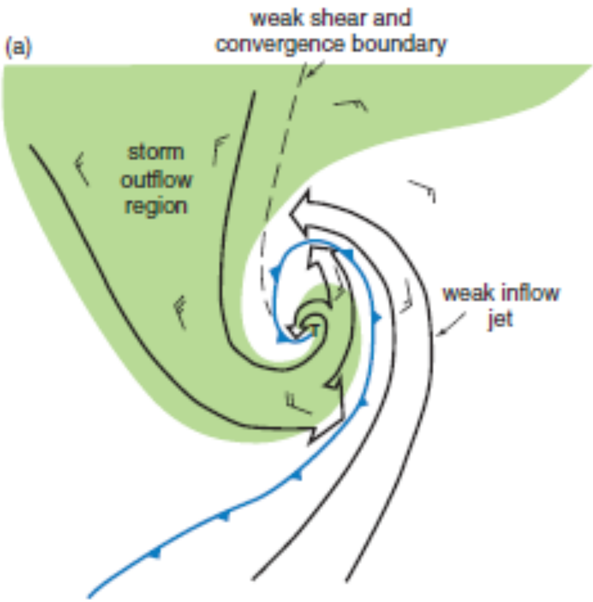


Brandes [1978]

Backward trajectories from the near-ground vertical vorticity maximum

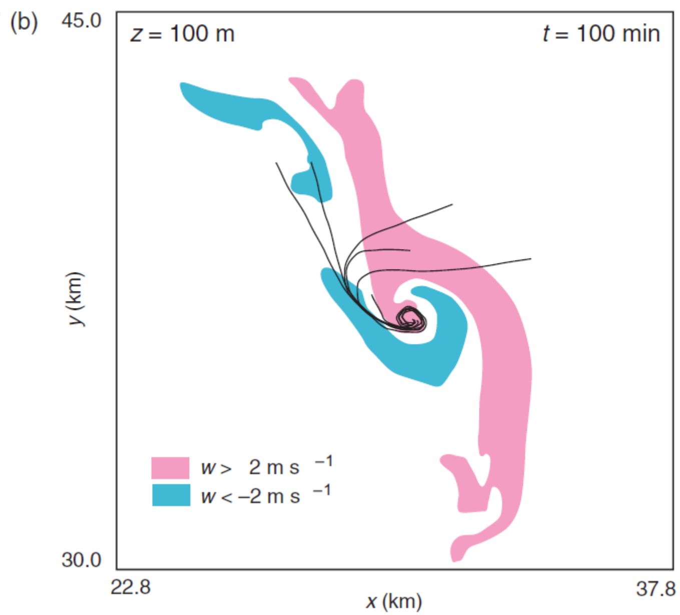


Wicker and Wilhelmson [1995]

a three-dimensional perspective from the southeast of trajectories entering a tornado that developed within a supercell simulation

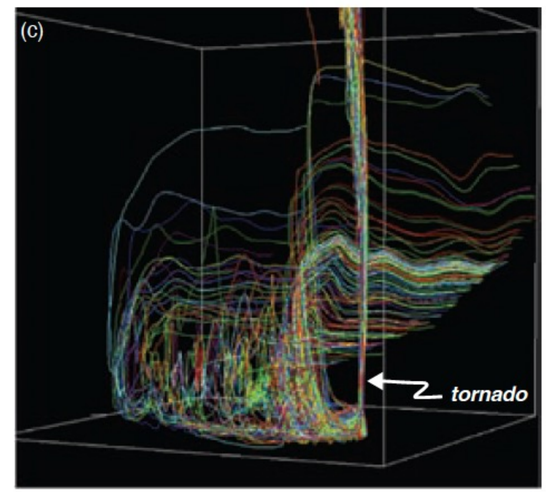


from Xue [2004]; courtesy of Ming Xue).

# Arches of baroclinically generated vortex line

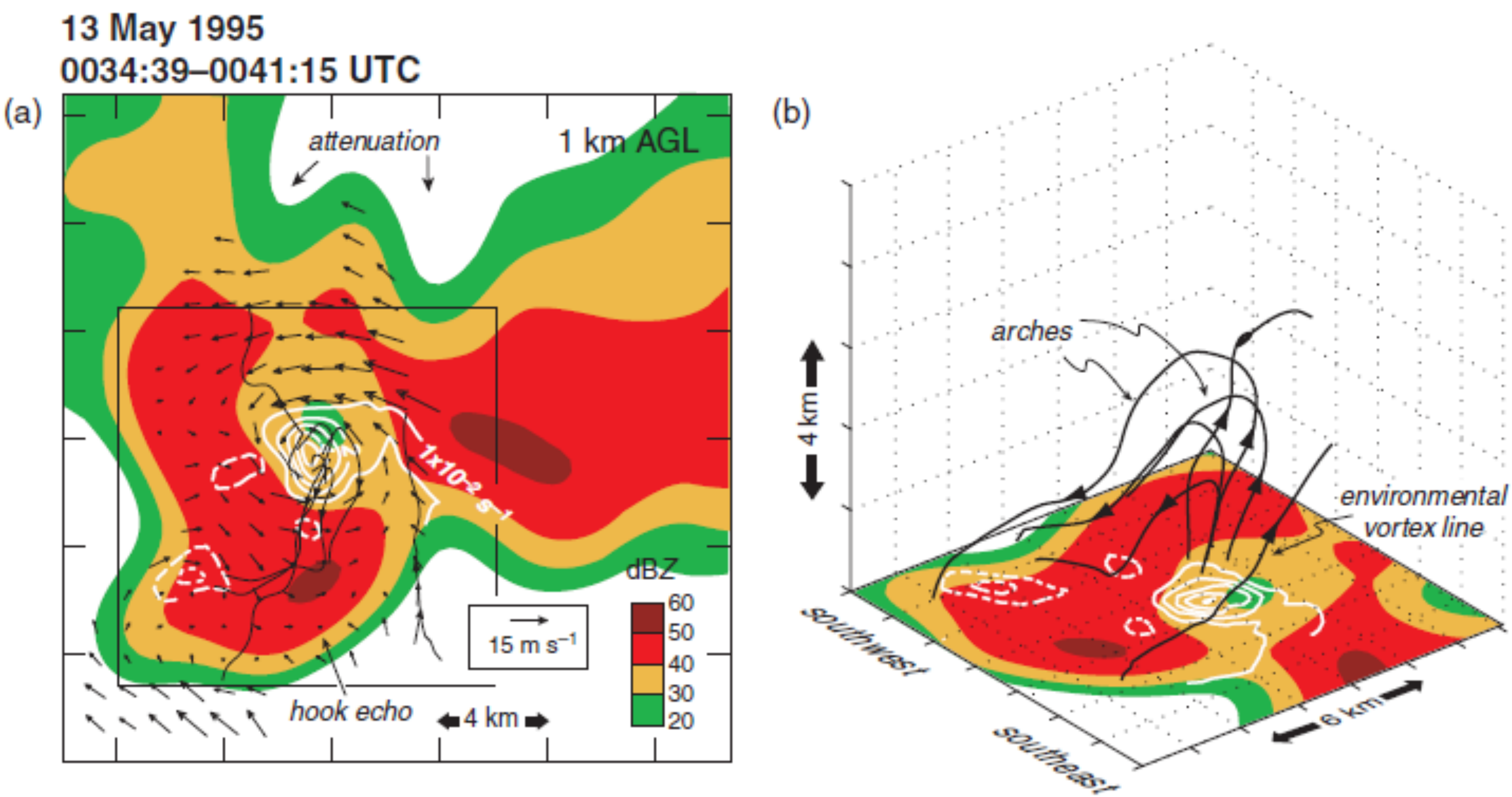


Dual-Doppler-derived storm relative wind

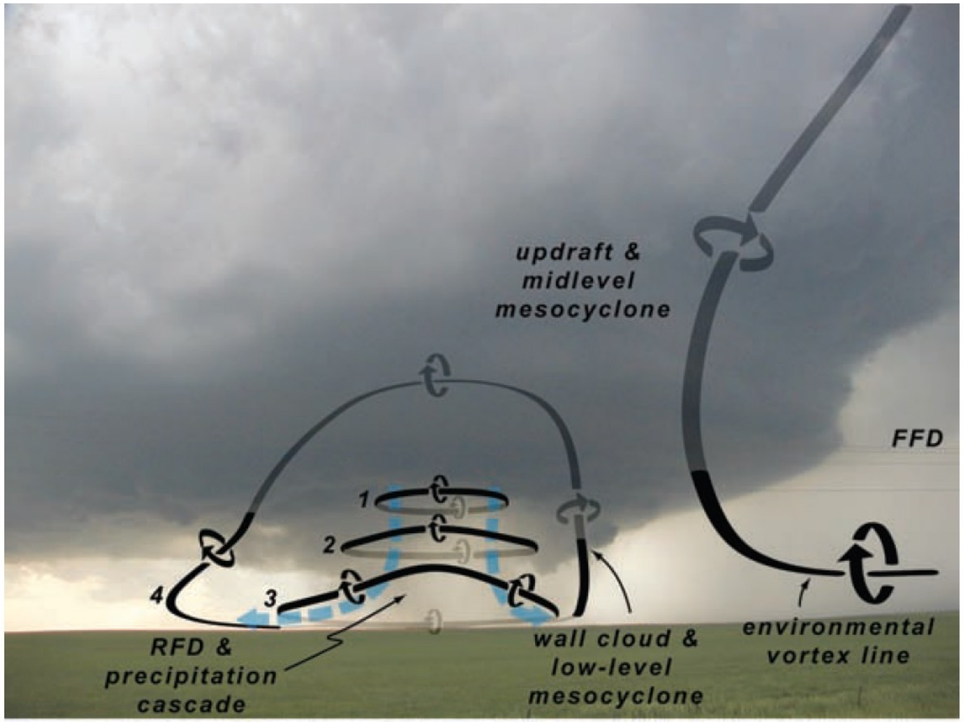


**Figure 10.7** Idealized evolution of vortex rings and arches inferred from the sample of supercells analyzed by Markowski *et al*. [2008], superimposed on a photograph of a supercell thunderstorm (courtesy of Jim Marquis; the view is from the south). The numerals 1–4 can indicate either a single vortex line seen at four different times in a sequence, or four different vortex lines at a single time but in different stages of evolution. An environmental vortex line is also shown.

# Arching by pure baroclinic process

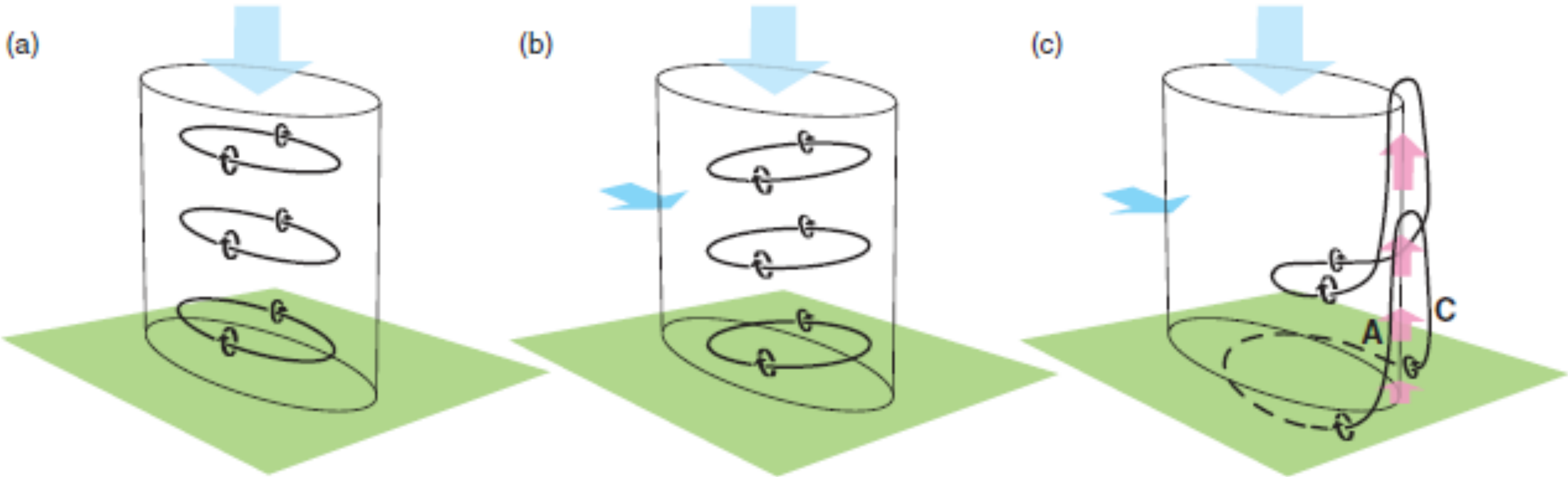

# Tornado Genesis (2)

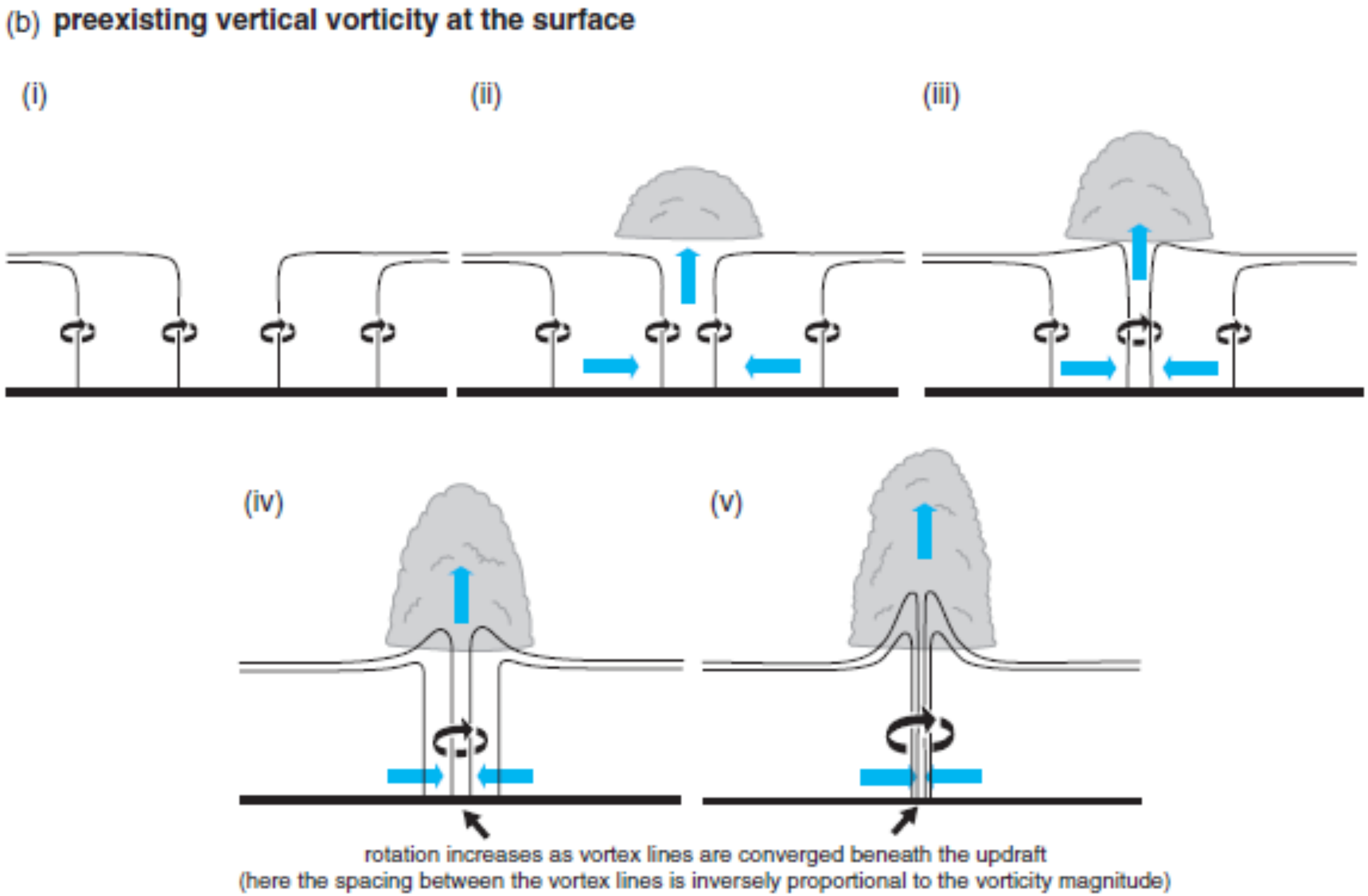

# Non-mesocyclonic tornadoes

Squall line tornadoes

- Often associated with meso-$\gamma$-scale vortices (mesovortcies)
- The squall line tornadoes are generally weak. EF2 above is very rare.

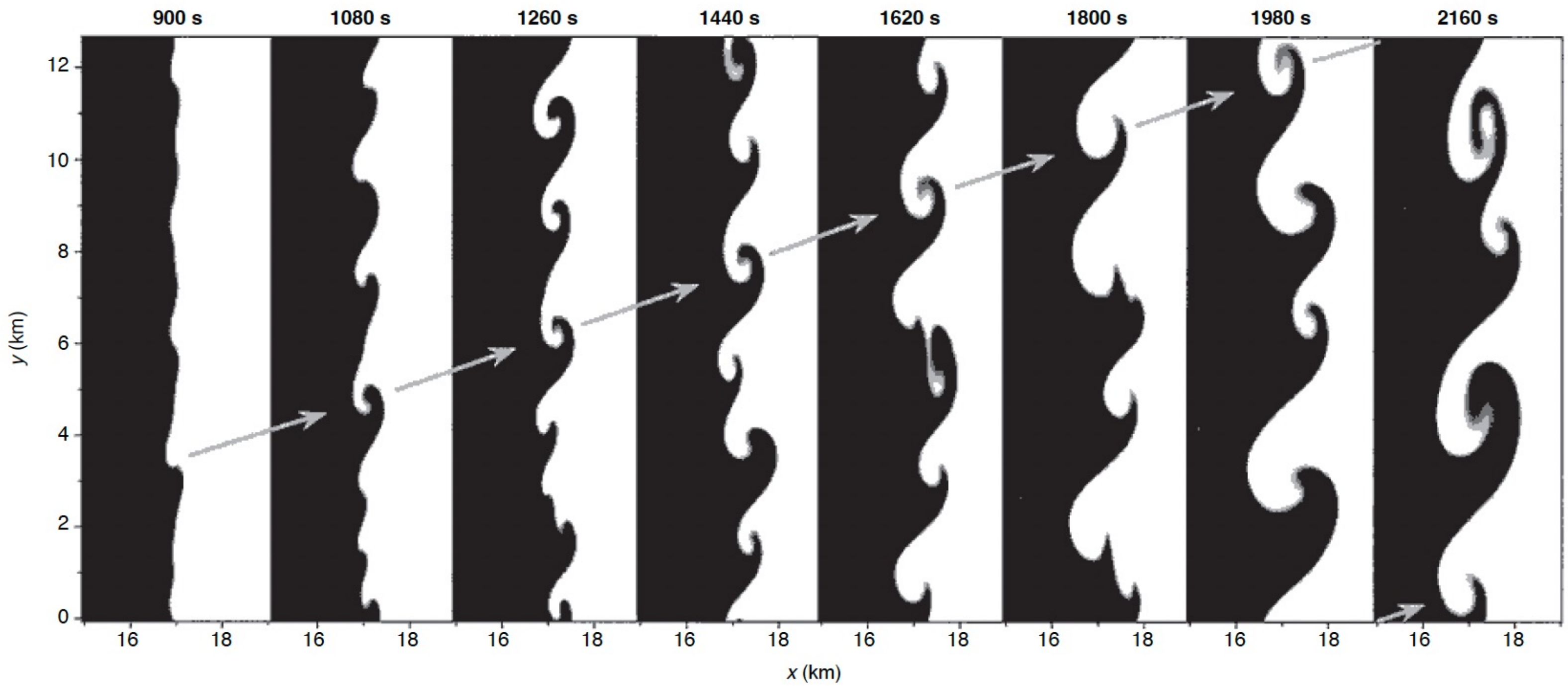


**Figure 10.9** Horizontal cross-section through the leading edge of a simulated outflow boundary at $z = 0.55$ km showing the development of misocyclone circulations as a result of horizontal shear instability. The abrupt shading change denotes the approximate $-3$ K perturbation potential temperature. (From Lee and Wilhelmson [1997a].)

**Figure 10.10** Landspouts near Lazbuddie, TX, on 4 June 1995. Photograph by Peter Blottman.

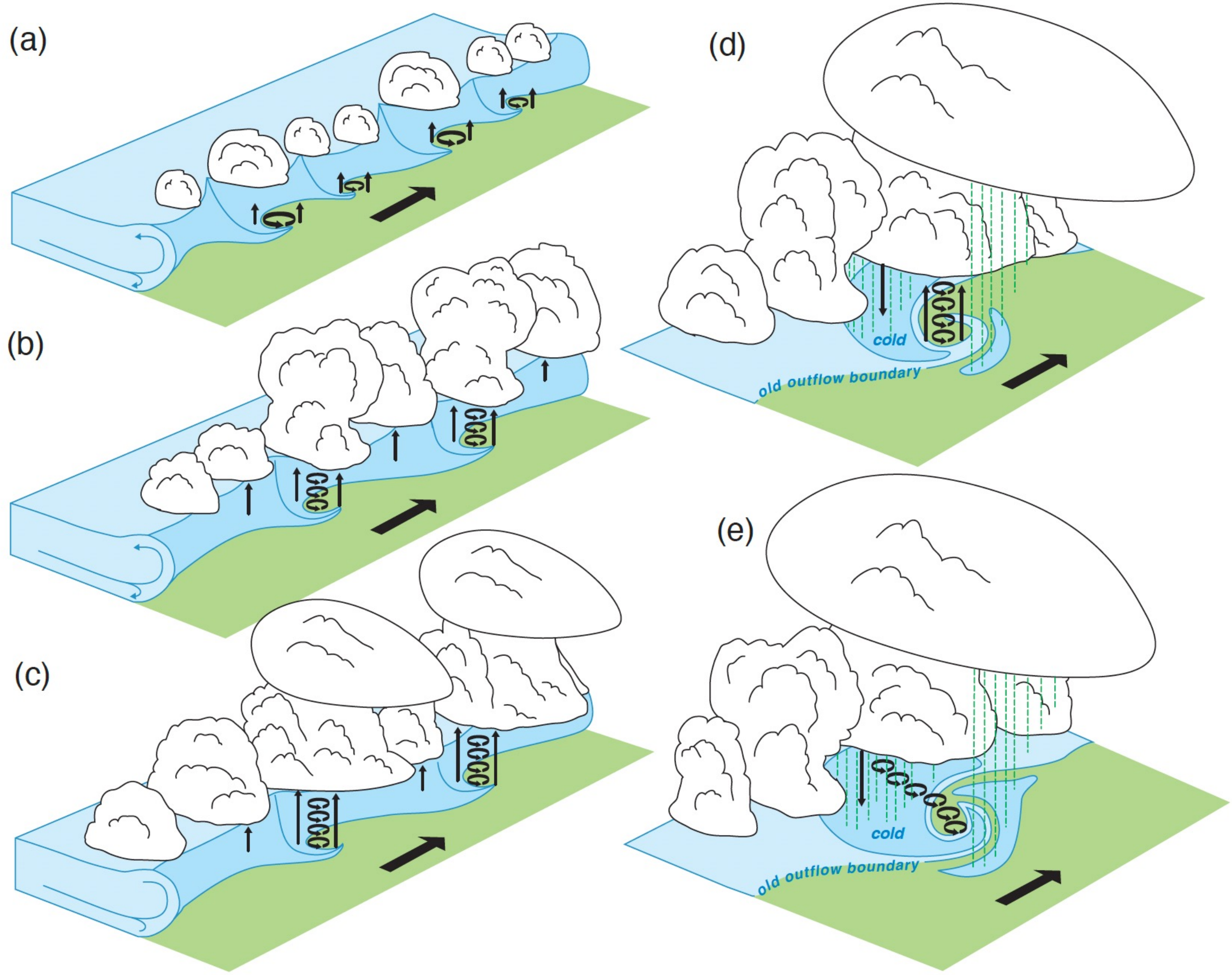


**Figure 10.11** Schematic presentation of the lifecycle stages of landspouts. The viewing perspective is from an elevated position looking northwest. See the text for details. The bold arrow indicates the ambient wind direction ahead of the air mass boundary. The diagrams for stages iv and v focus on just one member of the landspout family. (Adapted from Lee and Wilhelmson [1997b].)

**Figure 10.12** Photograph of a gustnado. Photograph taken by Chuck Doswell.

# Tornado forecasting

- The most fruitful strategy: combine radar observation and near-storm environment
- 25% of radar-detected mesocyclone are associated with tornadoes
- The strongest mesoscyclone are not necessarily associated with tornadoes

# Tornadic or nontornadic supercell?

- Boundary layer RH
- Low-level vertical shear

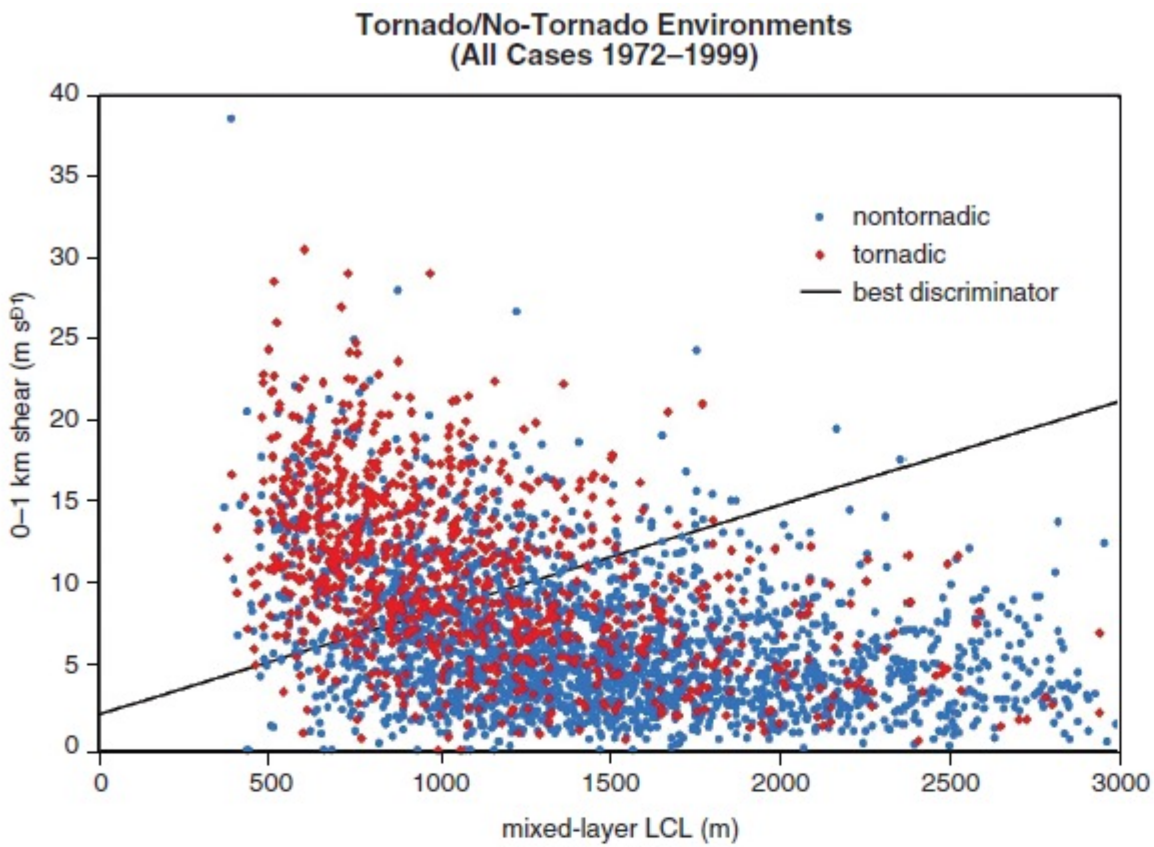

# Tornadic or nontornadic supercell?

- **Cold pool intensity**

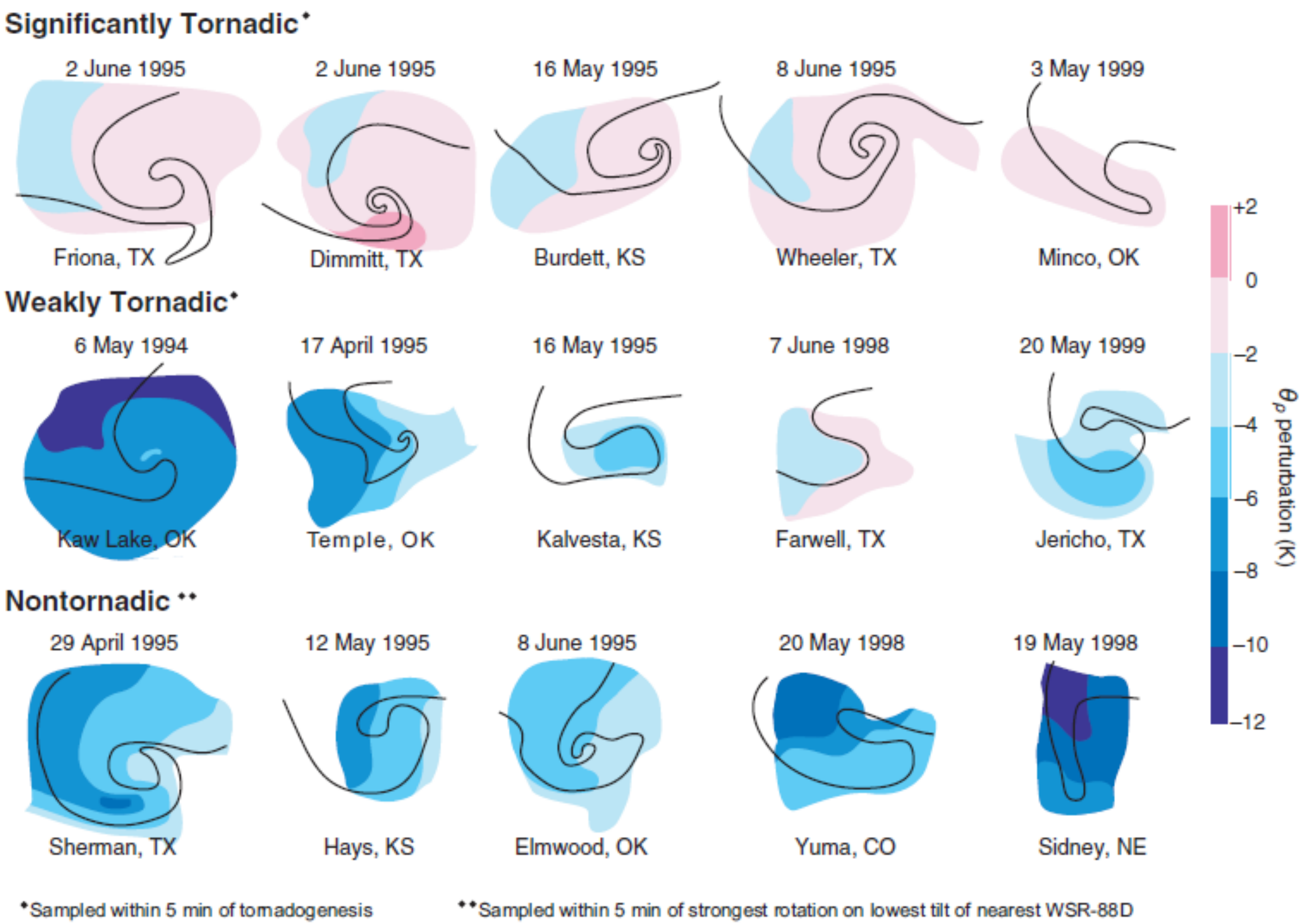

# Meso-$\alpha$ scale favorable condition

- Boundary layer RH & Low-level vertical shear
  - Define days of breakout of tornadoes
- Randomness
  - Meso-$\beta$-scale enhancement of boundary layer RH and low-level vertical shear

    Outflow boundary, warm front, sea breeze etc.

    - **Density gradient** generate horizontal vorticity, thus augment the environmental vertical shear
    - **Localized convergence** deepens the moist layer
- Storm-Boundary interaction
  - Not all these interactions are favorable
  - Whether the new airmass that the storm encounters has **larger CAPE, smaller CIN**

# Squall line tornado forecasting

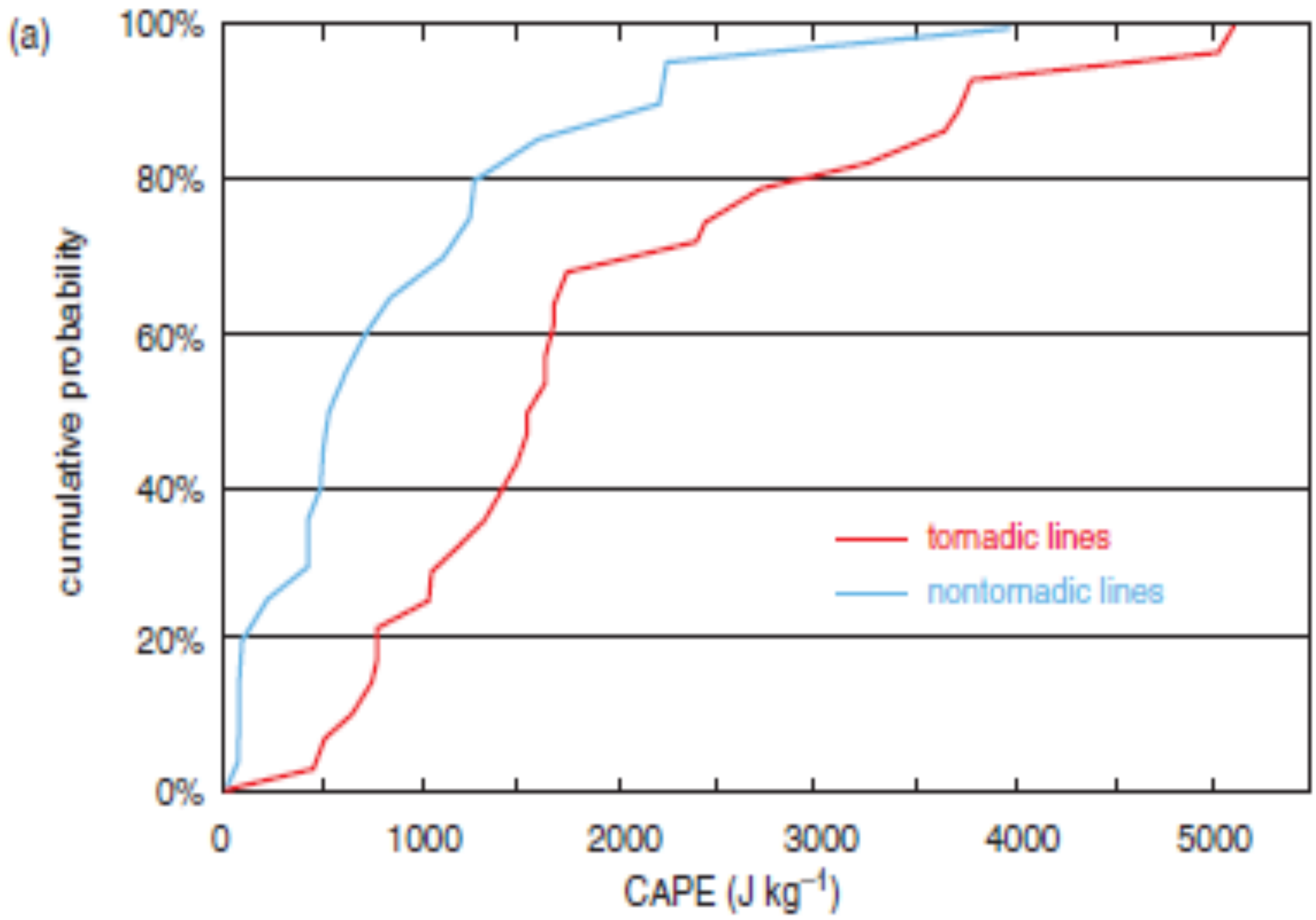

# Squall line tornado forecasting

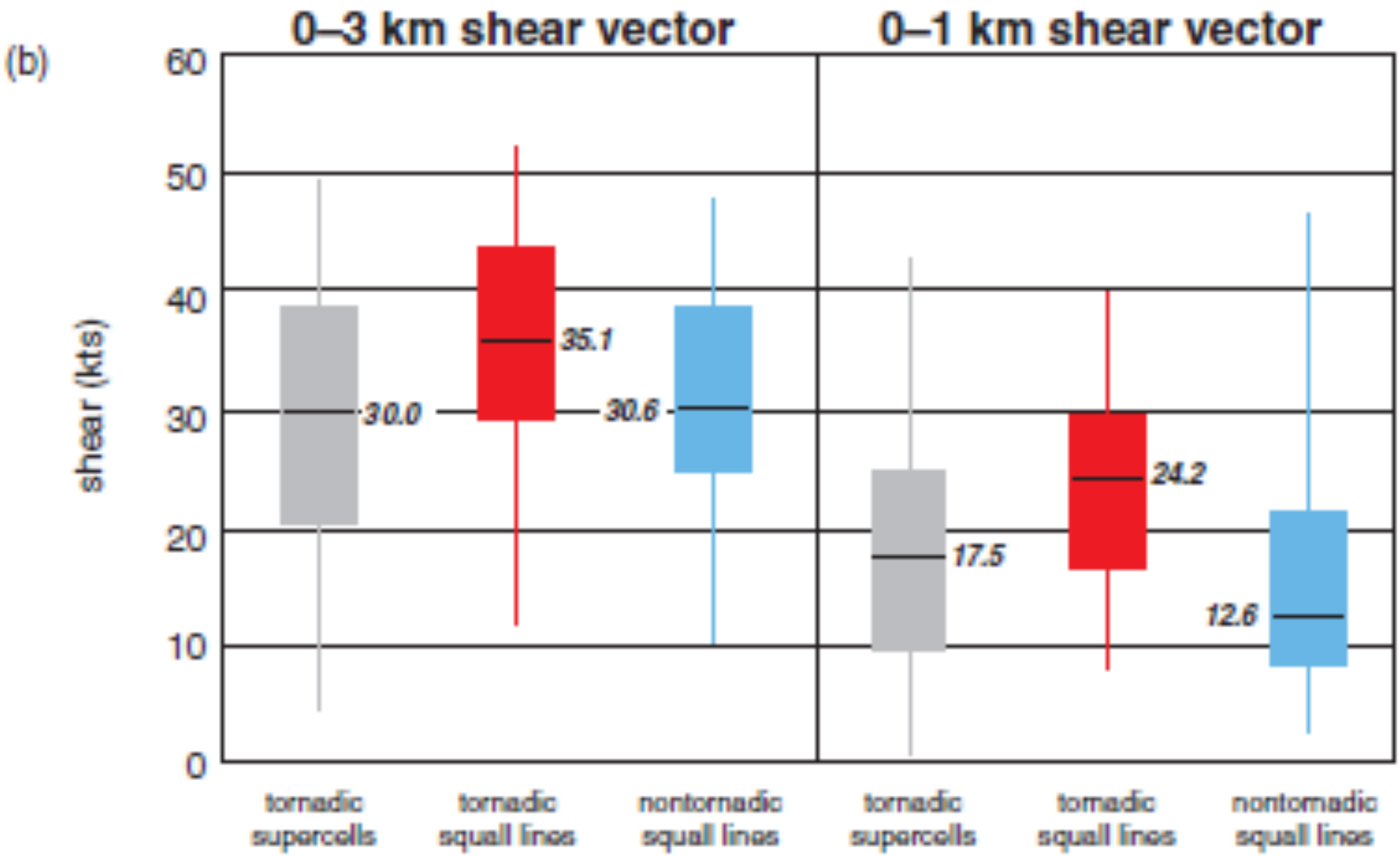

# Tornado structure

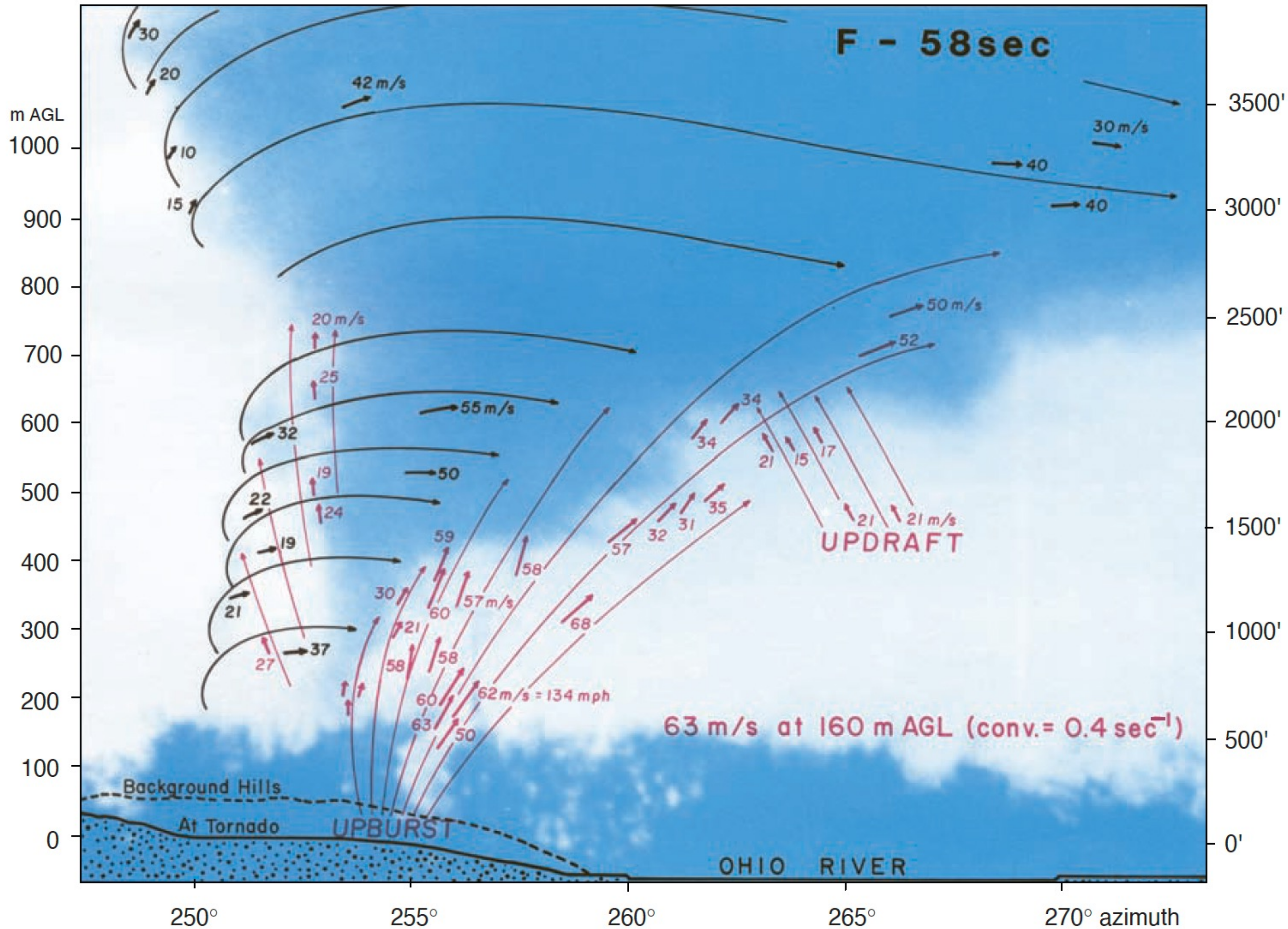


**Figure 10.17** Fujita's photogrammetric analysis of wind velocities in the Sayler Park, OH, tornado of 3 April 1974. Winds are in m $s^{-1}$. (From Fujita [1992].)

# Tornado structure

- Based on photogrametric studies, laboratory experiments and numerical simulations

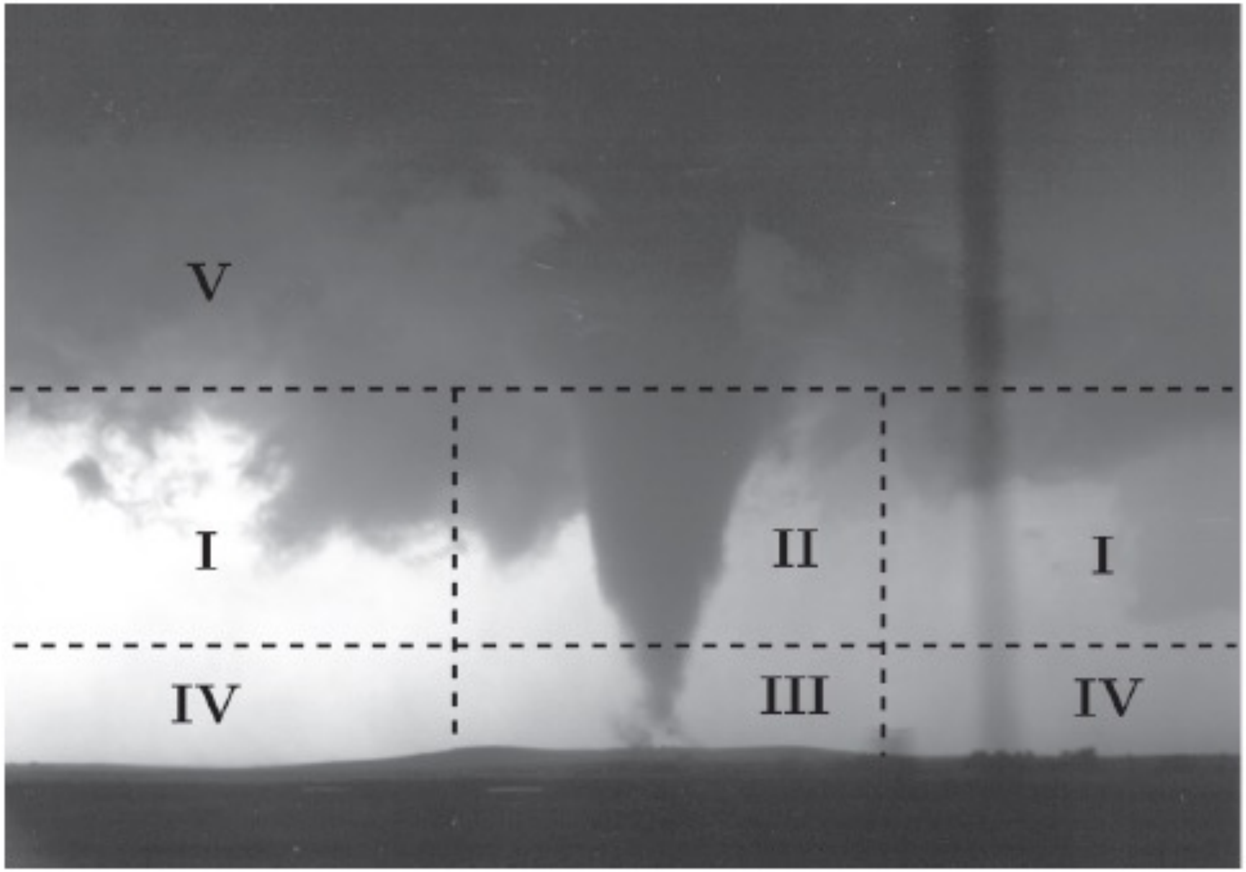

# Flow regions: Outer region (I)

Inward spiraling air

Conserve angular momentum

Spins faster as it approaches the tornado axis

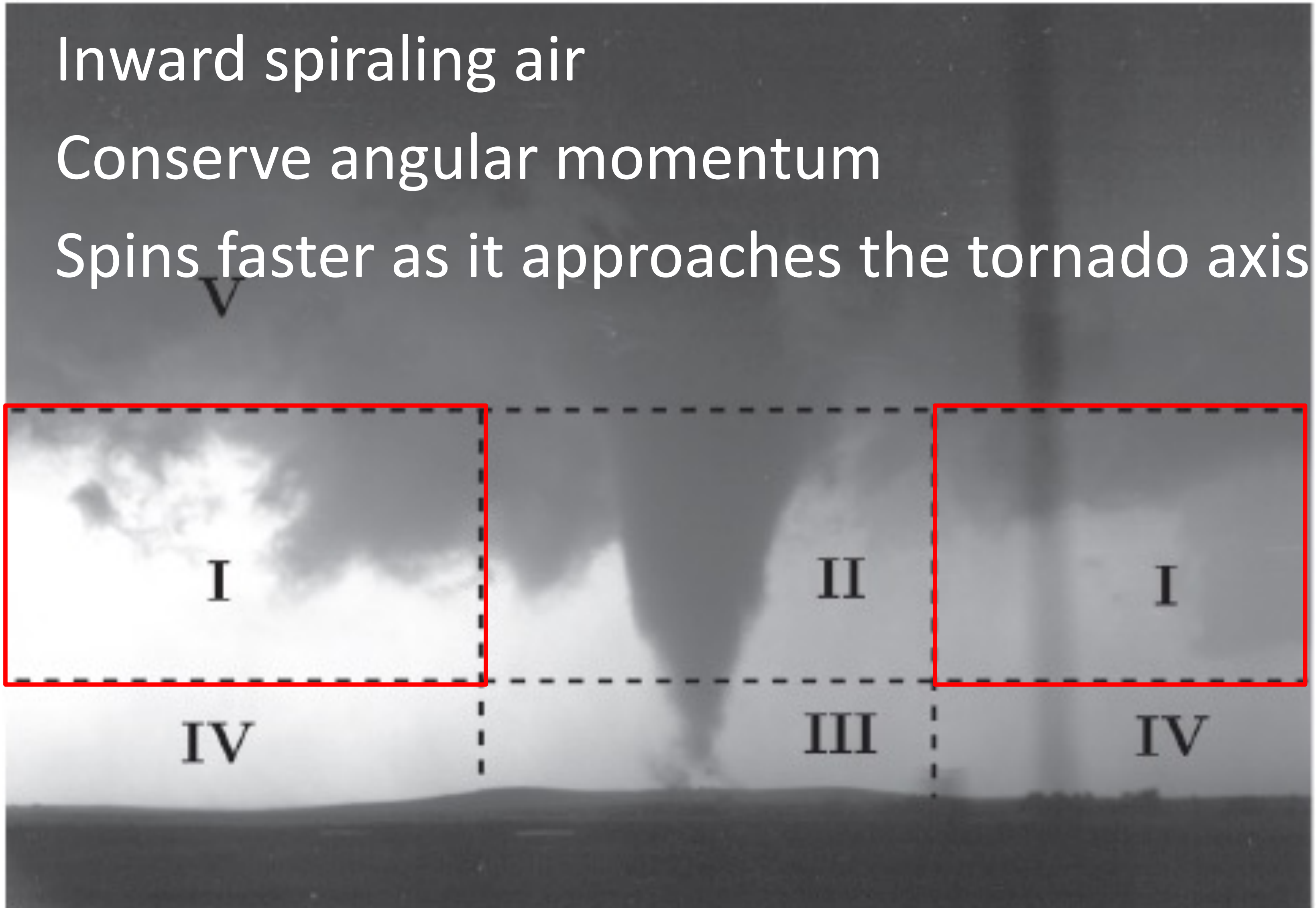

# Flow regions: Core region (II)

- From the axis to the maximum wind
- Contains a funnel cloud, a column of dust and debris from the ground
- Cyclostrophic  balance
- Almost no entrainment

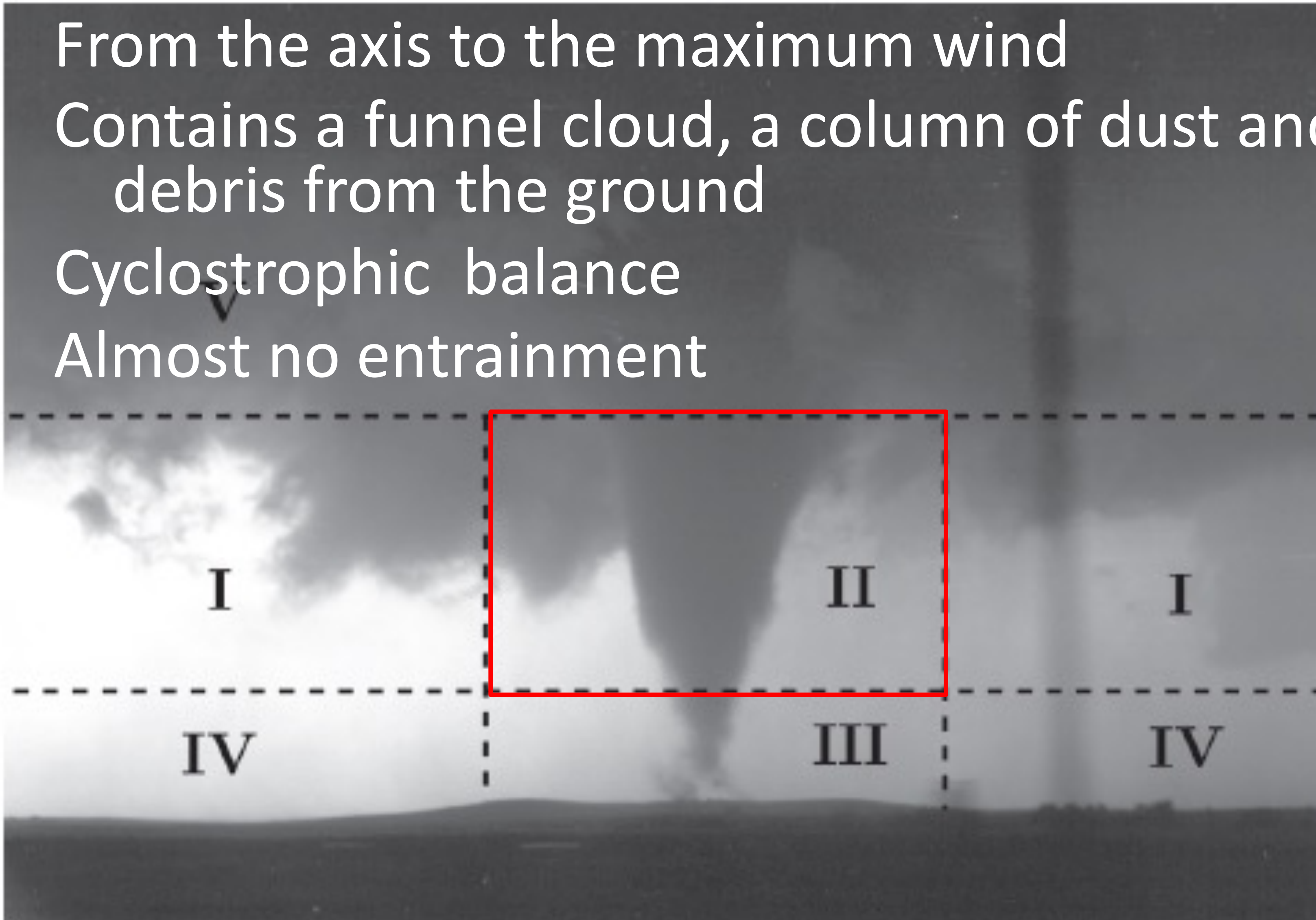

# Flow regions: Corner (III)

Flow turns upward from a primarily horizontal direction

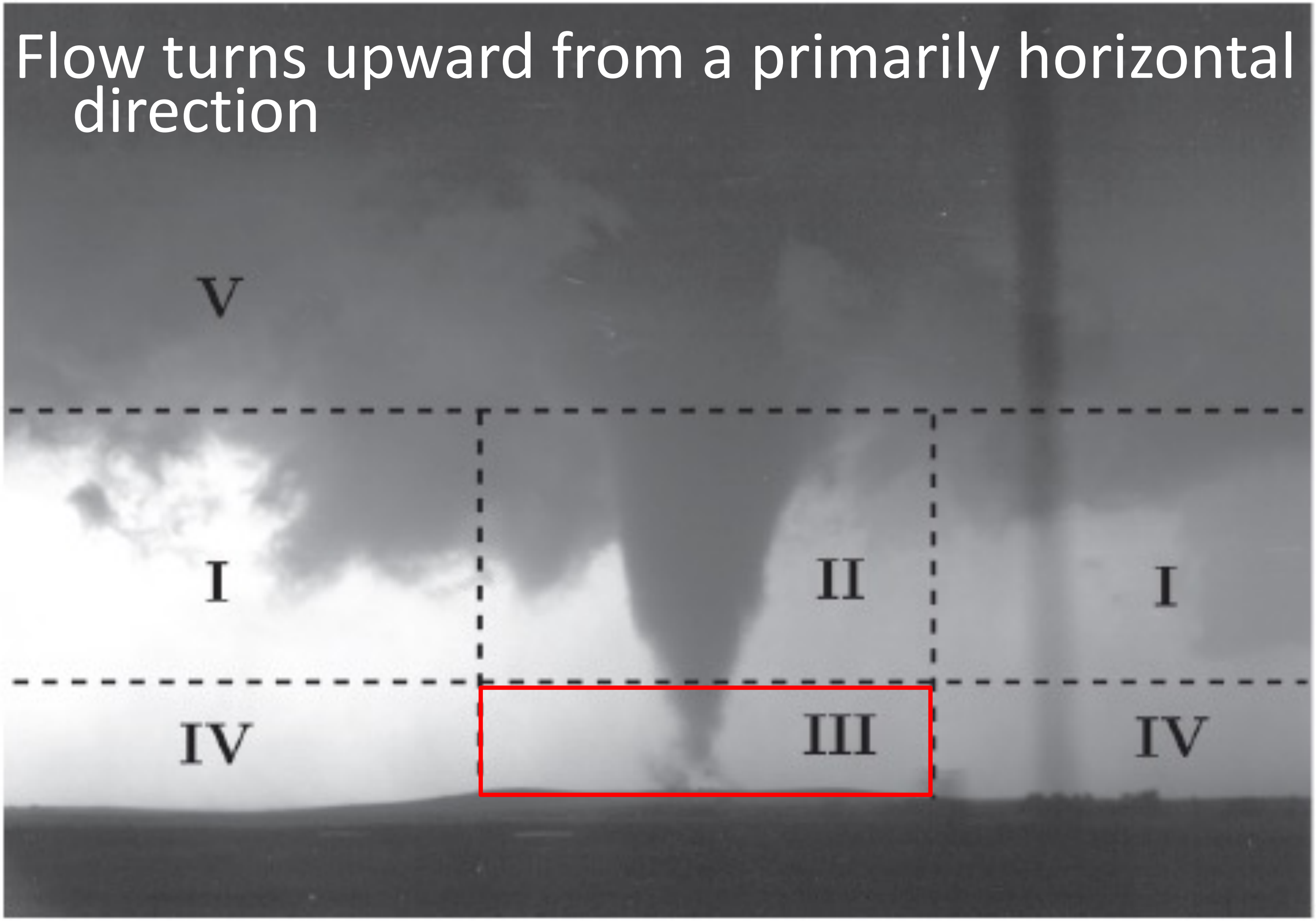

# Flow regions: Boundary layer (IV)

- 10-100m deep
- Turbulent
- Friction precludes cyclostrophic balance, thus inflow is produced
- Intense wind speed due to the inflow and convergence of angular momentum

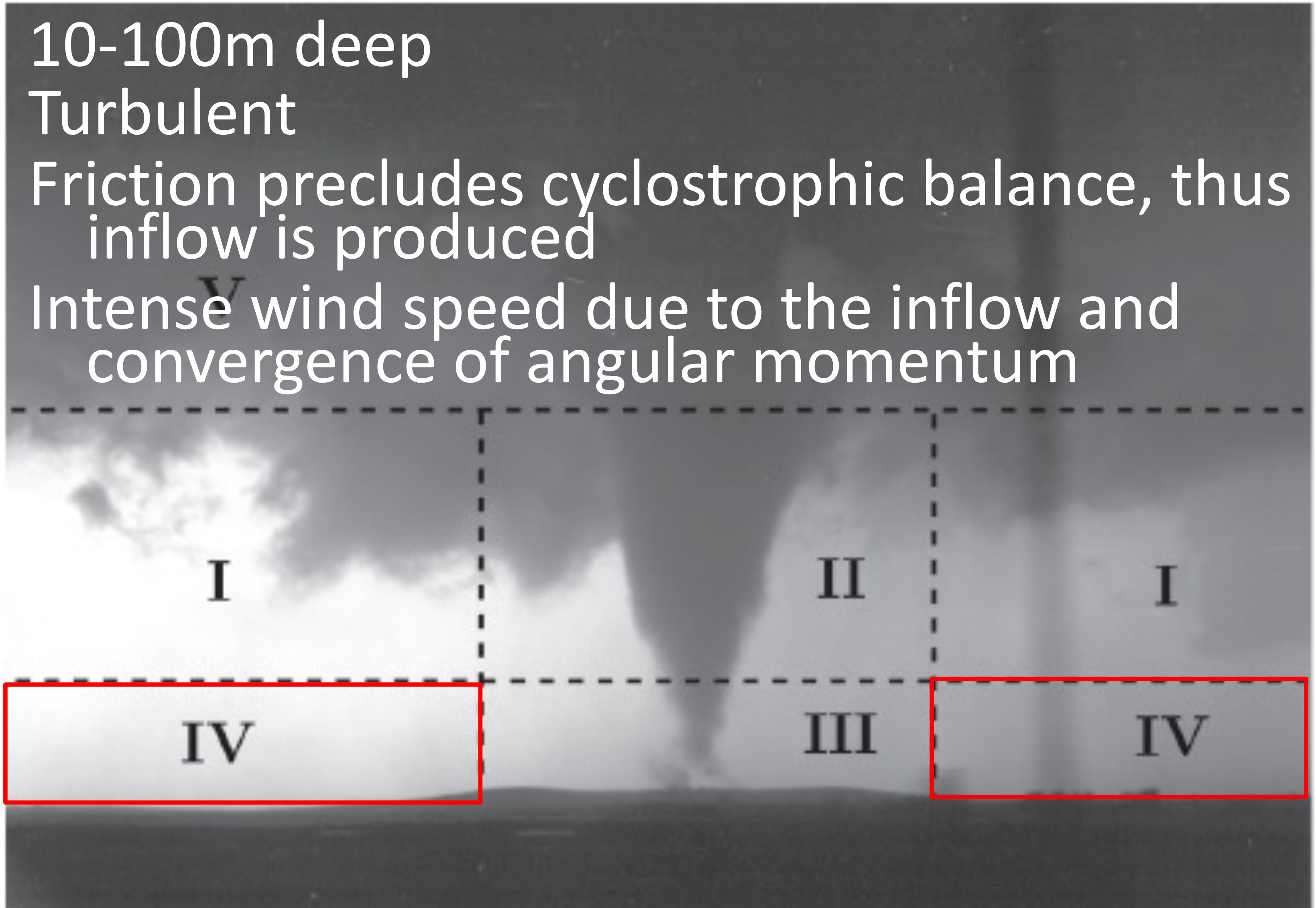

# Flow regions: Rotating updraft (V)

Large-scale parent updraft situated above the tornado

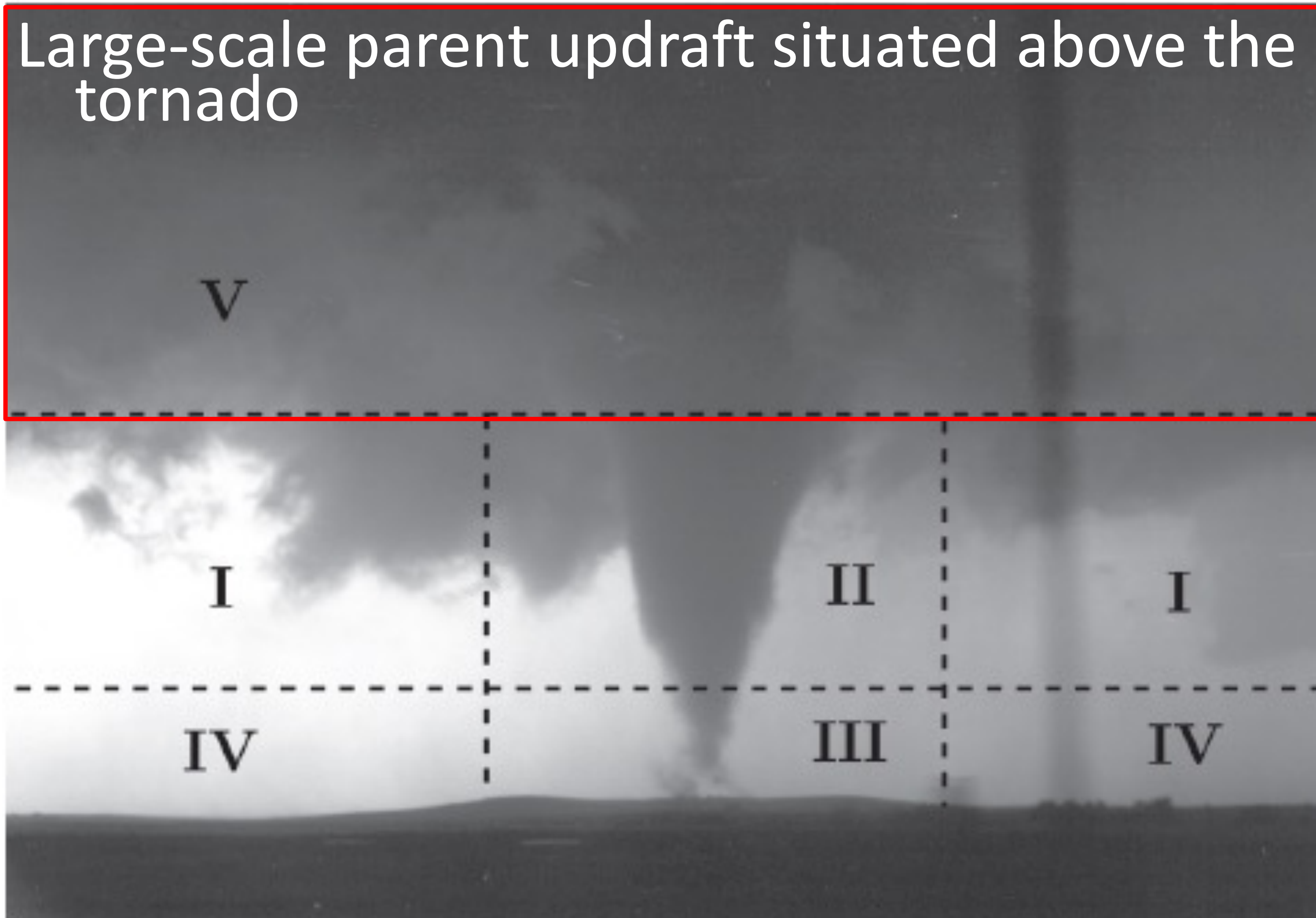

# Wind profiles: Rankine vortex

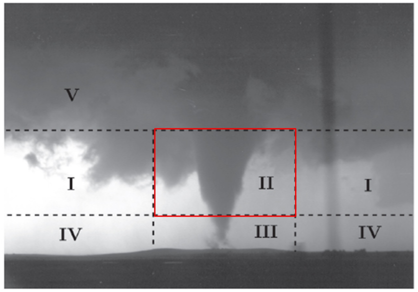


$v_{max}$ : the maximum tangential wind

$r_{max}$ : the radius of $v_{max}$

- Within $r_{max}$ : constant angular velocity v/r
- Outside $r_{max}$ : constant angular momentum vr

$$v = \begin{cases} v_{\max} r / r_{\max}, & r \leq r_{\max} \\ v_{\max} r_{\max} / r, & r > r_{\max} \end{cases}$$

- Cyclostrophic balance, applicable above the PBL

# Pressure profiles

Cyclostrophic balance in natural coordinates:

$$\frac{\rho v^2}{r} = \frac{\partial p'}{\partial r}$$

Assume P’ is only a function of r, integrate above equation from r to ∞, we have

$$\int_{p'(r)}^{p'_\infty} \mathrm{d}p = \int_r^\infty \frac{\rho v^2}{r} \mathrm{d}r,$$

$$\int_{p'(r)}^{p'_\infty} \mathrm{d}p = \int_r^\infty \frac{\rho v^2}{r} \mathrm{d}r, \qquad v = \begin{cases} v_{\max} r / r_{\max}, & r \le r_{\max} \\ v_{\max} r_{\max} / r, & r > r_{\max} \end{cases}$$

Assume $p'_\infty = 0$. the pressure field for $r > r_{\max}$ is

$$p'(r) = -\int_r^\infty \rho \left( \frac{v_{\max} r_{\max}}{r} \right)^2 \frac{\mathrm{d}r}{r}$$

$$= -\rho v_{\max}^2 r_{\max}^2 \left[ -\frac{1}{2r^2} \right]_r^\infty$$

$$= -\frac{1}{2} \rho v_{\max}^2 \frac{r_{\max}^2}{r^2} \quad \text{for } r > r_{\max}.$$

$$\int_{p'(r)}^{p'_\infty} \mathrm{d}p = \int_r^\infty \frac{\rho v^2}{r}\mathrm{d}r, \qquad v = \begin{cases} v_{\max} r/r_{\max}, & r \le r_{\max} \\ v_{\max} r_{\max}/r, & r > r_{\max} \end{cases}$$

For $r \le r_{\max}$, the pressure field is

$$p'(r) = -\int_r^{r_{\max}} \rho \left(\frac{v_{\max} r}{r_{\max}}\right)^2 \frac{\mathrm{d}r}{r}$$

$$- \int_{r_{\max}}^{\infty} \rho \left(\frac{v_{\max} r_{\max}}{r}\right)^2 \frac{\mathrm{d}r}{r}$$

$$= -\frac{\rho v_{\max}^2}{r_{\max}^2}\left[\frac{r^2}{2}\right]_r^{r_{\max}} - \rho v_{\max}^2 r_{\max}^2 \left[-\frac{1}{2r^2}\right]_{r_{\max}}^{\infty}$$

$$= -\rho v_{\max}^2 \left(1 - \frac{1}{2}\frac{r^2}{r_{\max}^2}\right) \quad \text{for } r \le r_{\max}$$

The minimum pressure is found at the vortex center

$$p'_{\min} = -\rho v_{\max}^2$$

For $\rho \sim 1 \text{ kg m}^{-3}$

$v_{\max} \sim 25 \text{ m s}^{-1}$

$p'_{\min} \sim 6 \text{ mb}$

only enough to lower the cloud base by approximately 60m.

$v_{\max} = 100 \text{ m s}^{-1}$

$p'_{\min} \sim 100 \text{ mb}$;

the cloud base lowers by ~1000 m, which would likely be near the ground

# Swirl ratio

$$S = \frac{v_0}{w_0}$$

- $V_0$ is the tangential velocity at $r_o$.
- $W_0$ is the mean vertical velocity at the top of the chamber

# Tornado structure

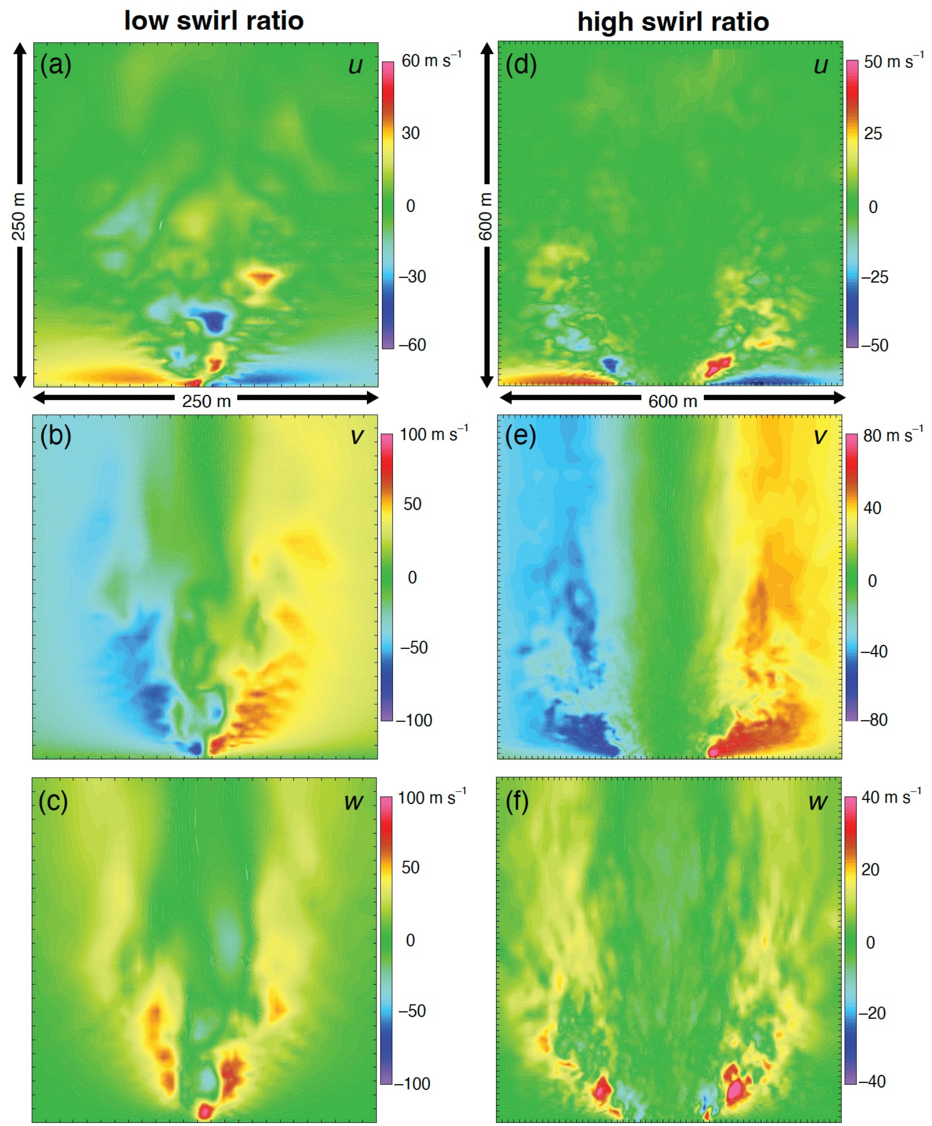


**Figure 10.18** (a)–(c) Vertical cross-sections of instantaneous radial ($u$), tangential ($v$), and vertical ($w$) velocities in a three-dimensional numerical simulation of a tornado having a low swirl ratio. The cross-sections are taken through the center of the tornado. (d)–(f) As in (a)–(c), but for a simulated tornado having a high swirl ratio. Courtesy of Dave Lewellen.

(a) Weak Swirl ratio —boundary layer separates and flow passes around the lower corner;

(S<1)

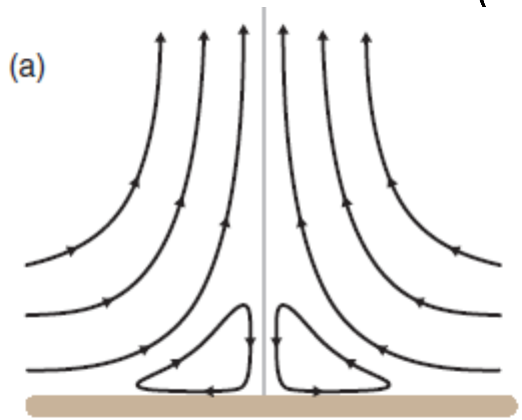


(b) one-celled vortex;

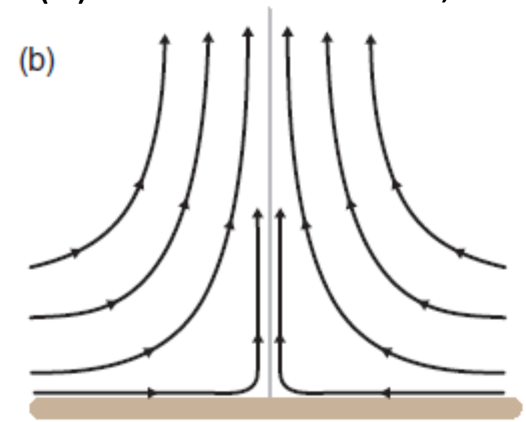


(c) one-celled vortex over the lower portion, two-celled vortex over the upper portion, separated by vortex breakdown

(S>2)

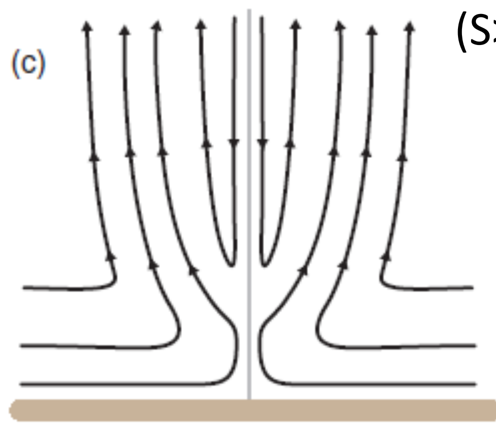


(d) two-celled vortex

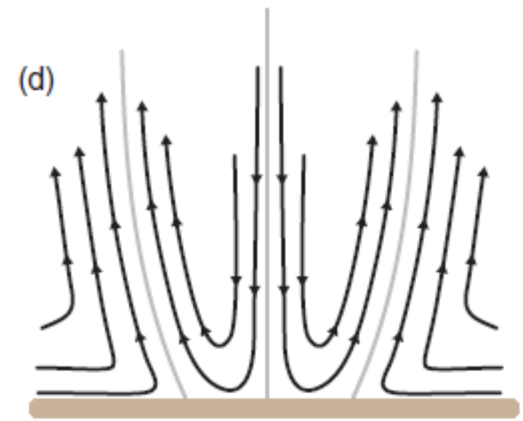


(e) multiple vortices.

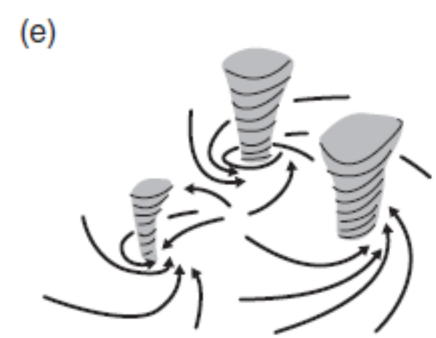

# Numerical simulation

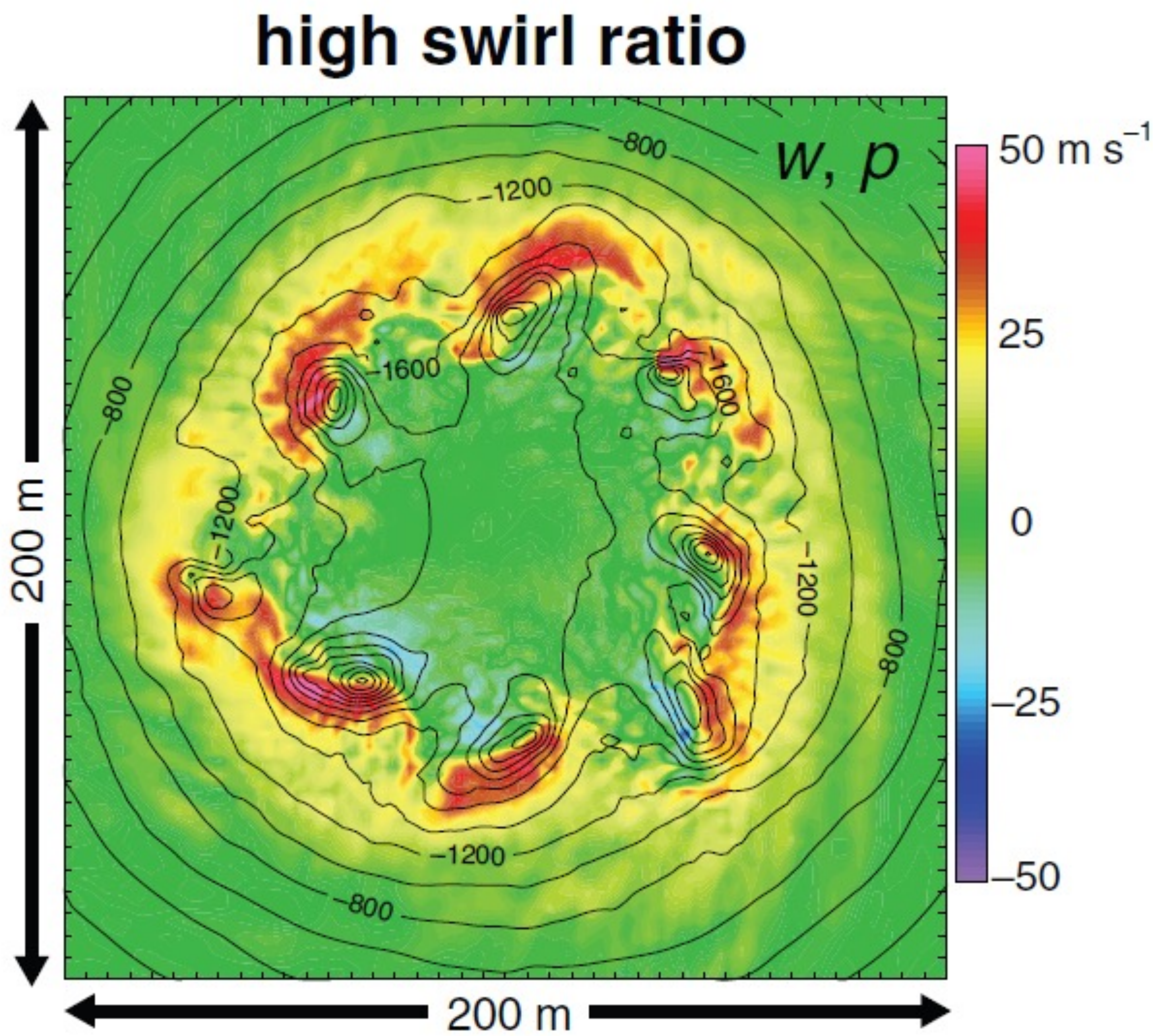

# Multiple vortex

## Chapter 5

# Hazards associated with DMC

- Tornado
- Straight Wind
- Hail
- Flash flood

# Nontornadic damaging straight line winds

- Almost always associated with precipitation cooled outflow

(Wind> 26 m/s)

  - Exception: inflow of supercell
- Produced by
  - Meso-$\gamma$-scale downdraft (downburst), highly divergent
    - Intense downdraft
    - RIJ: lesser downdraft that carrys large momentum from aloft
  - Meso-$\beta$-scale cold pools associated with horizontal pressure gradient large enough to produce damaging winds in the absence of strong downdraft. (merged outflow)
  - Vortices formed at the outflow boundary

# Damaging winds: (1) due to downdrafts

Downburst: defined to have
  Horizontal dimensions less than 10 km.

Macroburst:
  Larger than 4 km, 5-30 min

Microburst:
  Less than 4 km, 2-5min
  Very dangerous for airplane

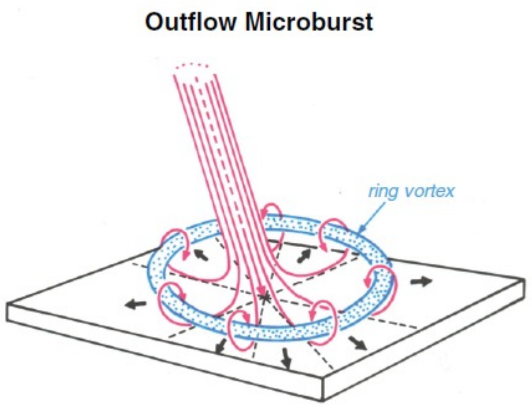


Fujita 1985

# Subclasses of microburst

- Wet microburst: Extensive precipitation reach the ground.
  - Most common
  - Negative buoyancy is generated by hydrometeor loading, evaporation, and hail melting.

# Subclasses of microbursts

- Dry microburst: precipitation fails to reach the ground.
  - Negative buoyancy is generated by evaporation
  - Deep boundary layer and high cloud base
  - Virga can be observed under the spawned convection

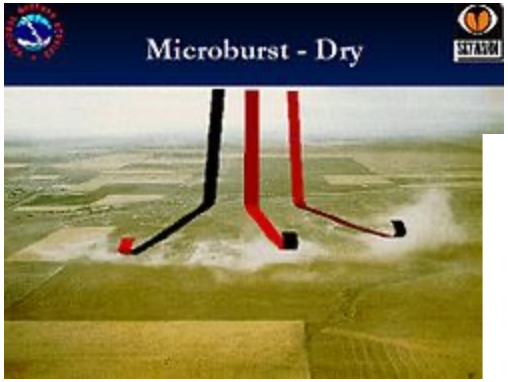


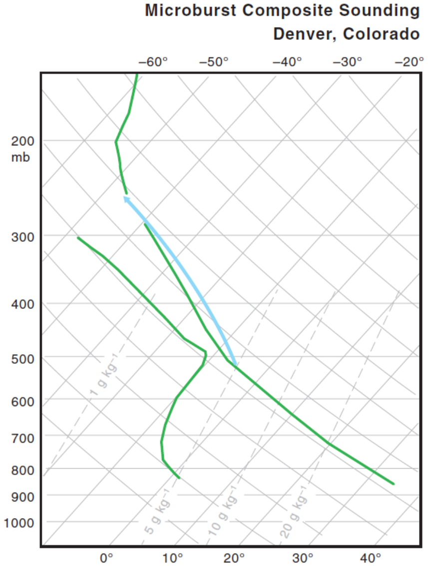

# Microburst

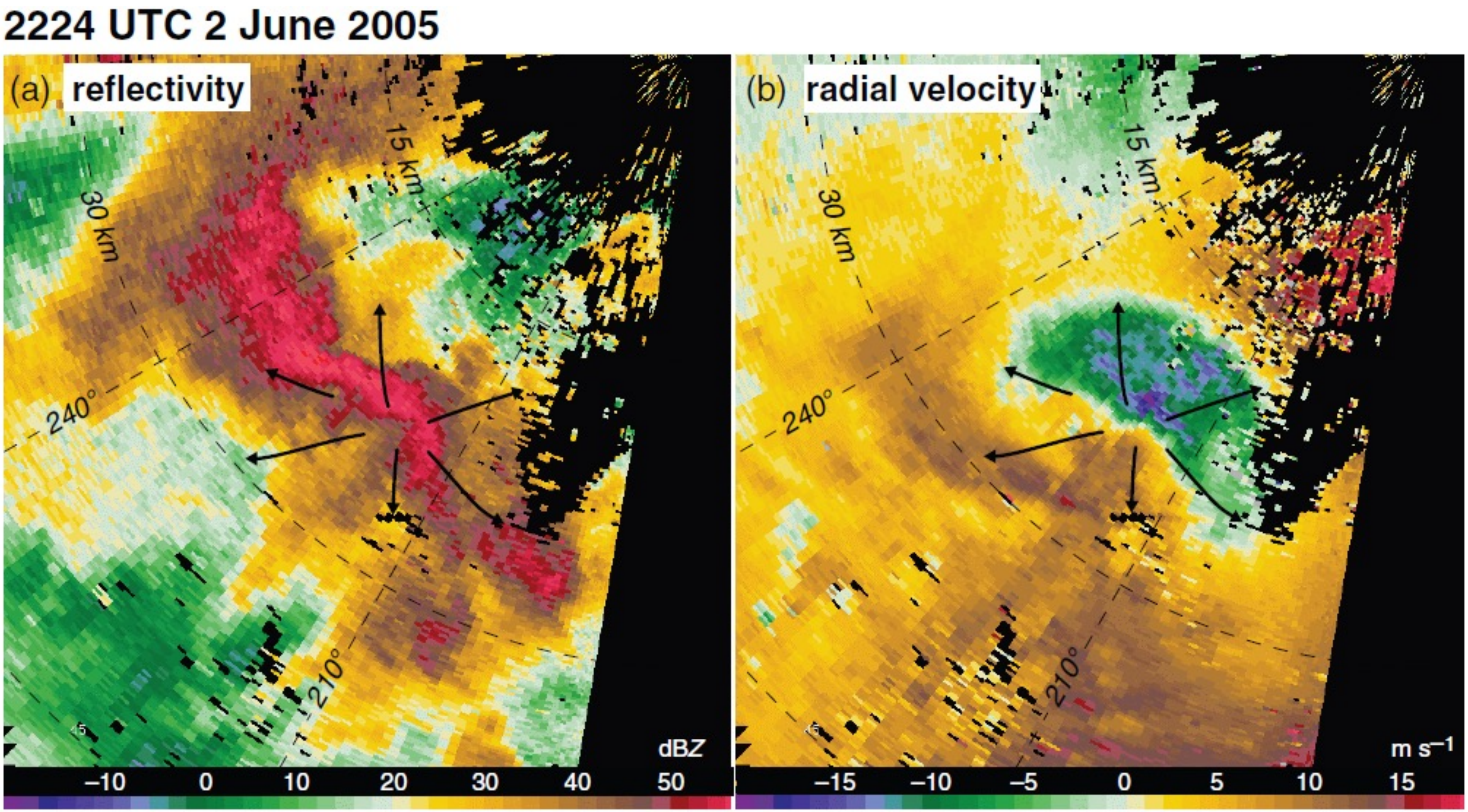

2224 UTC 2 June 2005
(a) reflectivity
15 km
30 km
240°
210°
dBZ
−10
0
10
20
30
40
50
(b) radial velocity
15 km
30 km
240°
210°
m s−1
−15
−10
−5
0
5
10
15

# Cross-section of a microburst

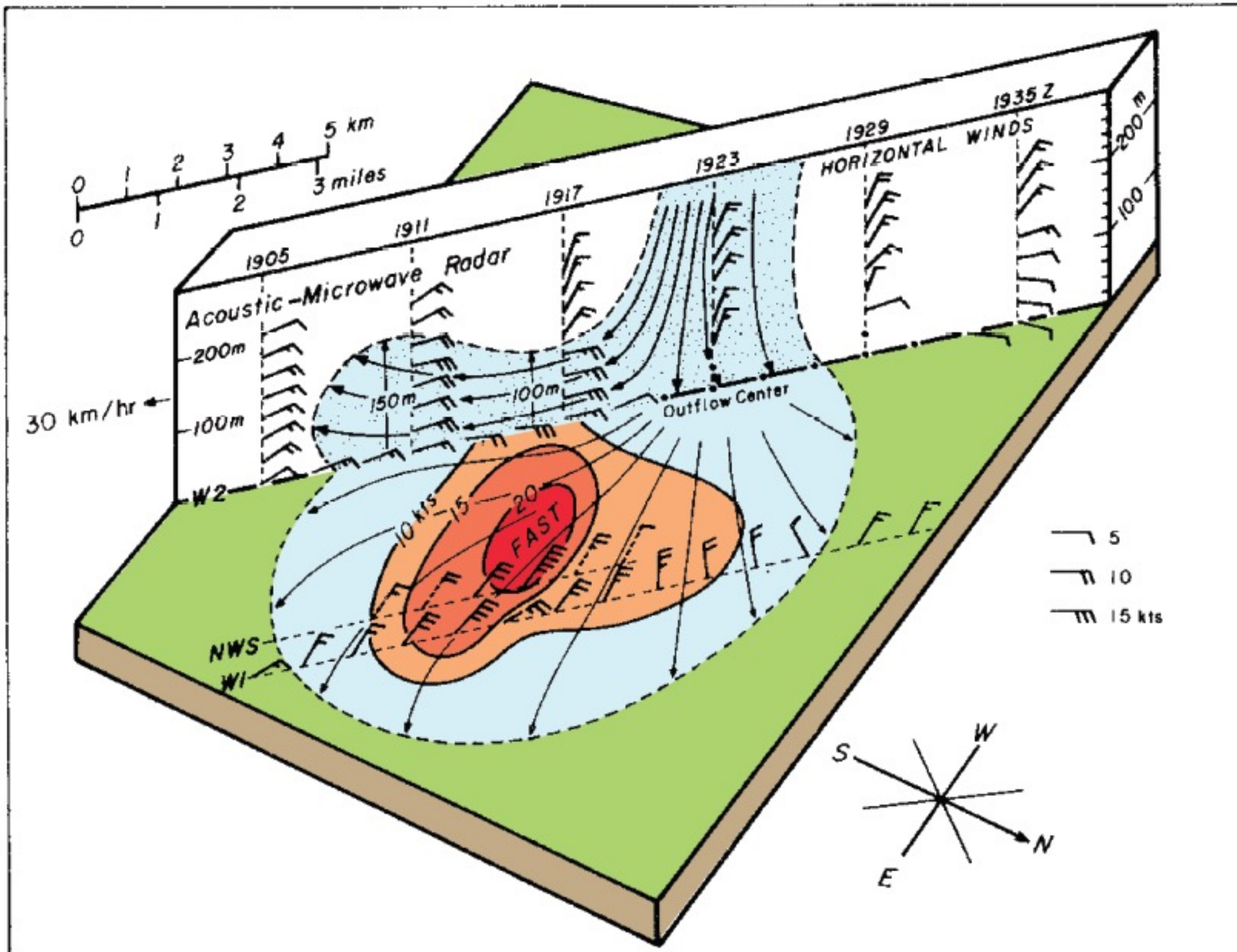


Fujita (1978)

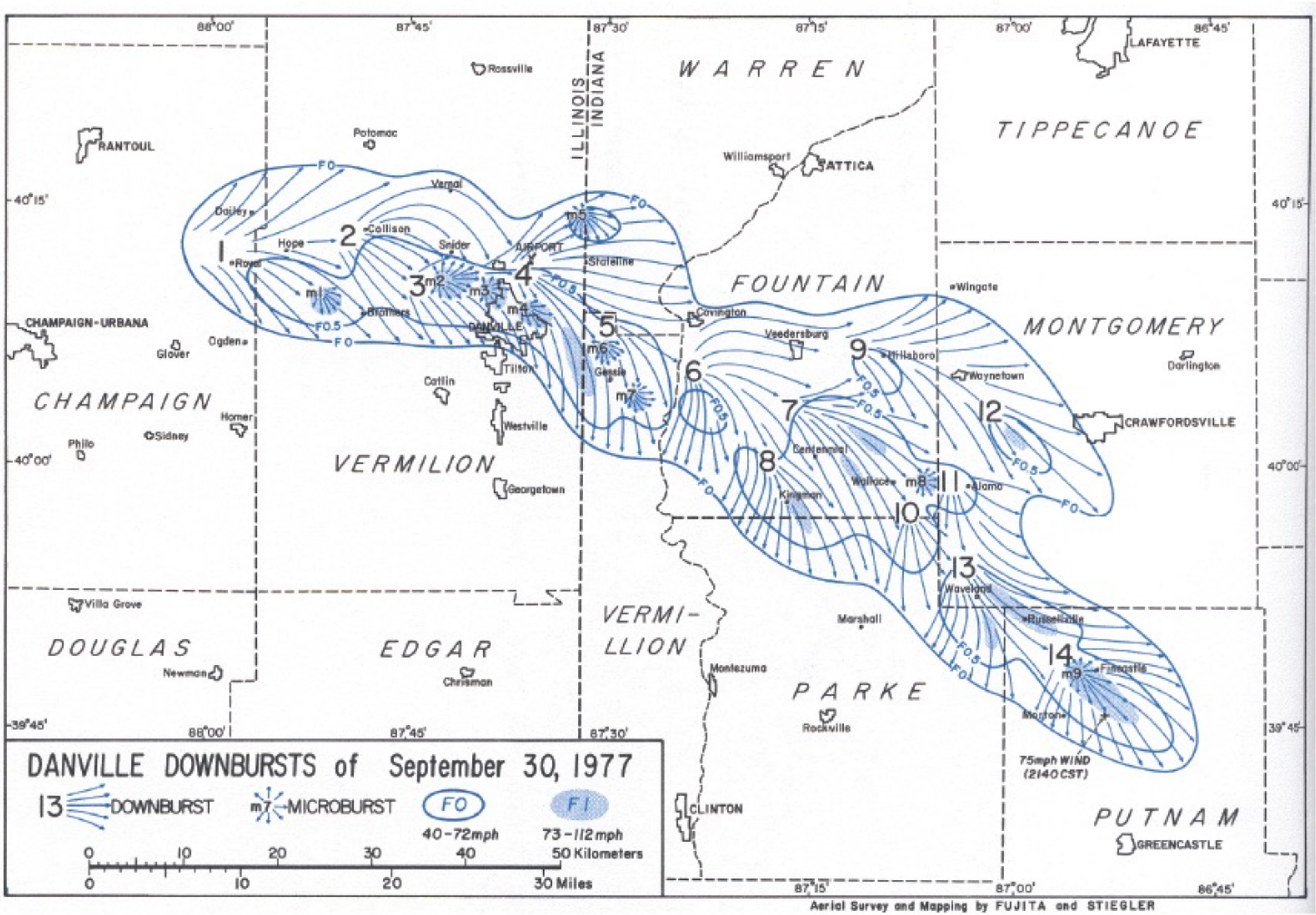
DANVILLE DOWNBURSTS of September 30, 1977
13 DOWNBURST
m7 MICROBURST
F0 40-72mph
F1 73-112mph
50 Kilometers
30 Miles
WARREN
TIPPECANOE
FOUNTAIN
MONTGOMERY
CHAMPAIGN
VERMILION
DOUGLAS
EDGAR
VERMILLION
PARKE
PUTNAM
ILLINOIS
INDIANA
RANTOUL
CHAMPAIGN-URBANA
DANVILLE
CRAWFORDSVILLE
LAFAYETTE
ATTICA
CLINTON
GREENCASTLE
75mph WIND (2140CST)
Aerial Survey and Mapping by FUJITA and STIEGLER

# 东方之星倾覆

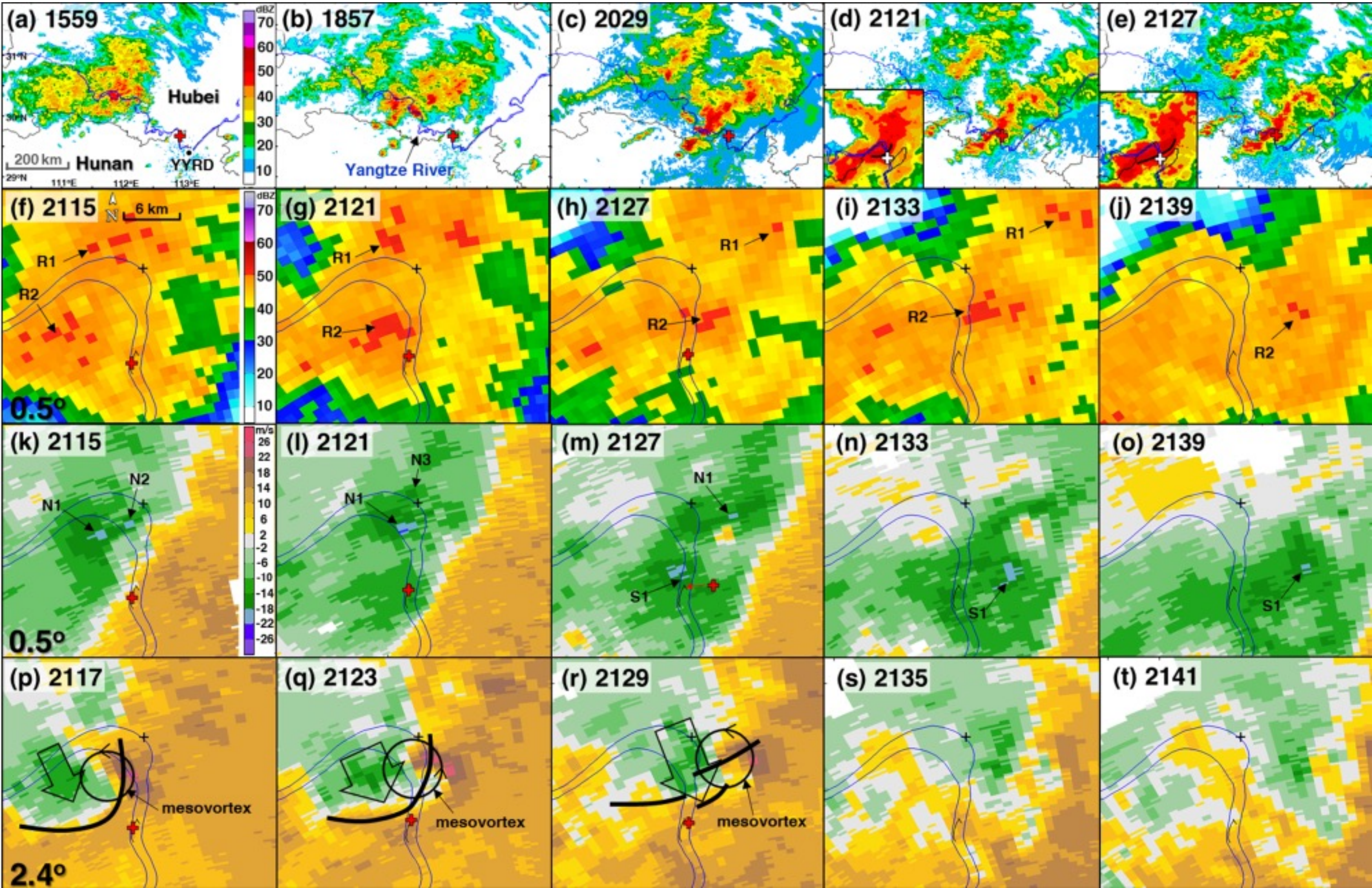

(a) 1559
(b) 1857
(c) 2029
(d) 2121
(e) 2127
Hubei
Hunan
YYRD
200 km
Yangtze River
dBZ
70
60
50
40
30
20
10
(f) 2115
(g) 2121
(h) 2127
(i) 2133
(j) 2139
6 km
R1
R2
0.5°
(k) 2115
(l) 2121
(m) 2127
(n) 2133
(o) 2139
m/s
N1
N2
N3
S1
0.5°
(p) 2117
(q) 2123
(r) 2129
(s) 2135
(t) 2141
mesovortex
2.4°

# 东方之星倾覆

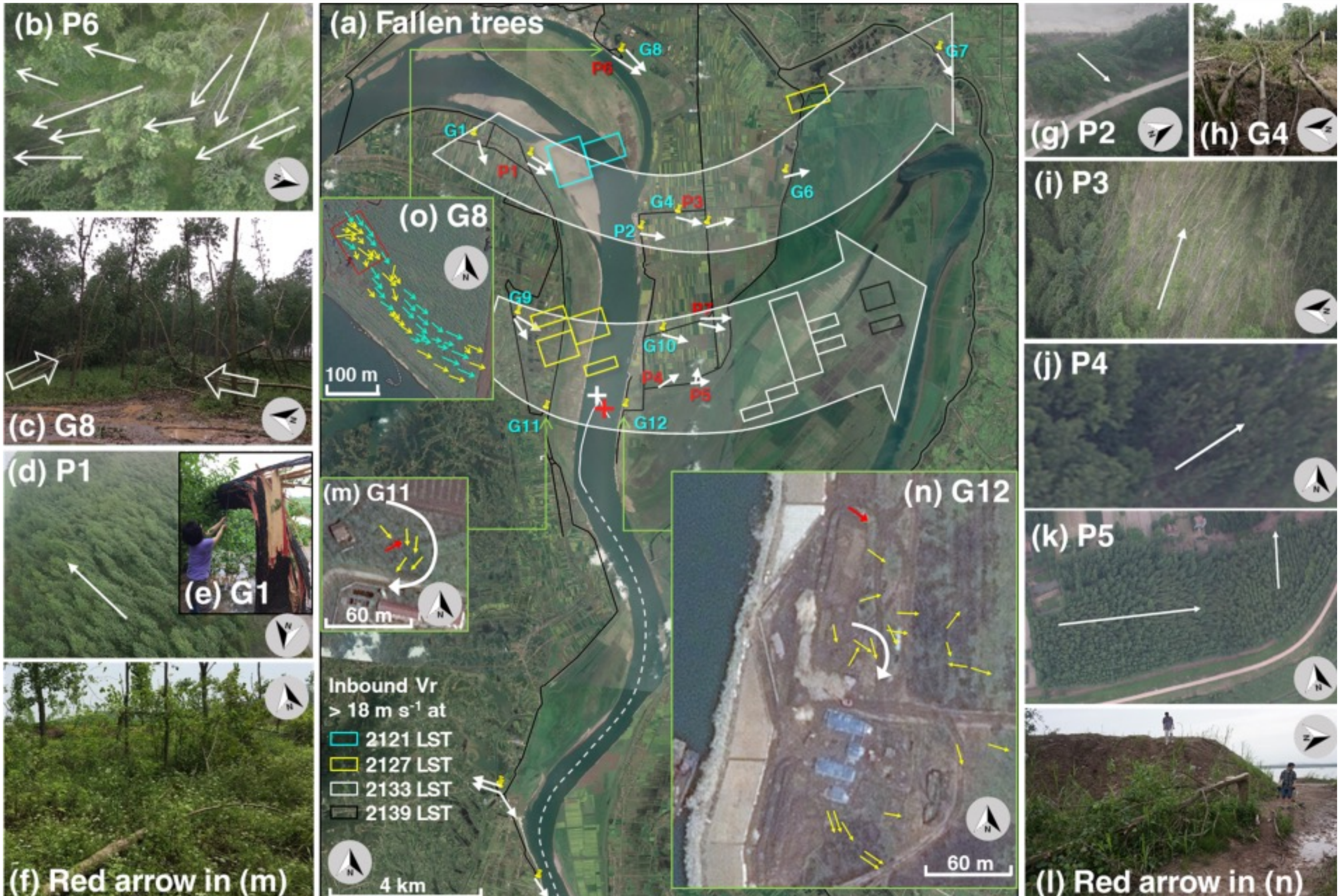

(b) P6
(c) G8
(d) P1
(e) G1
(f) Red arrow in (m)
(a) Fallen trees
G1
G2
G4
G6
G7
G8
G9
G10
G11
G12
P1
P2
P3
P4
P5
P6
P7
(o) G8
100 m
(m) G11
60 m
(n) G12
60 m
Inbound Vr
> 18 m s-1 at
2121 LST
2127 LST
2133 LST
2139 LST
4 km
(g) P2
(h) G4
(i) P3
(j) P4
(k) P5
(l) Red arrow in (n)

# 东方之星倾覆地点附近的为下击暴流

# The development of downdraft

$$\frac{\mathrm{d}w}{\mathrm{d}t} = \underbrace{-\frac{1}{\rho}\frac{\partial p'_{\mathrm{d}}}{\partial z}}_{\text{dynamic forcing}} + \underbrace{\left(-\frac{1}{\rho}\frac{\partial p'_{\mathrm{b}}}{\partial z} + B\right)}_{\text{thermodynamic forcing}},$$

Significant in the environment with high vertical shear

Dominant in downburst case

For well-behaved fields (i.e., $\nabla^2 p' \propto -p'$),

$$p' \propto \underbrace{\underbrace{e_{ij}^2}_{\text{splat}} \underbrace{-\frac{1}{2}|\omega|^2}_{\text{spin}}}_{\text{dynamic pressure perturbation}} \underbrace{-\frac{\partial B}{\partial z}}_{\text{buoyancy pressure perturbation}}.$$

# Pressure perturbation

At surface beneath the downburst

Bernoulli equation: $$p' \approx \overline{\rho}\left(\frac{v^2}{2} + \mathrm{DCAPE}\right)$$

v is the downdraft velocity a few km above the surface at a height where P' is small. $\overline{\rho}$ is the mean air density in this layer.

(at ~ 2km)

For $v \sim 10\,\mathrm{m\,s^{-1}}$, $\overline{\rho} \sim 1\,\mathrm{kg\,m^{-3}}$

and $\mathrm{DCAPE} \sim 200\,\mathrm{m^2\,s^{-2}}$, yields $p' \sim 2.5\,\mathrm{mb}$.

Limited by the estimation difficulty in DCAPE

# Buoyancy B

- Latent cooling
- Hydrometeor loading

$$\frac{B}{g} \approx \frac{\theta'}{\overline{\theta}} + 0.61 q_{\mathrm{v}}' - \frac{\mathrm{c_v}}{\mathrm{c_p}} \frac{p'}{\bar{p}} - q_{\mathrm{h}}$$

# Latent cooling

- Evaporation of liquid water
  - Below melting level
  - Dry PBL, mid-level entrainment
  - Although dryness is important in downdraft initiation, but the increase of dryness does not necessarily indicate the intensification of the downdraft
    - Dry condition may not initially produce strong updraft and much rainfall to evaporate

# Latent cooling

- Melting of ice
  - Below melting level
  - Increases as environmental RH increases
    - Hail stones maintains a higher $T_w$ due to less evaporation
    - Zero $T_w$ level is higher in moister environment

- Sublimation of ice
  - Confined on higher altitudes
  - Increases as environmental RH decreases

# Latent cooling

The potential temperature change of an air parcel at constant pressure

$$\delta\theta = \frac{\theta}{T}\frac{l}{c_p}\delta r_{\mathrm{h}}$$

*l* : specific latent heat

$r_h$ : hydrometeor mass that is either evaporated, melted, or sublimated.

*ϑ cools by approximately 2.5/0.3/2.8 K* for every 1 g kg−1 of hydrometeor mass that is evaporated/melted/sublimated.

# MCS simulations

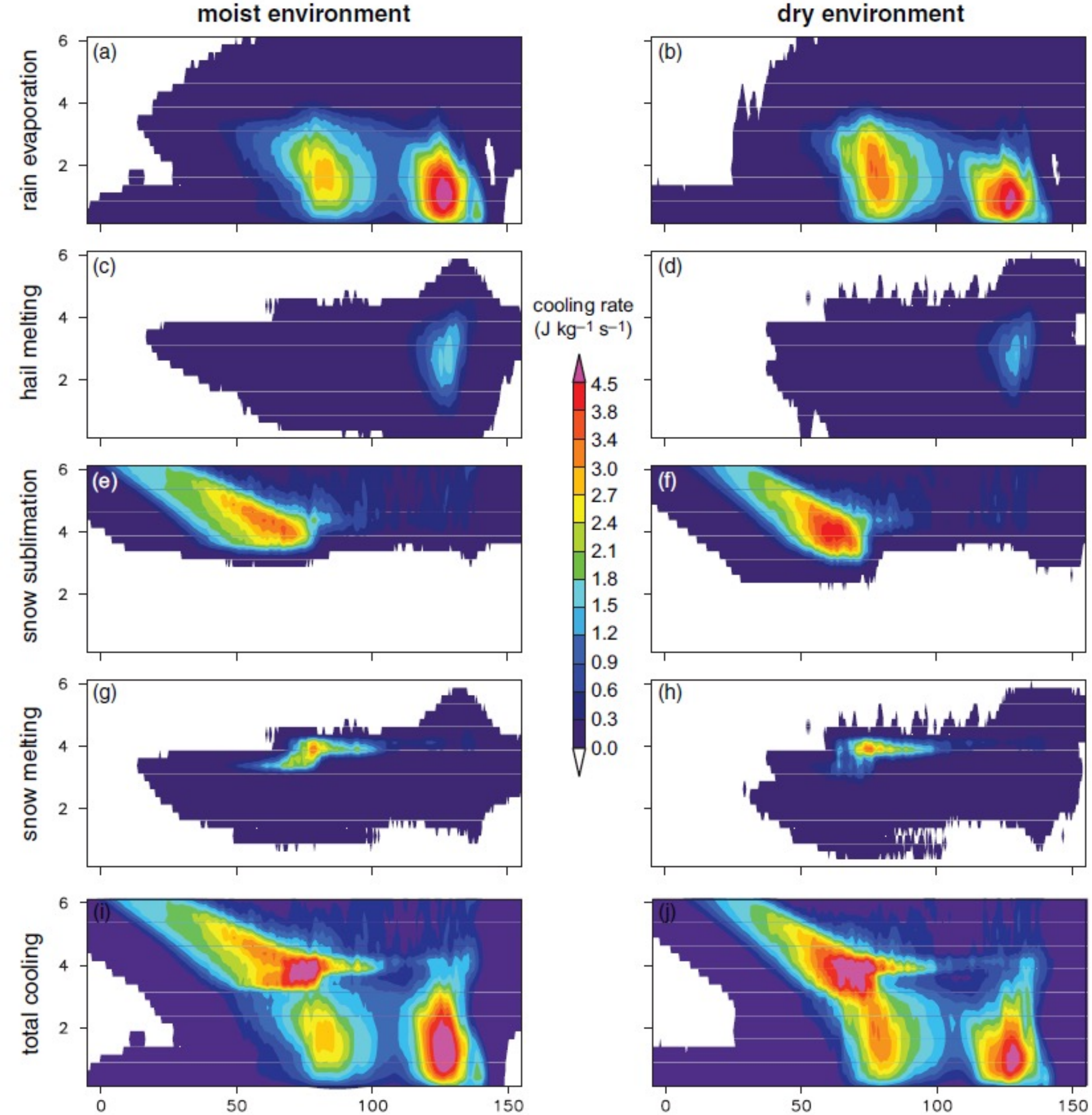


**Figure 10.29** Vertical cross-sections of line-averaged latent cooling rates in a pair of numerical simulations of a long-lived MCS. The panels in the left column (a, c, e, g, i) are from a simulation in which the environment has a relatively high relative humidity throughout the troposphere (the relative humidity decreases from 95% at the top of the boundary layer to 50% at the tropopause), whereas the panels in the right column (b, d, f, h, j) are from a simulation in which the midtropospheric environment has a 1.5 km-deep dry layer with relative humidity of only 10%. The CAPE in both simulations is 4000 J $kg^{-1}$. The melting level in both simulations is at approximately 4 km. The $x$ and $z$ axis labels are in kilometers. The latent cooling rates (J $kg^{-1}$ $s^{-1}$) from (a, b) rain evaporation, (c, d) hail melting, (e, f) snow sublimation, and (g, h) snow melting are shown 4 h into the simulations, as is (i, j) the total latent cooling rate. The evaporative cooling (and total latent cooling) in the moist environment immediately behind the gust front (the gust front is at $x = 150$ km) exceeds that in the dry environment (the domain-wide evaporative cooling and total latent cooling are also greater in the moist environment, although this is not as obvious from the panels above). Image courtesy of Richard James.

# Buoyancy B

- Latent cooling
- Hydrometeor loading

# Hydrometeor loading

$$B \approx g\left(\frac{\theta'}{\overline{\theta}} + 0.61 r'_{\mathrm{v}} - r_{\mathrm{h}}\right)$$

- For $r_h$ = *10 g kg−1, the contribution* to *B is the same as from a −3 K potential temperature* perturbation.

- Crucial in the initiation of downdraft

# Damaging winds: (2) in the absence of a strong downdrafts

- Very common in MCSs
- Generated by
  - Strong pressure gradient in the cold pool
  - Descending of rear-inflow-jet to the surface
  - Meso-$\gamma$-scale vorticies

# RIJ

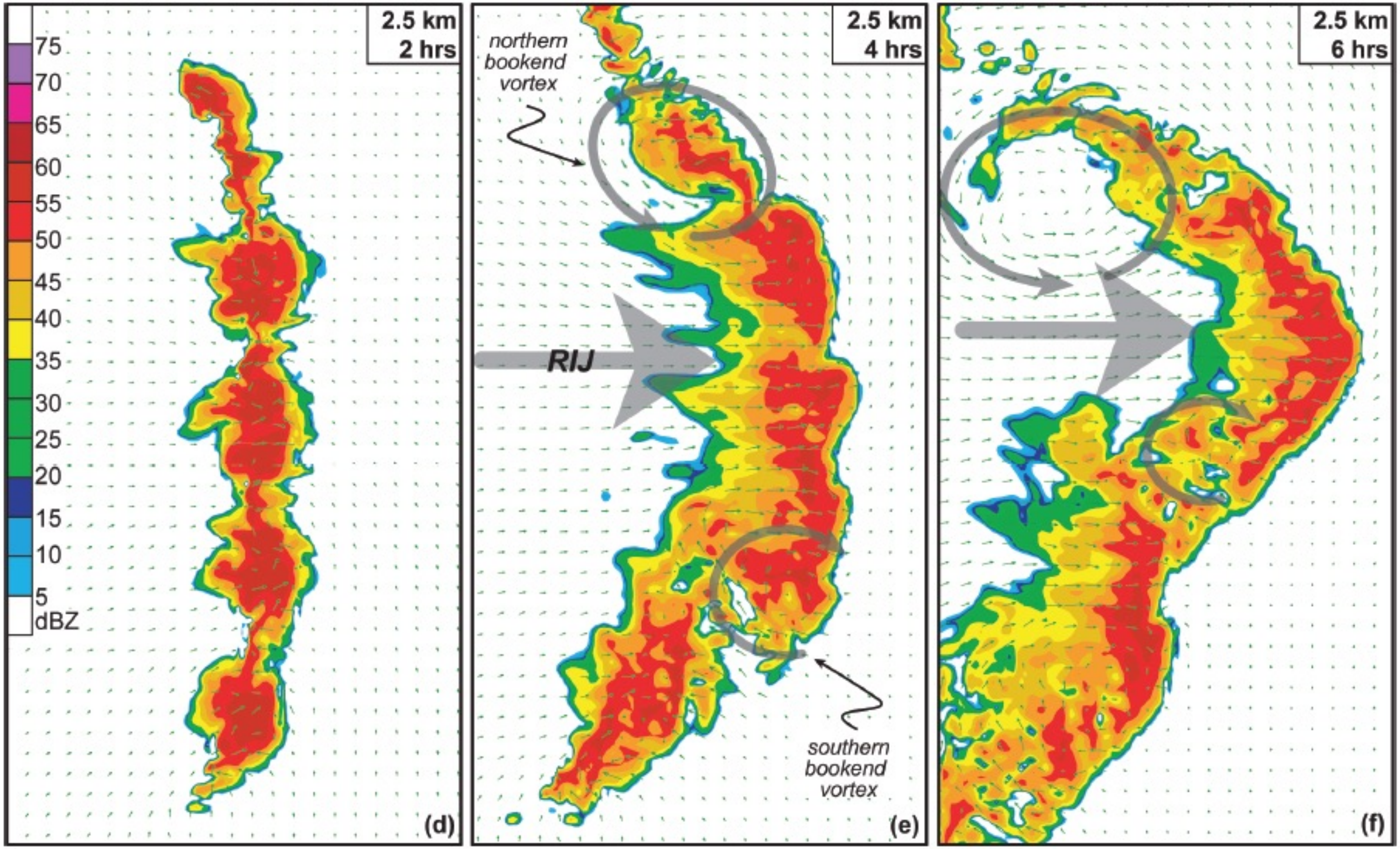
75
70
65
60
55
50
45
40
35
30
25
20
15
10
5
dBZ
2.5 km
2 hrs
(d)
2.5 km
4 hrs
northern
bookend
vortex
RIJ
southern
bookend
vortex
(e)
2.5 km
6 hrs
(f)

# Mesovorticies

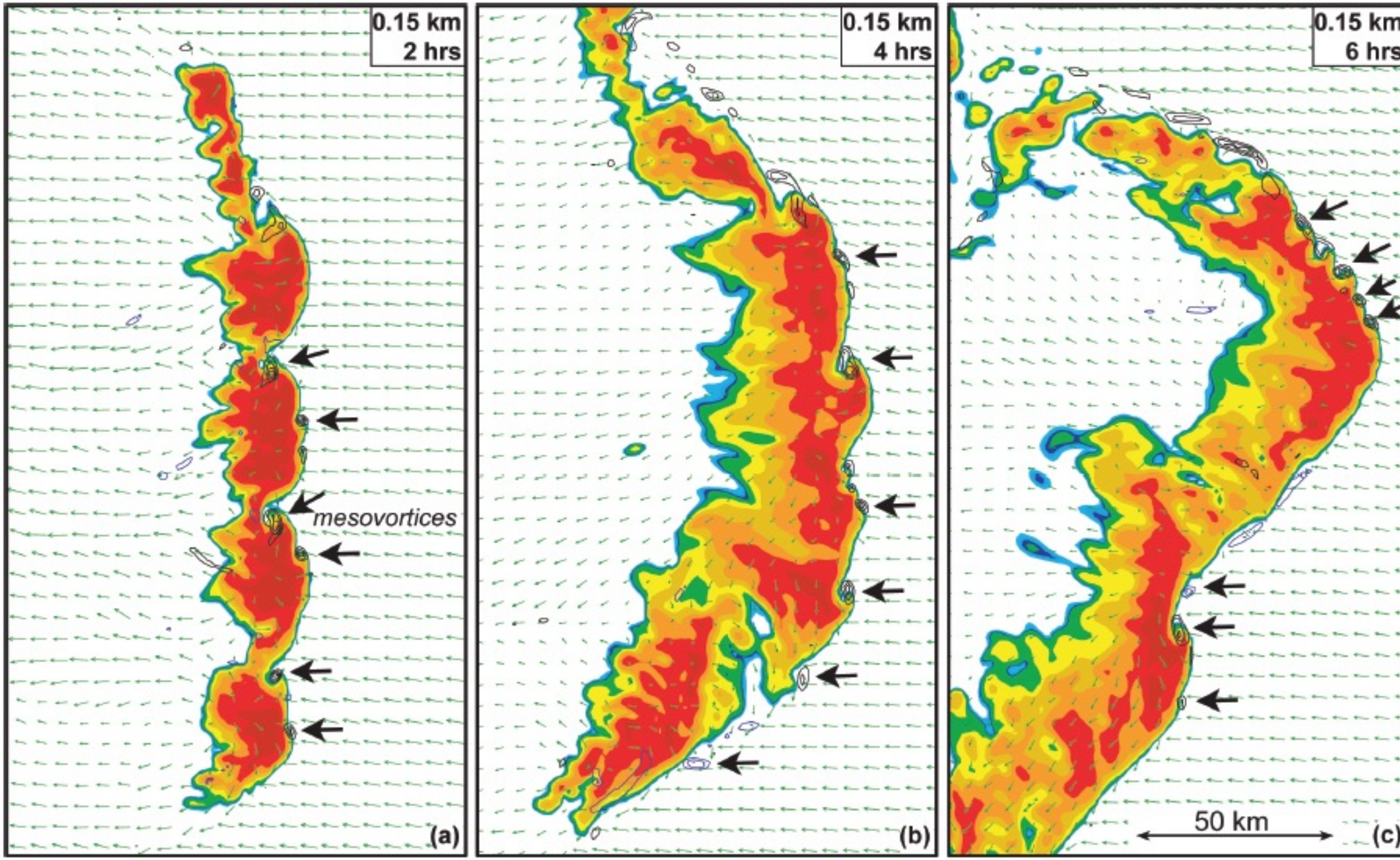

# Straight wind: Derecho

A widespread convectively induced straight-line windstorm.

- major axis > 400 km
- wind > 26 m/s
- time~ 10 h
- Specifically, the term is defined as any family of downburst clusters produced by an extratropical mesoscale convective system (bow echoes).

# Example

Guastini, C. T., and L. F. Bosart, 2016: Analysis of a Progressive Derecho Climatology and Associated Formation Environments. *Mon. Wea. Rev.*, **144**, 1363–1382, [https://doi.org/10.1175/MWR-D-15-0256.1](https://doi.org/10.1175/MWR-D-15-0256.1).

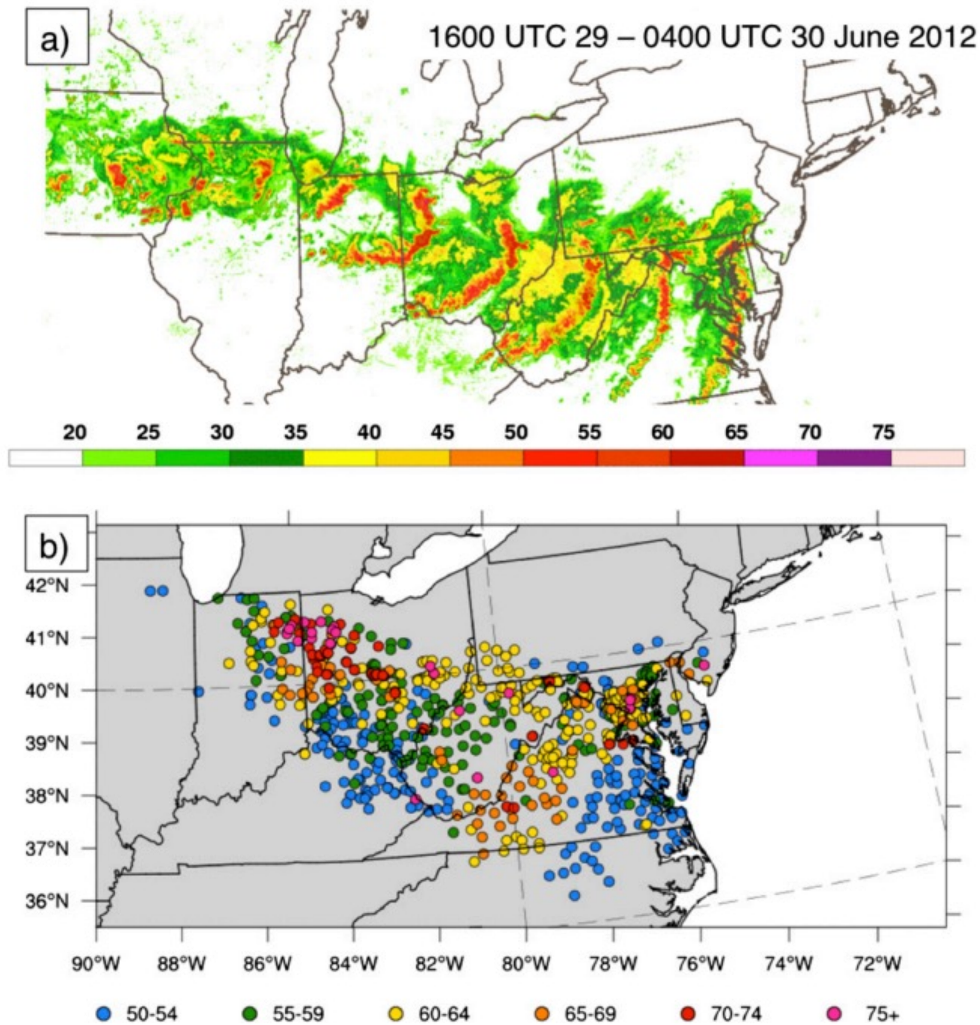


FIG. 1. (a) Radar continuity map every 2 h from 1600 UTC 29 Jun to 0400 UTC 30 Jun 2012. (b) Storm Prediction Center severe wind reports colored by wind speed (kt) for the 29–30 Jun 2012 progressive derecho. It is noted that many of the wind speeds contained in the Storm Prediction Center data are estimated.

# U.S. 1996-2013

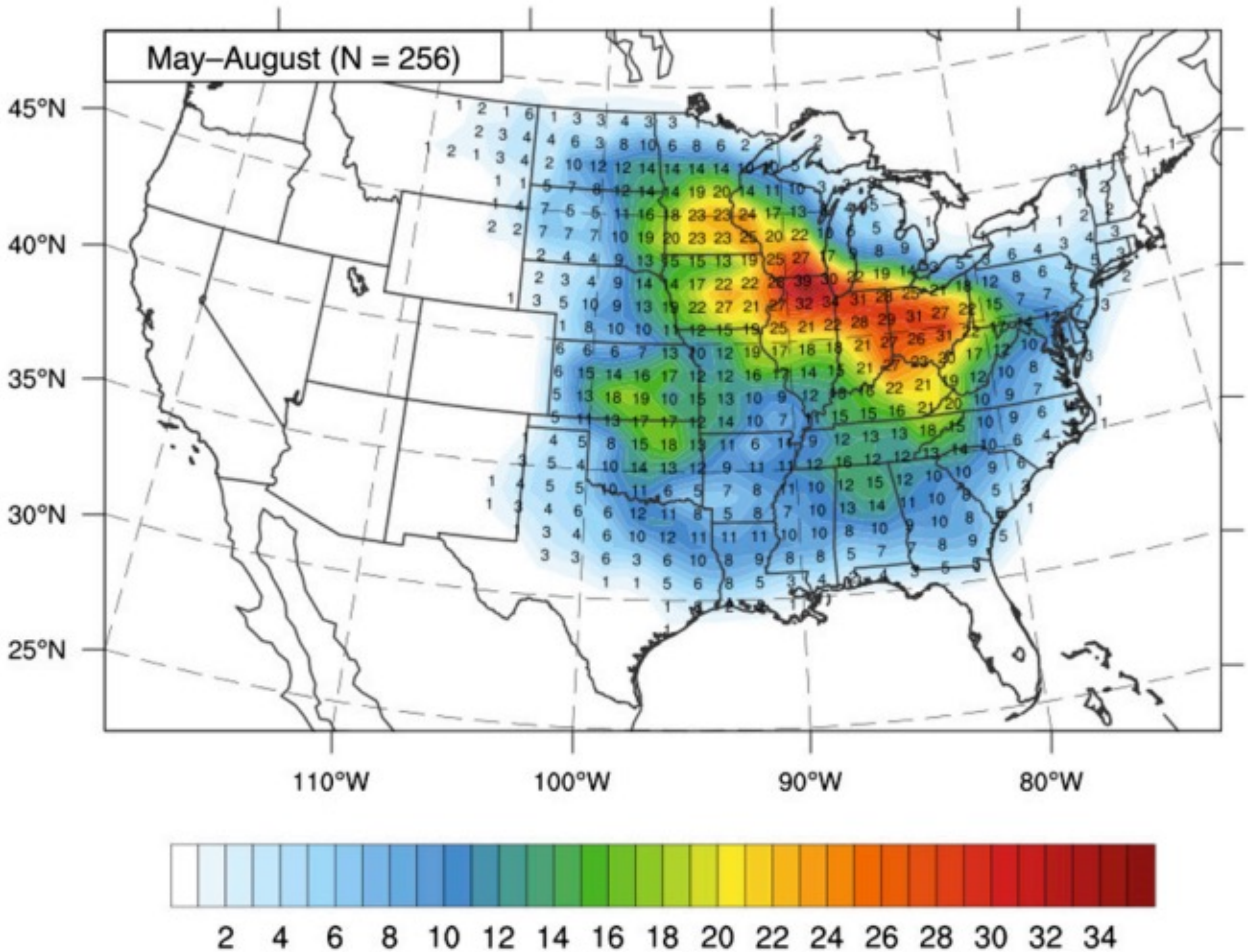


FIG. 4. Climatology of progressive derecho events for the warm season (May–August) of 1996–2013. The number of progressive derechos passing through a given 100 km × 100 km grid box over the 18-yr span is located at the center of the grid box and is plotted for those boxes containing at least one progressive derecho.

# 不同季节的分布

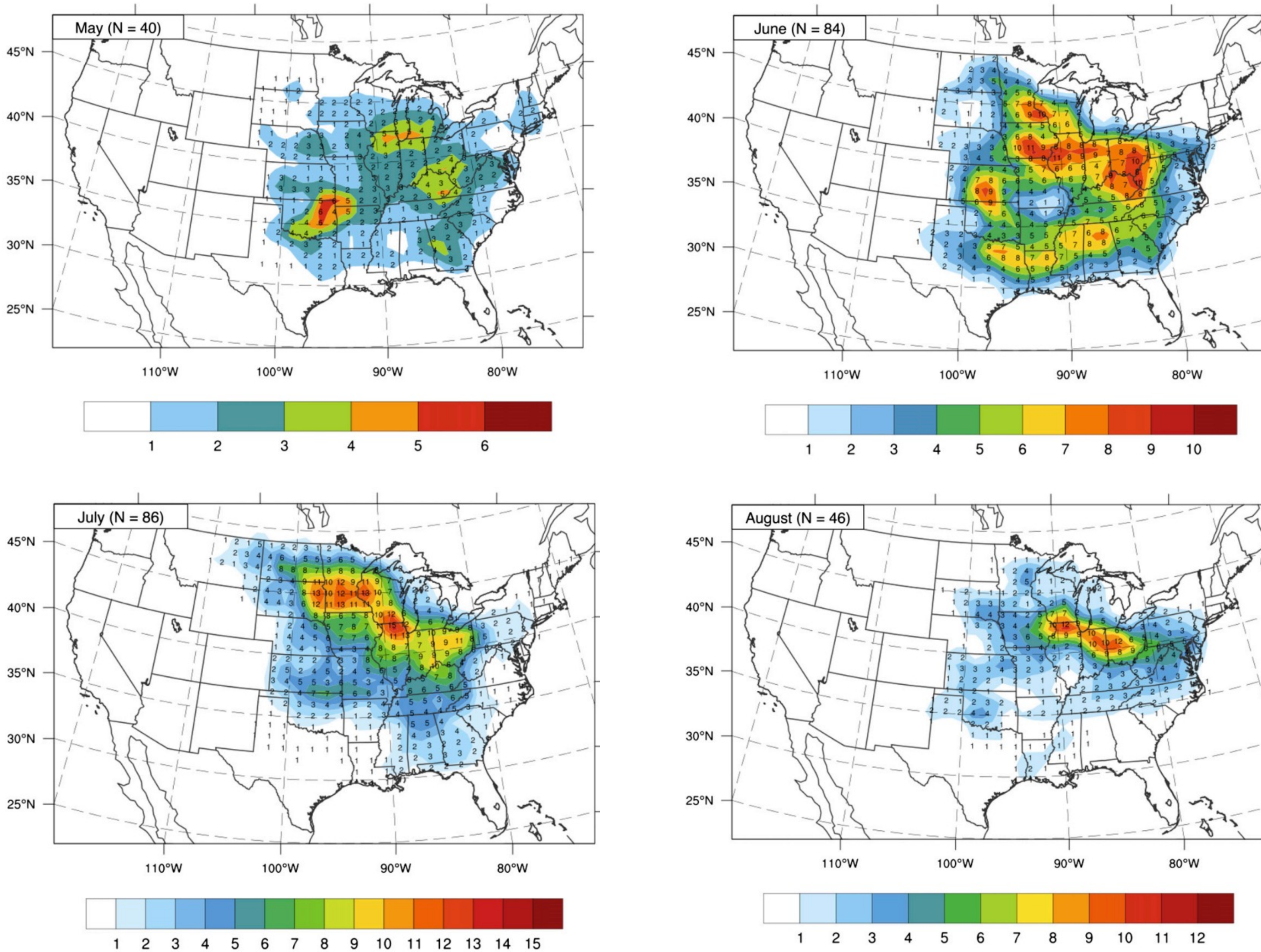

May (N = 40)
June (N = 84)
July (N = 86)
August (N = 46)
45°N
40°N
35°N
30°N
25°N
110°W
100°W
90°W
80°W
1 2 3 4 5 6
1 2 3 4 5 6 7 8 9 10
1 2 3 4 5 6 7 8 9 10 11 12 13 14 15
1 2 3 4 5 6 7 8 9 10 11 12

# Forecasting

## For isolated cell

- Identifying environments conducive to the formation of intense downdraft

## For MCSs

- Anticipating the formation of long-lived MCSs
  - Cold pool
  - Rear inflow jet descending
  - Mesovorticies

## For Supercells: RFD

# Chapter 5
# Hazards associated with DMC

- Tornado
- Straight Wind
- Hail
- Flash flood

# Hail formation and growth

- Form by collection of supercooled cloud droplets and raindrops
  - Most hydrometeors remain supercooled liquid
  - Freezing nuclei form a few ice particles in the updraft
  - Ice particle starts to descend after 5-10 min growth by vapor deposition
  - The supercooled liquid freezes immediately upon contacting and form spherical graupel (with diameters of a few millimeters )

# Hail formation and growth

– Formation of low-density ice layer
  - The growing ice particles become larger and falls faster, sweeping out more supercooled liquid

– Formation of clear ice layer
  - Once the growth rate becomes large, the hailstone temperature may be  above zero, owing to the increased energy transferred to the ice in the fusion process
  - The supercooled cloud droplets may not freezes immediately upon contact, but flow across the surface and fill in the gaps and thus increases the hail density, and form a layer of clear ice.

# Hail size

- The final size of the stone is decided by
  - Liquid water concentration
  - The time that the hail can reside in the region of high supercooled liquid water content
    - Updraft strength
    - Hail fall speed
    - Times of excursions through the updraft
- The size of hail that reaches the surface
  - Melting amount of hail
    - Increase: Falls in updraft with a high freezing level due to more moist air
    - Decrease: outside the cloud （dryer, lower wet-bulb-zero level ), or in downdraft (fall faster)

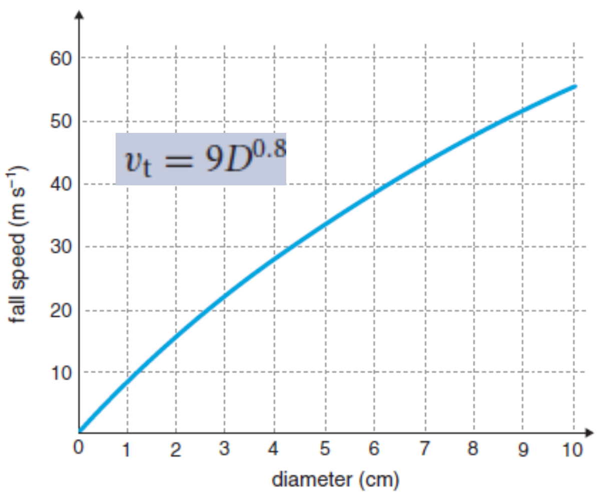

# Ideal condition for hail growth

- Hailstone fall speed matches the updraft velocity when the ice particle enters the portion of the updraft where the supercooled liquid water concentration is large
  - May grow to a diameter of 10 cm or larger
  - Falling hail approach the core of a tilted updraft, help to make the fall speed matched by the updraft
- If the updraft is too stronger, ice particles will be ejected to the anvil
- If the updraft is too weaker, ice particles will just falls out prematurely

# Forecasting the hail size that reaches the ground

- The maximum updraft speed
  - CAPE and shear
- The degree of melting
  - Level of Zero $T_w$
- Large CAPE and low Level of Zero $T_w$ are usually used to forecast large hail
- No observed apparent correlation between the hail size and CAPE or level of zero $T_w$
  - CAPE is not a good indicator for updraft when the parcel theory is not well satisfied

# Radar Signature of Hail

1956 UTC 22 July 2003

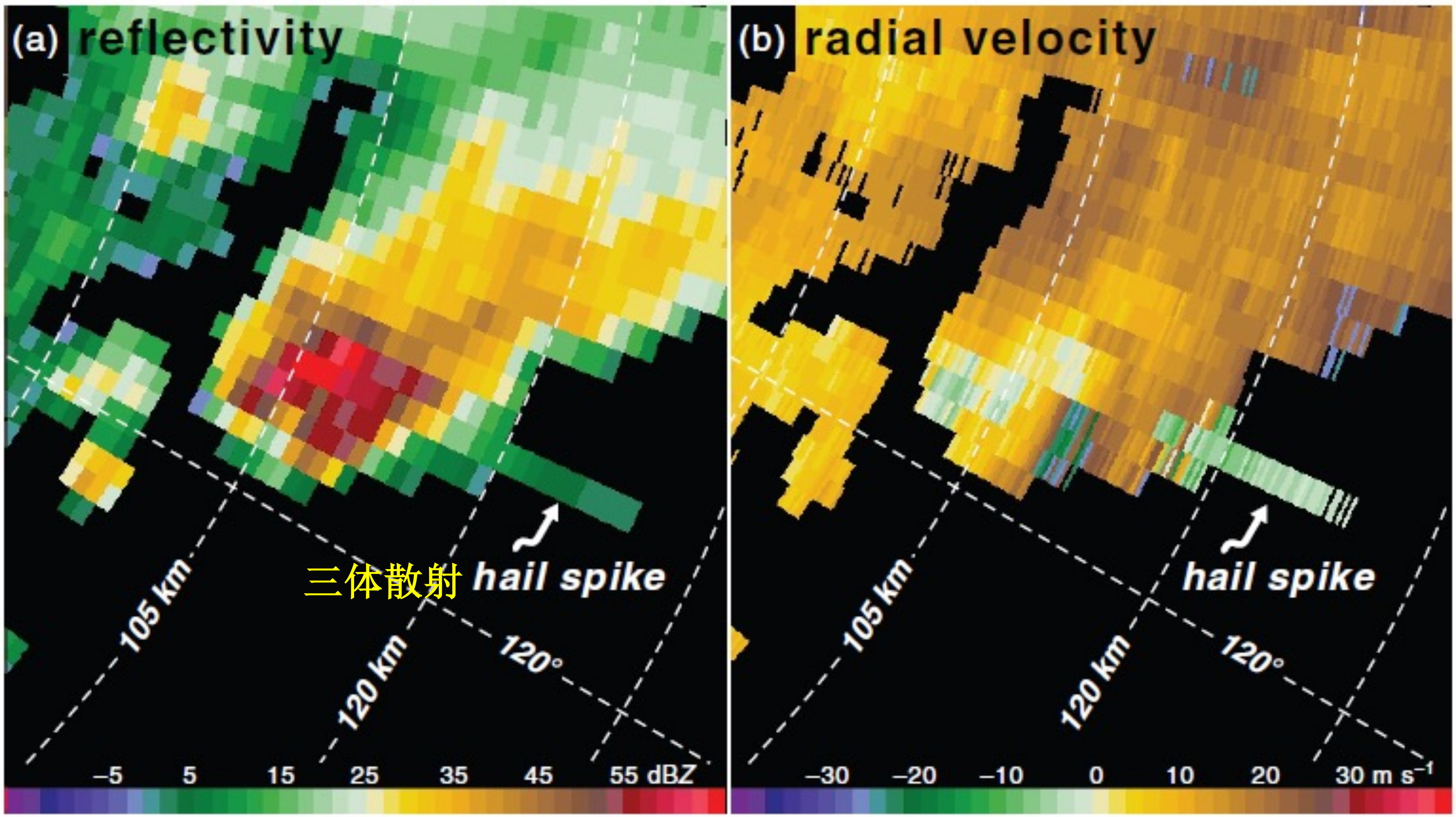

## Chapter 5

# Hazards associated with DMC

- Tornado
- Straight Wind
- Hail
- Flash flood

# Flash floods

- The deadliest hazard associated with convection worldwide
- Its nature is complicated by the interaction of meteorology and hydrology

The total accumulation of precipitation $P = \overline{R}D$

$\overline{R}$ : the average rainfall rate
D : the duration of the rainfall

# Duration

## Backbuilding MCS

- Rainfall duration is maximized when *cell motion is opposed by the propagation of the convective system*

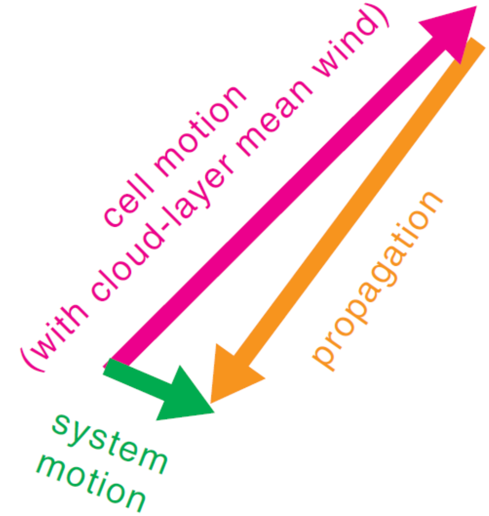


## Echo train

- High rain rate cell moves repeatedly over the same area

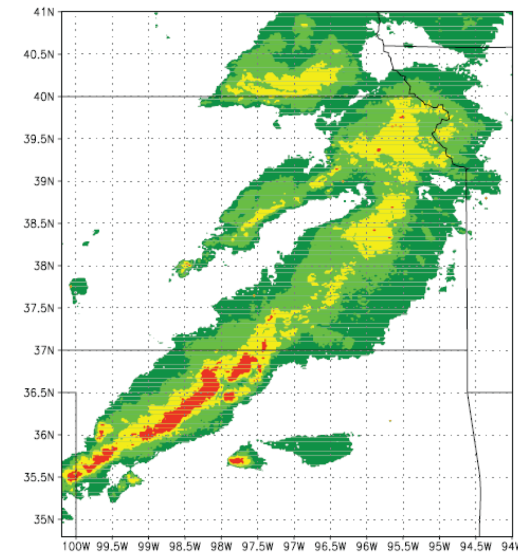

# Duration

- **MCS organization**

  LS MCSs are more prone to produce extreme rainfall accumulation, it moves slower than PS and TS MCSs

  – LS tends to have the opposite direction between cell motion and propagation

  – TS tends to have the same direction between cell motion and propagation

- **Convection structure**

  – Large stratiform precipitation region poses a greater threat

# Rain rate

Instantaneous rain rate $R = Ewr_{\mathrm{v}}$

E : precipitation efficiency , the ratio of the measured precipitation rate at the ground to the water vapor flux through the cloud base

# E vs. vertical wind shear

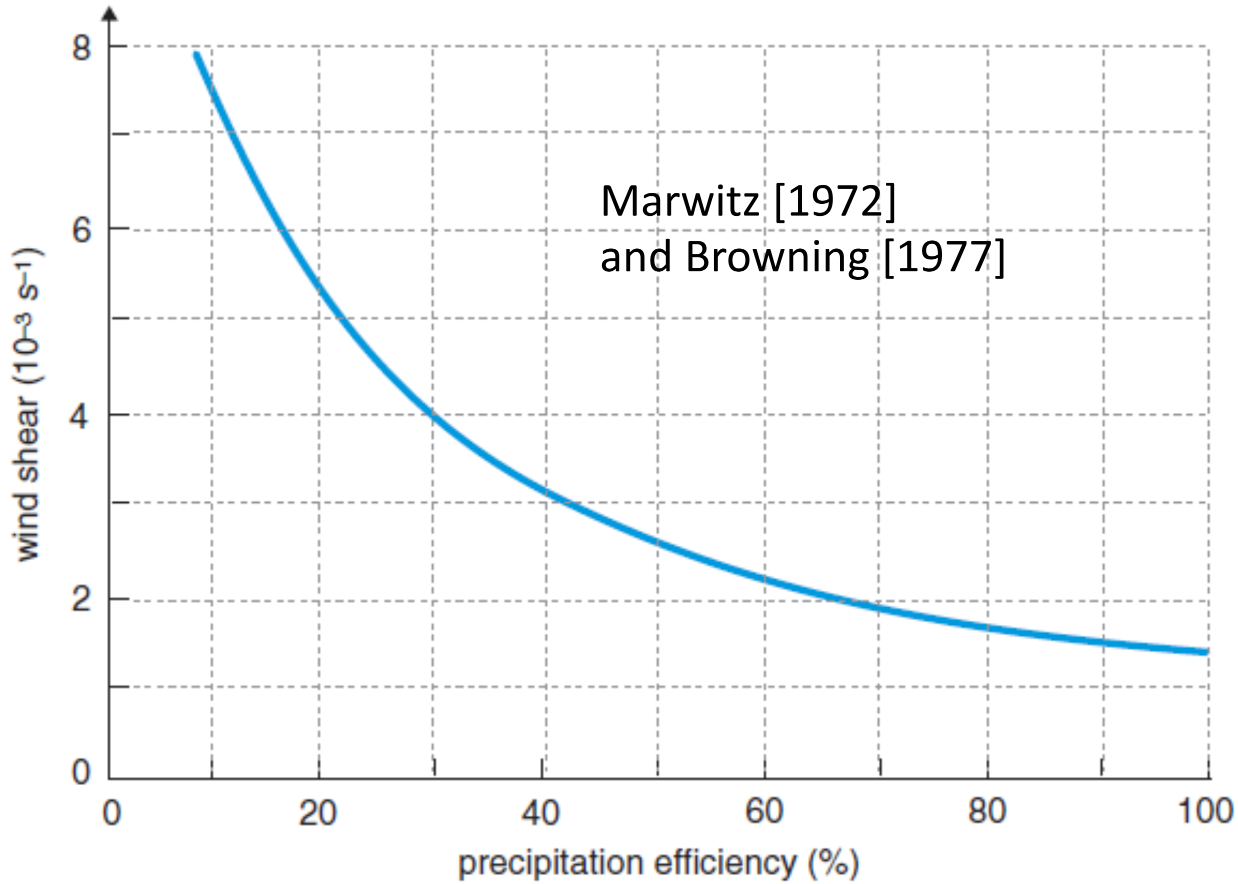


The determination of E is error-prone

# E vs. vertical wind shear

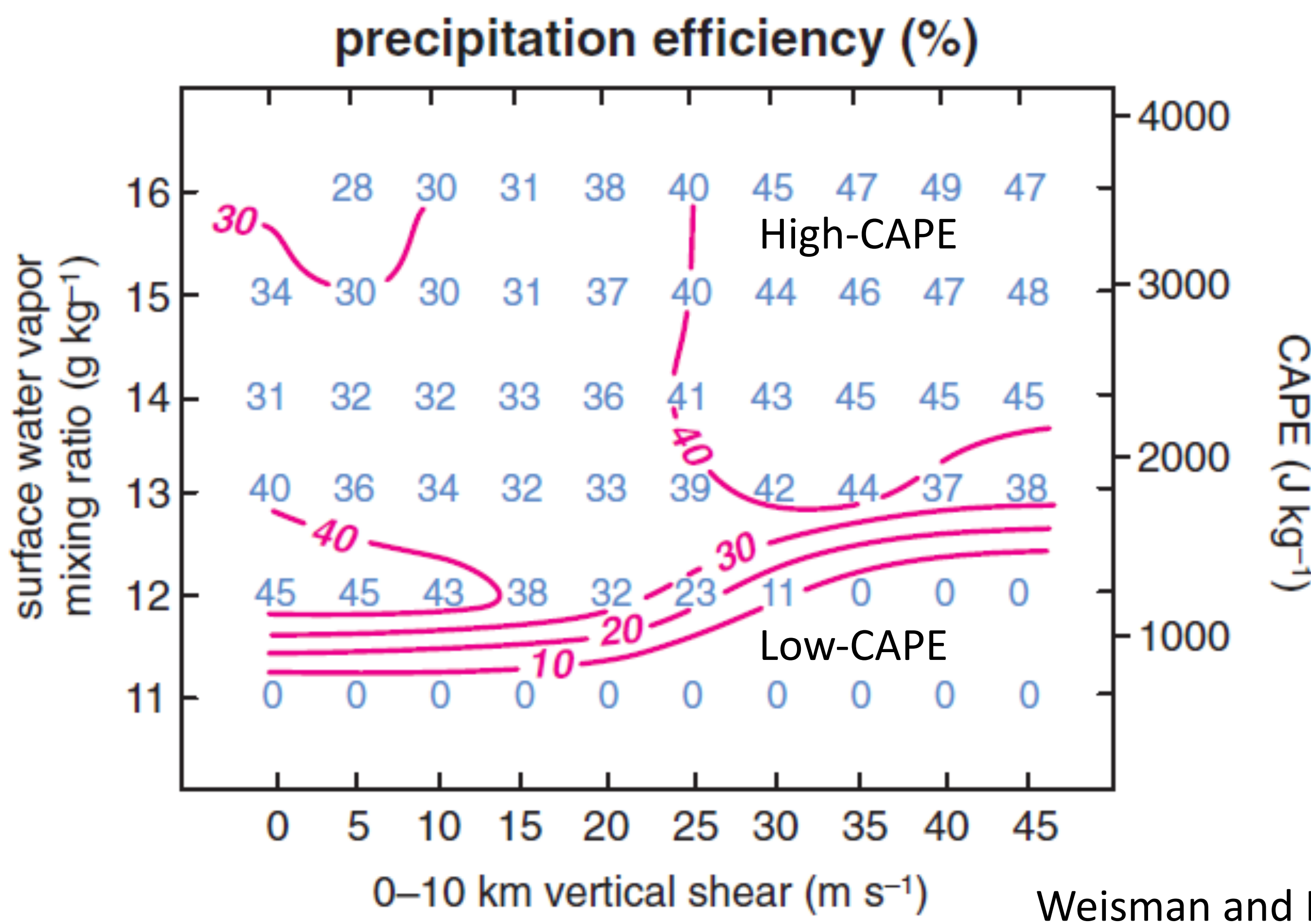


Weisman and Klemp (1982)

They used a very simple warm-rain microphysics parameterization

# E vs. vertical wind shear

- **Detrimental**: Entrainment tends to increase with increased shear
  - The precipitation falls farther from the updraft, more entrainment, more evaporation
- **Beneficial**: convection tends to be better organized or long-lived in stronger vertical shear environment

# E vs. RH

- E increases if RH increases
  - Less evaporation
- **Isolated updraft** has less E than those embedded in a larger cloud system due to more entrainment

# Forecasting E is tricky

- It involved microphysical process
  - Depth of cloud layer below and above freezing level
    - Warm rain process are more threatening
  - Cell merger increases E
    - Less entrainment
    - Larger collision and coalescence rate due to the possible merging of two different drop-size distribution

# Ingredients of flash flood from DMC

- Slow storm motion  (D)
- Large low-level water vapor concentration in the presence of strong updraft (R)
- Large environmental relative humidity (E)
- A significant cloud depth below the freezing level  (E)
- Weak vertical shear (E)

# Ingredients of flash flood from DMC

- In DMC, E is generally high, mesoscale Effects could make things worse
  - Cell merger
  - Backbuilding convection along slow-moving or stalled fronts
  - Backbuilding due to lifting by a convectively generated gravity wave
  - Topographic effects

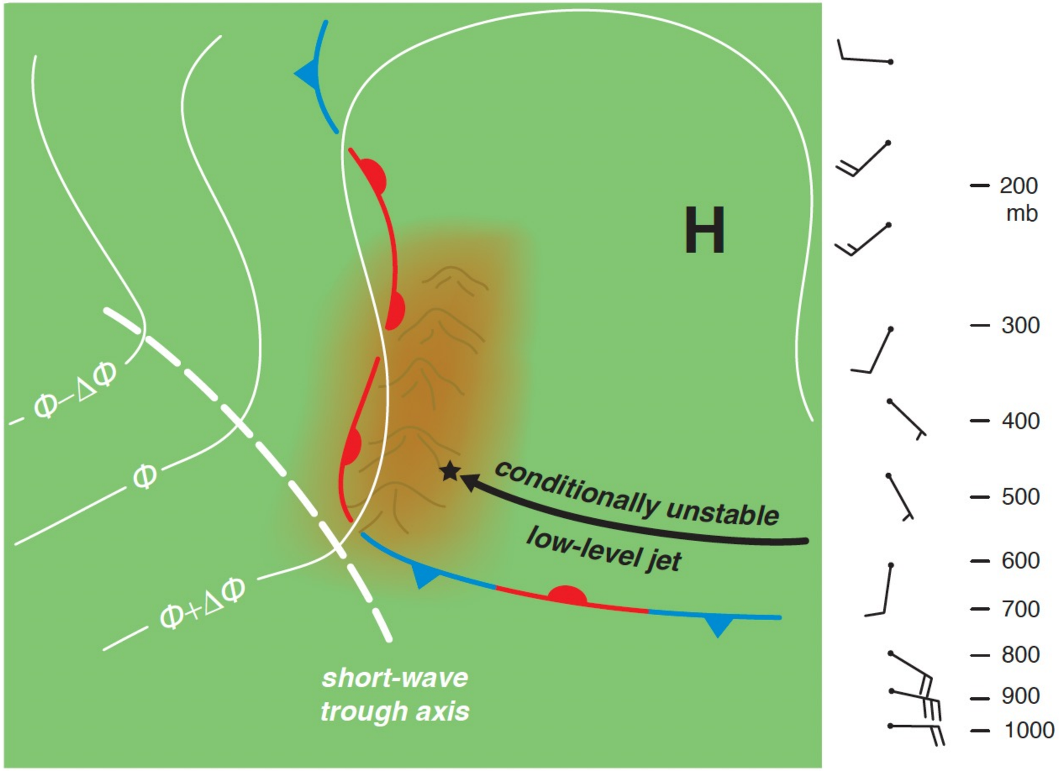


**Figure 10.43** Composite illustration of typical synoptic-scale conditions associated with severe orographic flash flood events. The worst flooding occurs in the vicinity of the star, which also marks the location represented by the vertical wind profile shown on the right (wind barbs are in knots). The flood-producing convection tends to be initiated downstream of a negatively tilted, midtropospheric short-wave trough (white midlevel height contours are indicated schematically) in an environment of weak southerly winds and divergence aloft. The short-wave trough contributes to the destabilization of the environment and advection of midlevel moisture into the threat area. At the surface, the most prominent feature is a large high-pressure system (the center of the high is indicated with a black letter 'H') downstream of a midtropospheric ridge axis. A slow-moving or stalled front is typically found to the south, and a postfrontal band of strong, conditionally unstable, moist easterly winds flows upslope and initiates new cells repeatedly over approximately the same area. Slow updraft motions, nearly stationary convective system motion as a result of the new cell generation being tied to the terrain, a moist and warm sounding, and weak vertical wind shear all contribute to the heavy precipitation accumulations. (Adapted from Pontrelli *et al*. [1999].)